NASA CONTRACTOR REPORT

NASA-CR-468

NASA CR-468

BASIC STUDIES ON VORTEX STABILIZED RADIATION SOURCES FOR IMPROVED SOLAR SIMULATION

by Delbert G. Van Ornum

Prepared under Contract No. NASw-858 *by*
GIANNINI SCIENTIFIC CORPORATION
Santa Ana, Calif.
for

NATIONAL AERONAUTICS AND SPACE ADMINISTRATION - WASHINGTON, D. C. - MAY 1966

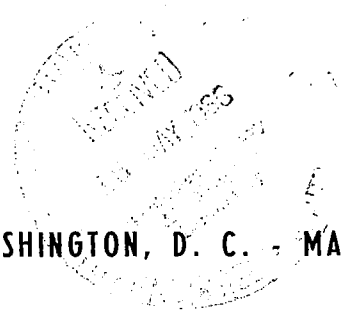

NASA CR-468

BASIC STUDIES ON VORTEX STABILIZED RADIATION SOURCES FOR IMPROVED SOLAR SIMULATION

By Delbert G. Van Ornum

Prepared under Contract No. NASw-858 by
GIANNINI SCIENTIFIC CORPORATION
Santa Ana, Calif.

for

NATIONAL AERONAUTICS AND SPACE ADMINISTRATION

For sale by the Clearinghouse for Federal Scientific and Technical Information
Springfield, Virginia 22151 – Price $3.00

ABSTRACT

The ultimate objective of this investigation was to improve the simulation of the solar spectrum as observed in space. The discrepancies between the spectral energy distribution found in argon vortex arc radiation and the zero air mass solar radiation were studied. To improve the spectrum, various elements were selected and added to the arc so that their broadened line radiations would fill in deficient zones. The additives were gases, or solid compounds injected into the arc itself and filtered out of the gas stream before recirculation. Measurement of the spectral output of the argon arc with injected titanium, barium, sodium, hydrogen, lanthanum and mercury led to a better understanding of both line and continuum radiation physics. From the line radiation approach, improved simulation of the solar spectrum was obtained by adding small amounts of hydrogen and barium to the argon vortex. From the continuum approach, excellent simulation was achieved by use of pure xenon in a high pressure vortex arc.

TABLE OF CONTENTS

LIST OF FIGURES

LIST OF FIGURES
(continued)

1.0 INTRODUCTION

This report presents the results of basic studies aimed at improving the simulation of the solar spectrum as observed in space by the use of the gas vortex stabilized arc. The vortex stabilized arc is a useful source of radiation for simulation and perhaps duplication of solar radiation. First, a large power handling capability has been demonstrated with some units having been operated at 150 kw input power. Second, the average radiance for the entire arc column considerably exceeds the radiance of the sun and, as large solid angles are optically available, large single arc solar simulators are possible. Third, the radiation of vortex arc units of more than 15 kw input power becomes essentially a continuum with a relatively minor line contribution. The radiation of a 25 kw argon vortex arc, for example, has a continuum which compares well with the carbon arc spectrum. The visible portion of the argon vortex arc spectrum, however, deviates considerably from the spectrum of the sun in space and an excess of intermediate ultraviolet is present.

The work reported deals largely with the argon vortex. Figure 1.1 Vortex Arc Configuration, sketches the essential features of a vortex unit. An outer fused silica tube is often used and is placed just outside the cylinder shown. The incoming argon passes between the two fused silica tubes, then enters the arc chamber volume through nozzles at the cathode end. The gas then spirals, forming a vortex as it moves radially inward to exhaust through an axial exhaust at the face of the anode. Both electrodes and the tube ends are cooled by forced circulation of water. With the striking of the arc, the electrons and argon ions are confined to a cylindrical column between the cathode tip and the anode bore. The resulting arc is very much like an ideal Maecker model (Ref. 1.1) with average current density nearly uniform throughout its length. The arcs studied in this program have been around 10 mm in length and 3 mm to 5 mm in diameter depending on the actual experimental device used. The vortex volt-ampere characteristics are strikingly different from those of a static short arc of similar electrode gap. The vortex arc voltages are always much higher than for the static arc. The vortex arc is cylindrical in shape and lacks the large anode flare observed with static short arcs.

A comparison of the spectrum of the argon vortex operated at 25 kw with the solar spectrum in space (Ref. 1.2) shows three important discrepancies: an excess in the ultraviolet, a deficiency between 0.45μ and 0.70μ, and an excess around 0.8μ. Figure 1.2, Spectral Distribution: Argon VSRS vs Sun, portrays these points. The argon spectral power drops by about half after 1.4 microns but maintains a fairly

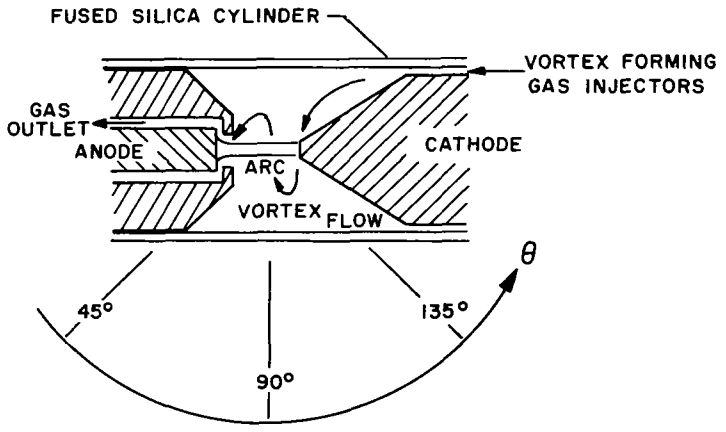

FIGURE 1.1 - VORTEX ARC CONFIGURATION

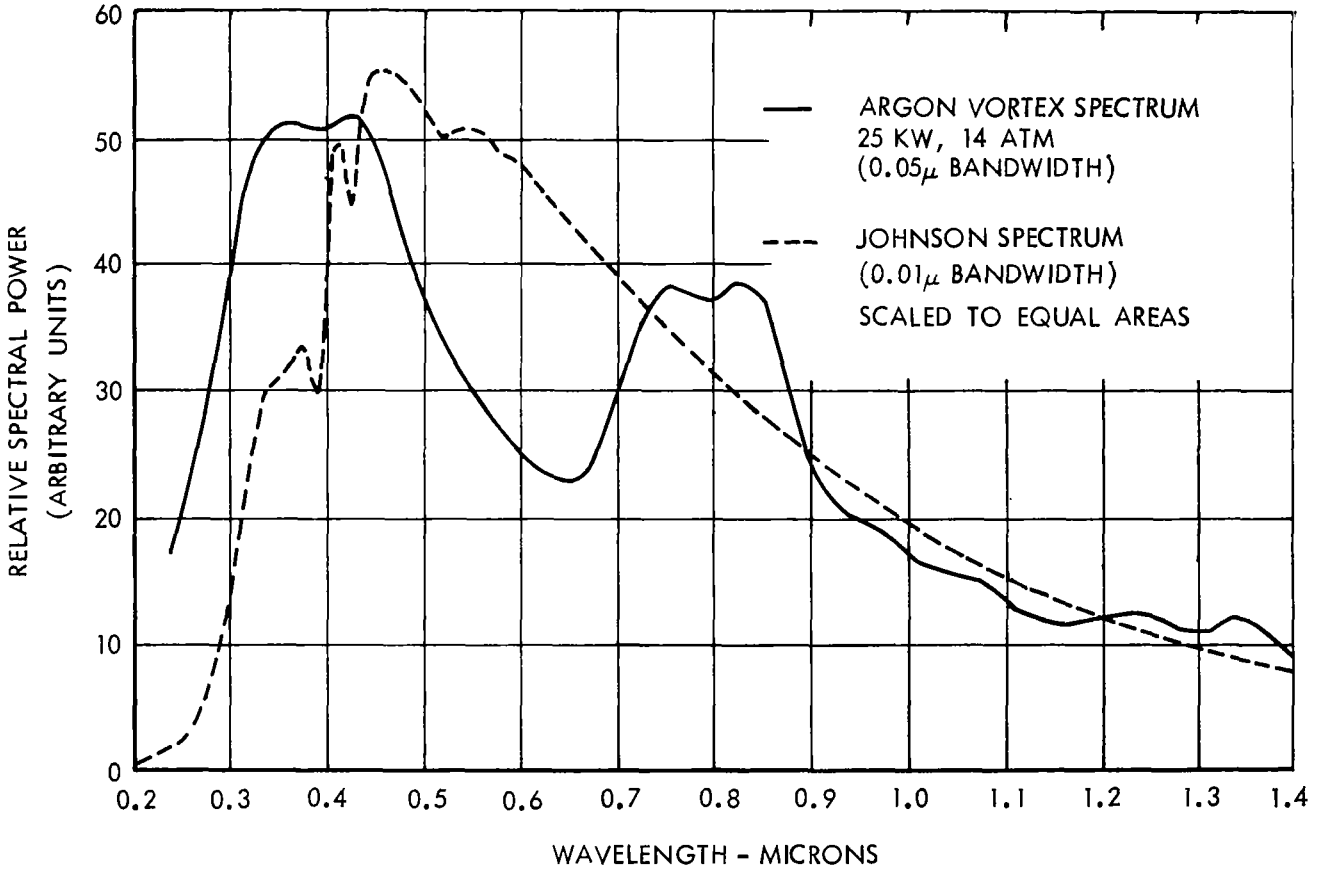

FIGURE 1.2 - SPECTRAL DISTRIBUTION: ARGON VSRS VS SUN

smooth decreasing continuum out to the fused silica cutoff. In actual simulator systems using fused silica for transmission and vaporized aluminum mirrors overcoated with silicon monoxide for reflection, spectral losses must be considered. Relatively large losses will occur in the ultraviolet, thus minimizing this excess. The peak at 0.8μ will also be reduced as the reflectivity of aluminum dips in the near infrared. The deficiency between 0.45μ and 0.70μ is more important, and most of the effort of the project being reported deals with means of increasing radiation in these wavelengths. It is interesting to note that this visible light deficiency of argon persists to very high input powers, see Figure 1.3, Spectral Distribution Argon Axial Bore Vortex, it is less significant at 60 kw, however, than at 21 kw.

Examination of the argon spectrum with a fairly narrow bandpass, say 5 Å, shows that at low input power and low pressure the radiation is composed of a fairly weak continuum with strong lines around 0.4μ and 0.8μ. As power and pressure are increased, the continuum increases until at around 25 kw and 14 atmospheres it is the dominant feature of the spectrum. Unfortunately the continuum radiation of an inert gas tends to have more than one peak (Ref. 1.3, 1.4 and 1.5), and in this case the 0.45μ to 0.70μ deficiency of argon persists.

The first approach to the spectral match problem was to add to the arc various elements so selected that their broadened line radiations would fill in the deficient zone in the visible. The spectral result, if successful, would be much like the increased radiation around 0.8μ which is caused in part by a large number of broadened argon lines. The additive can be a gas which takes part in the complete recirculation cycle or it can be a solid or liquid compound or element ejected into the arc itself and then filtered out of the gas stream before recirculation.

The physics involved in selecting desirable additive elements is complex. An understanding of conditions within the arc is necessary for achievement of a successful program. The energy levels of the electron of excited argon are a very important factor in determining plasma conditions. Figure 1.4, Energy Level Diagram of Argon I, shows that both the resonance level and ionization potential are very high, 11.8 ev and 15.8 ev respectively. Figure 1.5, Probability of Excitation of Argon and Neon, (Ref. 1.6), points out that electrons with at least these energies are necessary for the radiation process. Once ions are formed, continuum radiation will occur as electrons with low energy recombine with these ions.

The radial dimension of an arc is controlled by the mean free path of electrons throughout its volume. The mean free path is inversely proportional to the product of

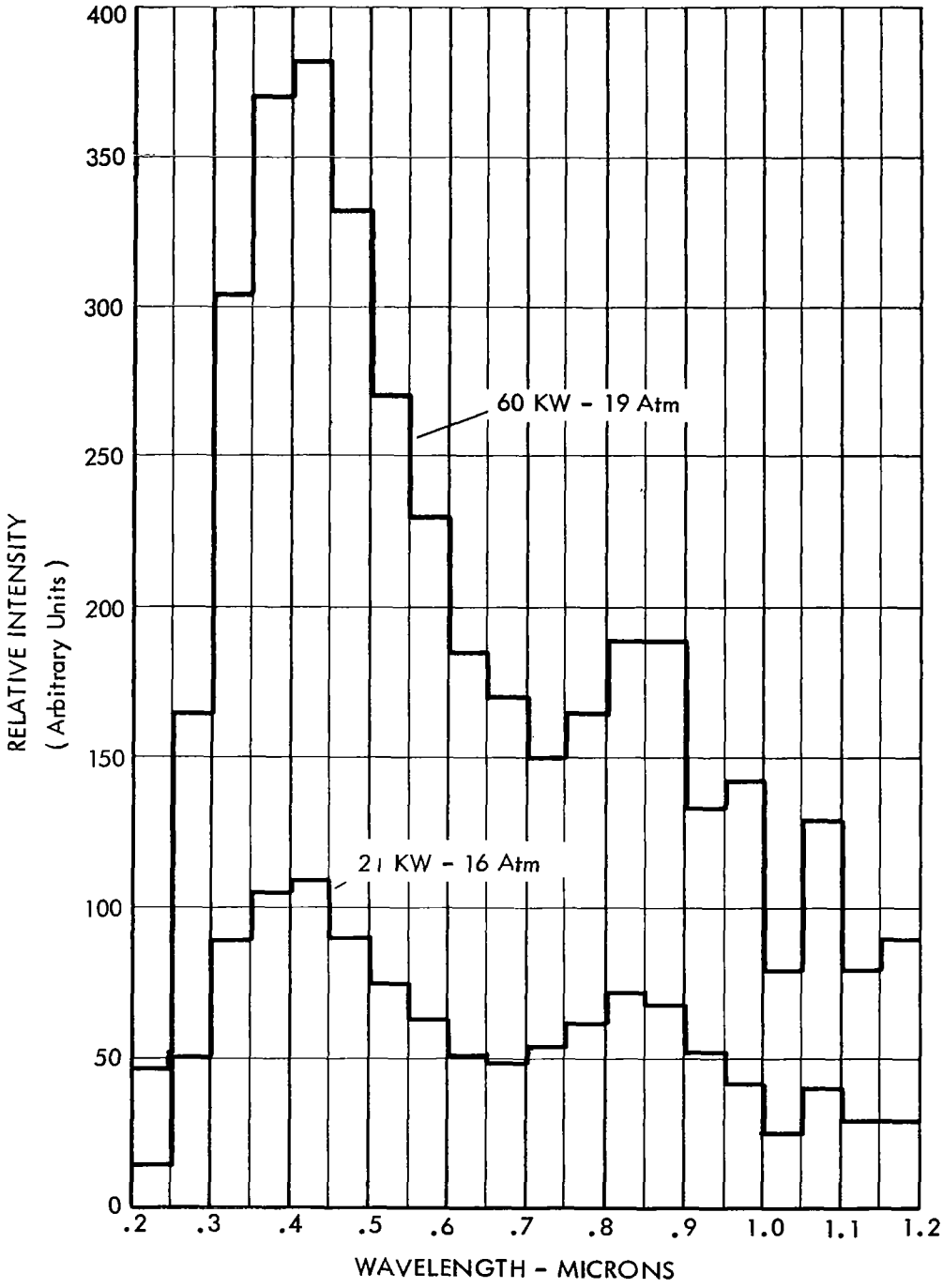

FIGURE 1.3 - SPECTRAL DISTRIBUTION: ARGON AXIAL BORE VORTEX

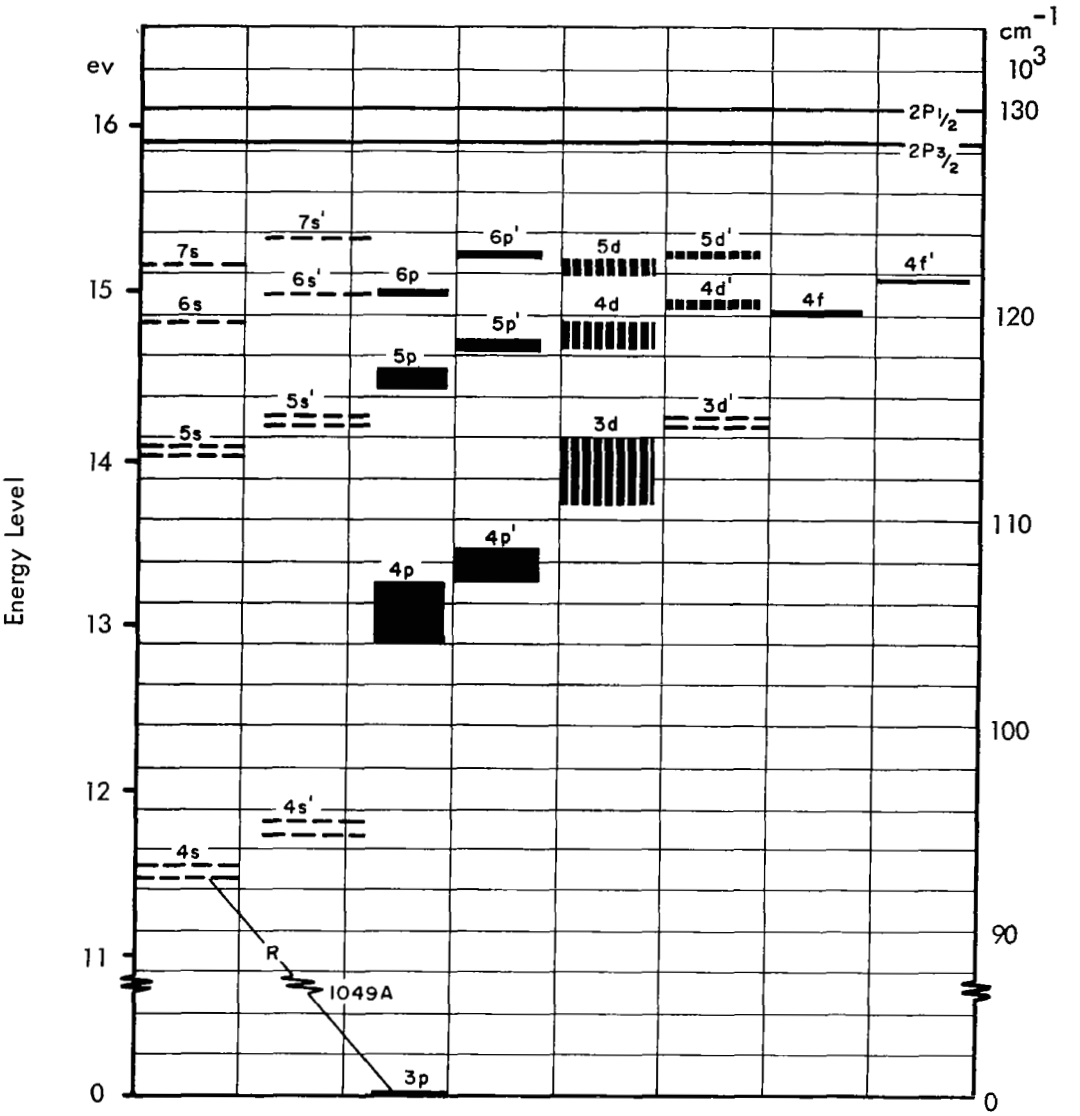

FIGURE 1.4 - ENERGY LEVEL DIAGRAM OF ARGON I

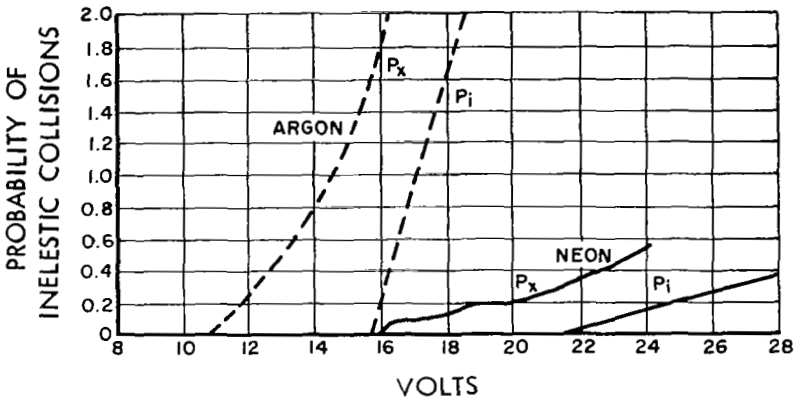

FIGURE 1.5 - PROBABILITY OF EXCITATION AND IONIZATION IN ARGON AND NEON

the atomic number density of the arc gas and its electron collision cross section. As the vortex flow maintains a cool high density gas very close to the arc axis, electron mean free path will decrease very rapidly as an electron moves out from the arc core. The vortex arc can then be visualized as a core with high energy electrons leaving the electron emission zone on the cathode and moving along the axis of the radiating arc to very near the anode surface, where an abrupt increase in gas number density reduces the mean free path. Around this core is a thin cylindrical shell of recombining slow electrons, ions, and neutral atoms limited to relatively low energy by the small mean free path, or in other words, high atomic number density, maintained by the vortex gas flow.

A provisional understanding of the radiation processes resulting in the argon spectrum of Figure 1.2 follows a study of the energy level diagram of Argon I. Most static short arcs with the inert gases produce radiation which peaks spectrally with the electronic transitions just above the resonance level, that is for argon, 4p - 4s transitions. The vortex arc with its higher voltage and related radial constriction tends to have strong excitation at higher levels up to the effective ionization potential. 5p - 4s and higher transitions produce larger amounts of radiation. Since 4p - 4s transitions emit photons with wavelengths peaking around 0.8μ, and 5p - 4s around 0.42μ, and 6p - 4s near 0.36μ, the observed spectrum seems reasonable. With narrow bandwidth study, this simple explanation fails since the actual spectrum is composed of an intense continuum with two broad peaks, one near 0.4μ and the other near 0.8μ. Added to these continuum peaks are the broadened line radiations which position the apparent peaks.

Two methods of improving the simulation of solar radiation are therefore evident. One method would inject other elements or compounds into the plasma of a convenient gas such as argon for the purpose of adding broadened line radiation in spectral regions requiring extra radiant power. The other method would basically ignore line radiations and work toward a plasma gas which would have a continuum peaking near 0.47μ, the peak of the Johnson spectrum. Both approaches were investigated in this project.

2.0 EXPERIMENTAL EQUIPMENT

2.1 Vortex Stabilized Arc

The arc used in most of the experimental work is sketched in Figure 2.1, Water Cooled Tube Vortex Arc with Powder Injection. This vortex arc has a number of unusual features. Water is used to cool the electrodes and also flows between the

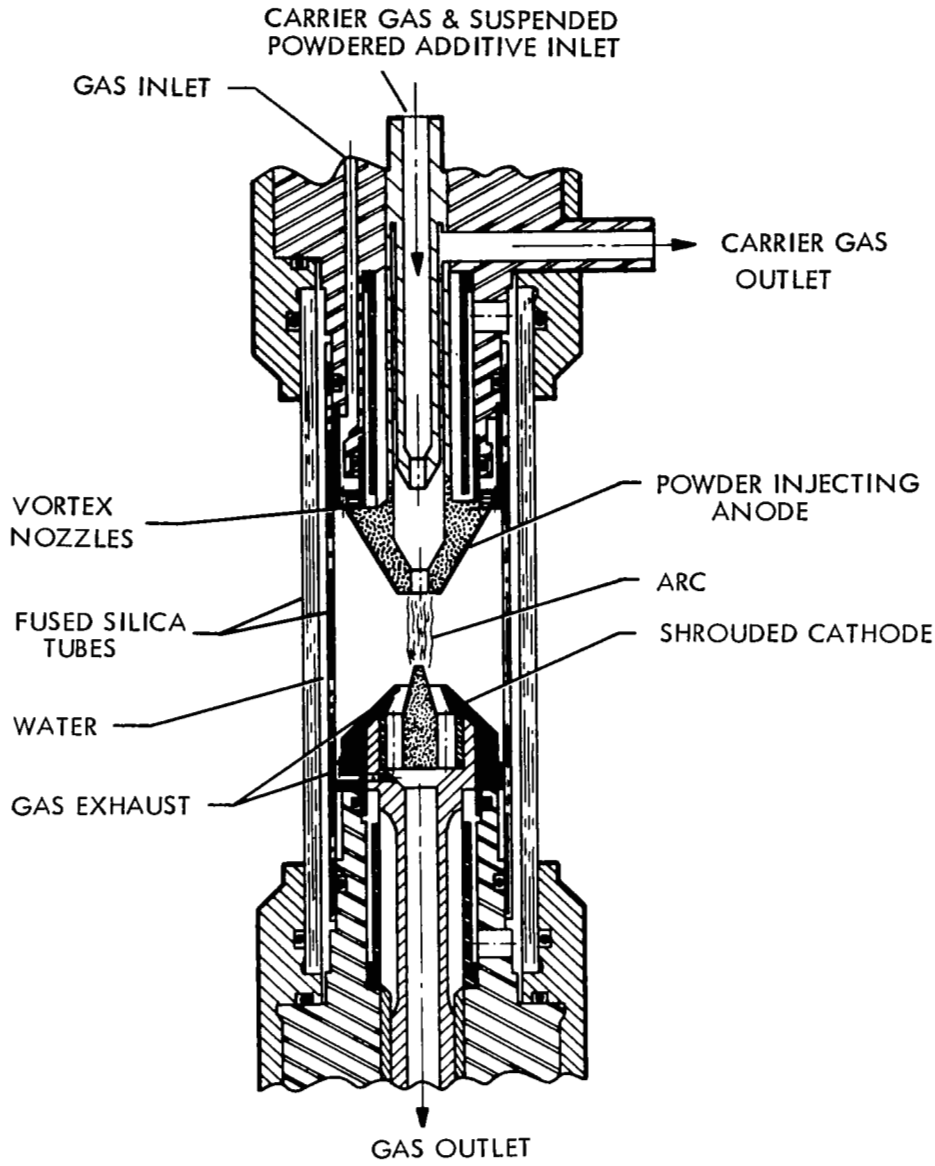

FIGURE 2.1 - WATER COOLED TUBE VORTEX ARC WITH POWDER INJECTION

two fused silica tubes. The outer fused silica tube is thus kept at quite low temperatures even with very high radiation fluxes. For example, this unit has operated with 35 kw input power to the arc and certainly more than 10 kw of radiant power transmitted through the tubing. The drawing is full size with the outside diameter of the outer tube being 35 mm. The gas forming the vortex and stabilizing the arc enters the arc chamber through vortex nozzles arranged in a ring around the anode electrode. The spinning gas exhausts through an annular opening around the pointed cathode. A small amount of gas is also exhausted around the large diameter of the cathode electrode. It was also possible to exhaust some of the arc gas through the central orifice in the anode. This vortex arc can be operated without powdered additives and considerable data were taken with this mode of operation in order to determine the plasma composition of the argon arc.

To study the radiation changes caused by additives, a carrier gas identical to the majority arc gas, usually argon, was introduced to the central cavity in the anode through the nozzle sketched. A substantial improvement was made on methods of injecting additive powders into an arc. Injection of the powders with carrier gas directly into the arc (i.e. on arc centerline) causes instability due to the cold carrier gas. This instability problem was eliminated with the electrode and injection device shown in Figure 2.1. This device operates in the following manner; the suspended powder and carrier gas enter the powder injecting anode, and are accelerated to a high velocity by the nozzle section. The high velocity imparted to the powder particles at the nozzle is sufficient to carry them through the anode orifice and into the arc core, while the carrier gas is bled off and returned to the low pressure side of the argon circulation pump. The cold carrier gas is not allowed to pass through the orifice and disturb the arc. The experimental work was conducted with the carrier gas outlet flow set slightly higher than the carrier gas inlet flow. This means that gas flow to make up the difference must flow out of the arc chamber through the anode orifice against the incoming powder. In spite of this counterflow the momentum of the powder carries it into the arc.

2.2 Gas Recirculating and Powder Injection System

The vortex arc unit was operated with a complete gas recirculating system. The powdered additives were introduced to the carrier gas in a motor driven cylindrical hopper. The general setup is shown by Figure 2.2.1, Schematic of Argon Recirculating Vortex Arc System. The experimental arcs were usually run at 150 to 200 psi, or considering the small pressure drop in the recirculating system, pressures of 10 to 14 atmospheres in the arc plasma.

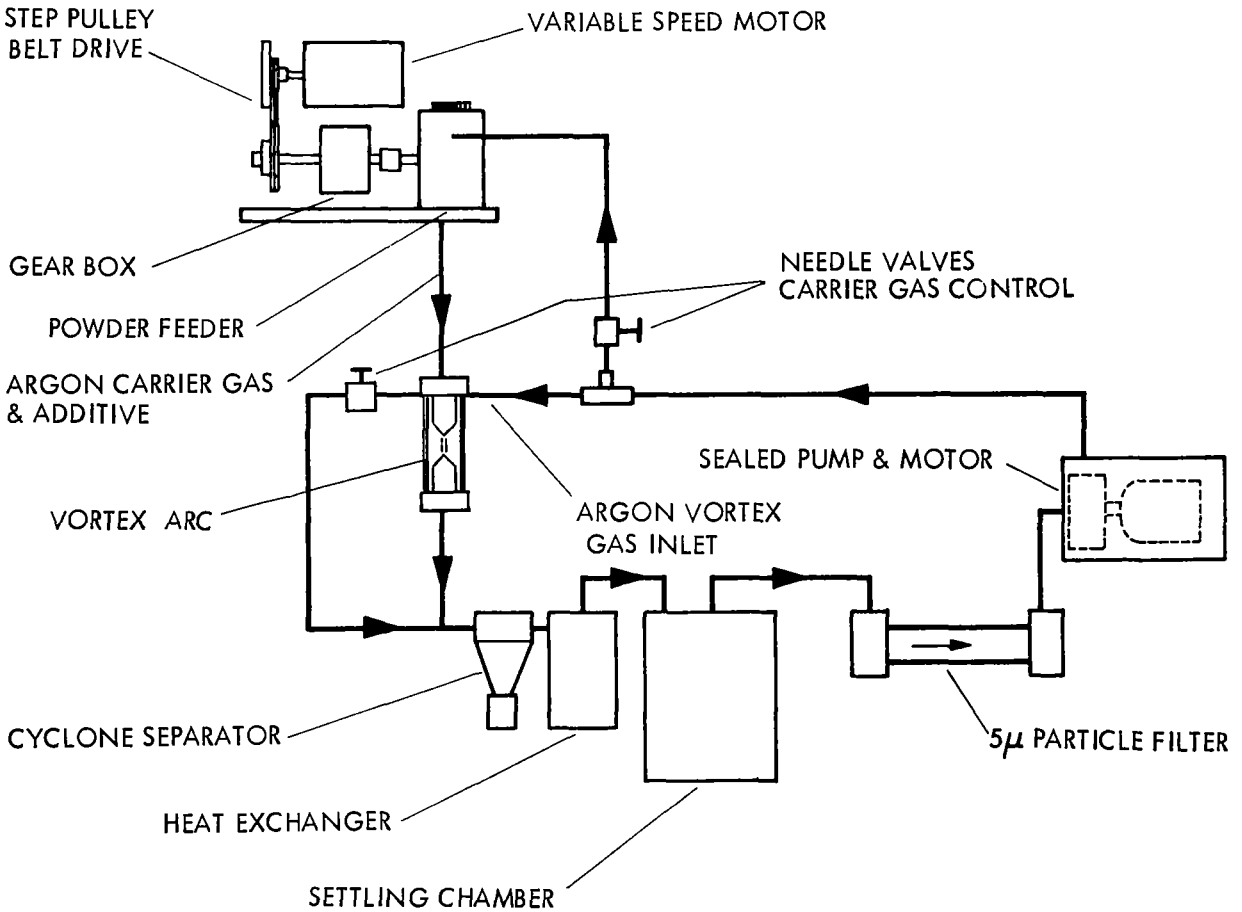

FIGURE 2.2.1 - SCHEMATIC OF ARGON RECIRCULATING VORTEX ARC SYSTEM

The powder feed device consists of a sealed housing with an internal rotating drum into which the powder to be fed is placed. See Figure 2.2.2. Small quantities of powder fill the tangential holes drilled thru the drum wall and are carried around to the outlet port, where the carrier gas, which is fed to the inside of the drum, forces the powder out of the hole and carries it entrained to the arc chamber. The device has two advantages:

The tangential metering holes are positively emptied by the carrier gas flowing thru them.

The powder is prevented from packing and subsequent clogging by the tumbling action of the rotating drum.

The hot exhaust gas and powder leaving the cathode are exhausted into a cyclone separator which removes the bulk of the entrained powder. The gas then moves to a heat exchanger (gas to water) and on through a settling chamber and fine filter to the sealed recirculating pump.

Figure 2.2.3 is a photograph of the water cooled tube vortex arc showing the conical cyclone separator and cylindrical heat exchanger. The black cylinder to the left of the vortex arc chamber houses an achromatic lens used for forming an image on a distant screen. This image was useful in visual monitoring of arc conditions.

2.3 Microradiance Measurement Technique

The microradiance of arcs was studied with apparatus as shown in Figure 2.3. The arc column, standing vertically in the figure, is imaged by two spherical mirrors on the arc image plane. This plane is pierced by an 0.018 inch diameter orifice. A calibrated thermopile is carefully adjusted to receive all arc radiation passing through this orifice. The 46 cm focal length mirror is attached to a long arm which is rotated by a fine screw thread. The position of this arm is monitored by a 10 turn potentiometer whose output is fed to the x axis of an x-y recorder, thus giving the radial position. As the mirror rotates, the image sweeps the 0.018 orifice, and by recording thermopile voltage on the y axis, a profile is obtained. The axial position of the detector and orifice are transferred from station to station along the axis of the arc (at arc image plane) by a micrometer lead screw. Radial profiles are obtained at each station and then reduced to microradiance contours.

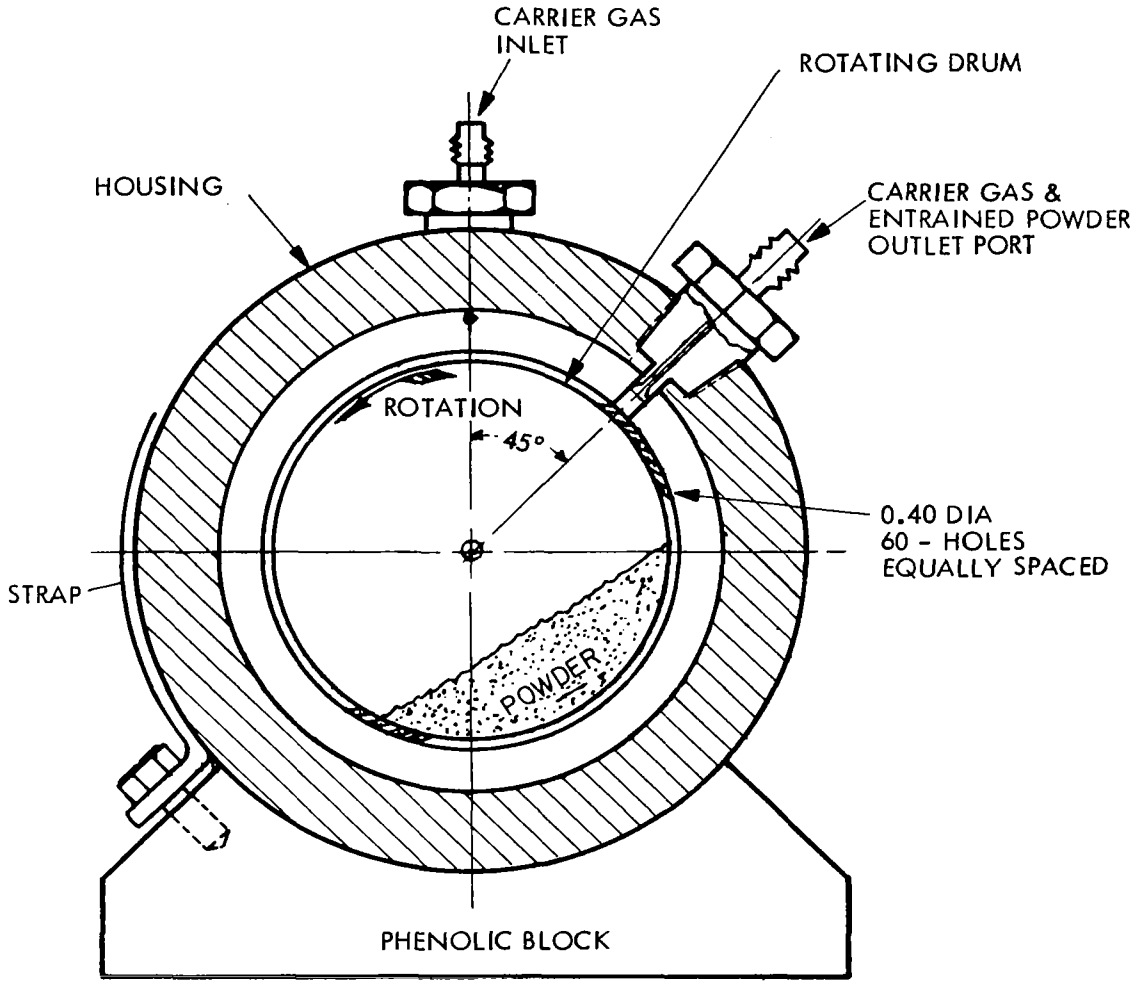

FIGURE 2.2.2 - POWDER FEED DRUM

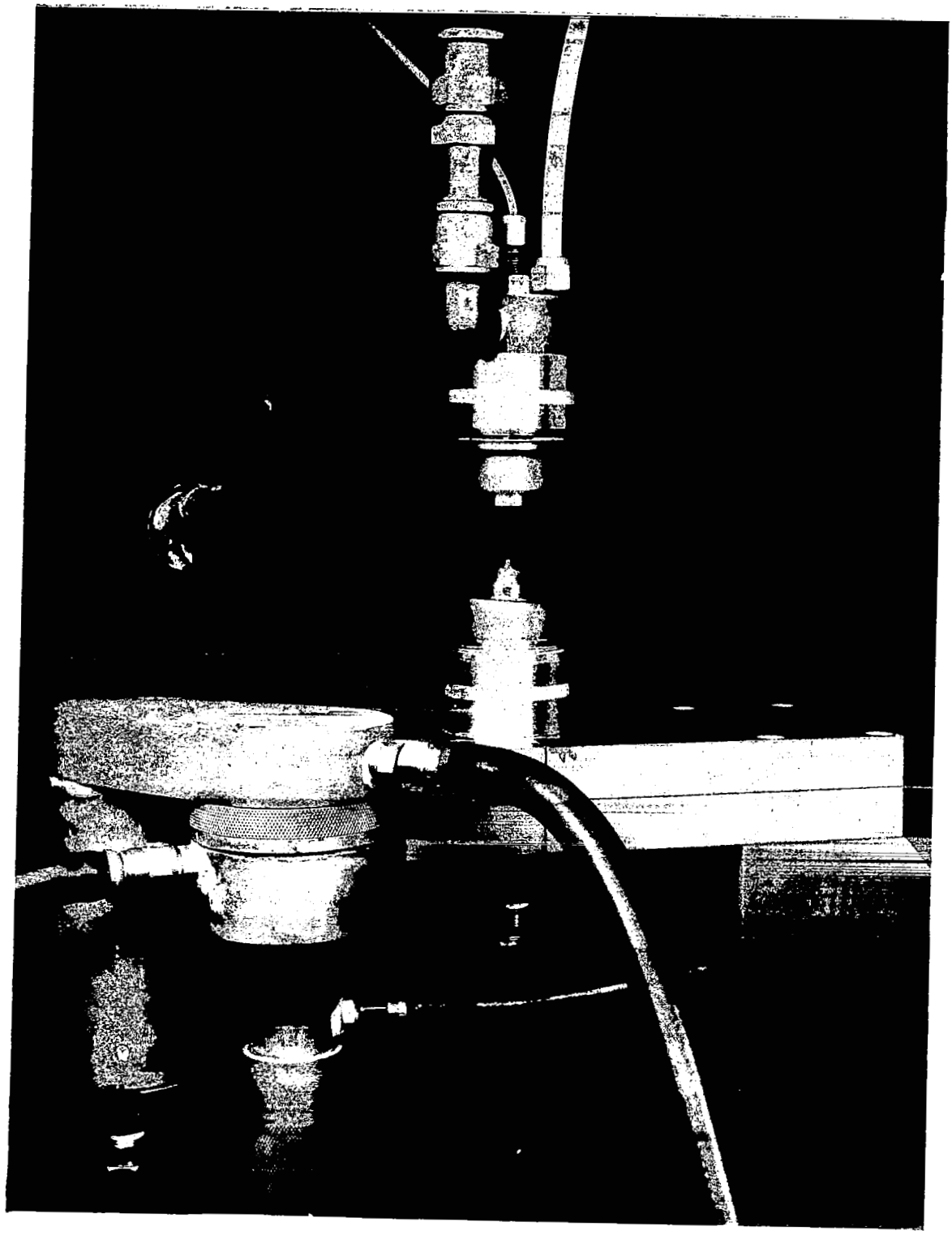

FIGURE 2.2.3 WATER COOLED TUBE VORTEX ARC

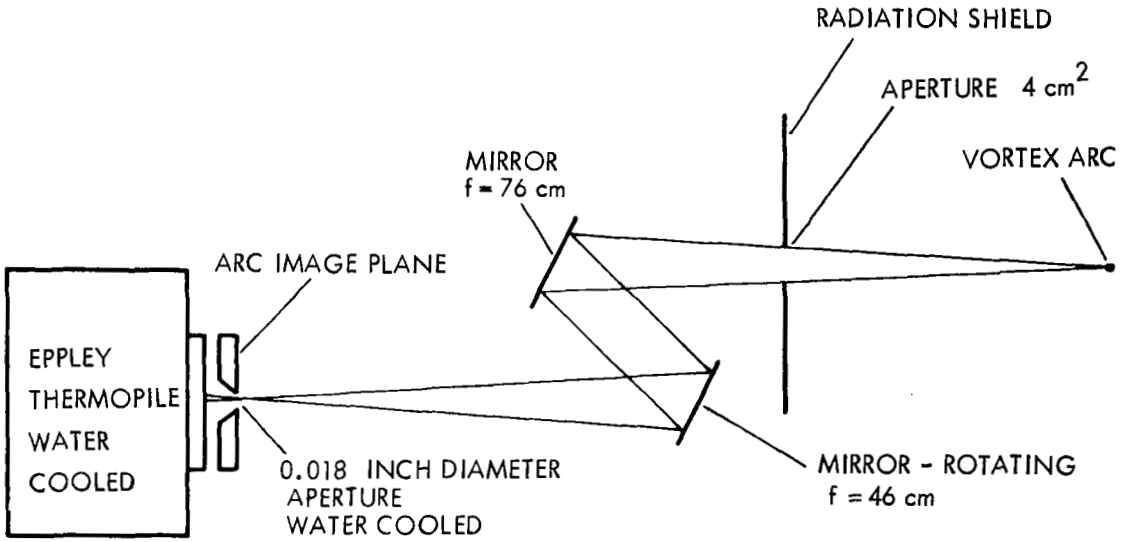

FIGURE 2.3 - MICRORADIANCE OPTICS

2.4 Spectroscopic and Radiometric Instrumentation

A Bausch & Lomb 250 mm monochromator with a 600 lines mm^{-1} grating was used to study the arc spectrum over the wavelengths 0.2μ to 1.4μ. A schematic sketch showing the optical system is shown in Figure 2.4.1. The two mirror arc imaging system is identical to that described under Microradiance, Section 2.3. The 46 cm focal length mirror is mounted on a long arm which can be rotated slowly by a fine screw thread. The position of this arm may be used as the x axis input of an x-y recorder. The rotation of the mirror moves the arc image over the entrance slit of the monochromator thus allowing a scan of the radiation originating in different portions of the arc at any selected wavelength. In the more usual application of the monochromator the wavelength position is monitored by potentiometer to supply the x axis to an x-y recorder. The detector output is recorded on the y axis.

The detectors used were lead sulfide (Ektron), S-1 photomultiplier (RCA 7102) and S-5 photomultiplier (RCA 1P28). The lead sulfide was used in a simple D.C. bridge circuit for wavelengths between 0.3μ and 1.4μ. Very little zero drift was experienced while observing wavelengths between 0.4μ and 1.4μ and continuous recording of output voltage was possible. For wavelengths between 0.3μ and 0.4μ a significant zero drift occurred. This was minimized by manual chopping and a slow point by point plot of radiation output. The spectral response of PbS approaches a constant quantum efficiency making it a very useful detector in study of spectral distributions.

The S-1 photomultiplier was used in the wavelength range from 0.6μ to 1.0μ and the S-5 from 0.2μ to 0.6μ. The sharp spectral peaking of the photoemission phenomenon limits the usefulness of these detectors in study of wide band spectral distributions; they are, however, extremely valuable for narrow band, low spectral power measurements.

A special fluorescent detector was used for work between 0.2μ and 0.34μ. A thick white layer of sodium salicylate was painted on a Corning 3-75 filter and then mounted immediately before a 1P28 (S-5) photomultiplier. Figure 2.4.2 shows recorder outputs for the 3-75 filter only and 3-75 with sodium salicylate combination. Sodium salicylate has a constant quantum efficiency in fluorescence over a wide spectral range, 0.09μ to 0.34μ (Ref. 2.4.1). The emission spectrum of sodium salicylate peaks at about 0.41μ and extends from 0.36μ (10%) to 0.48μ (10%) (Ref. 2.4.2). The 3-75 cutoff filter reduces transmission of all wavelengths shorter than 0.35μ to a small recorder output. This output is due to both transmission and scatter but is essentially flat. When sodium salicylate is painted on the first surface

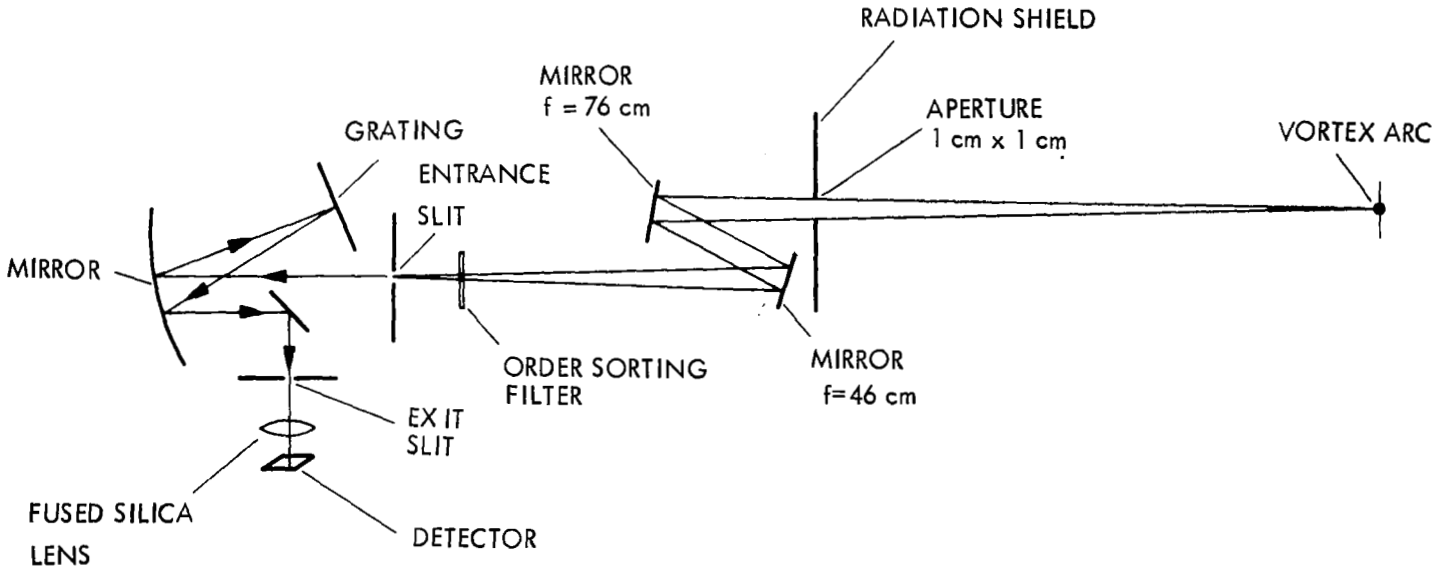

FIGURE 2.4.1 - MONOCHROMATOR OPTICS

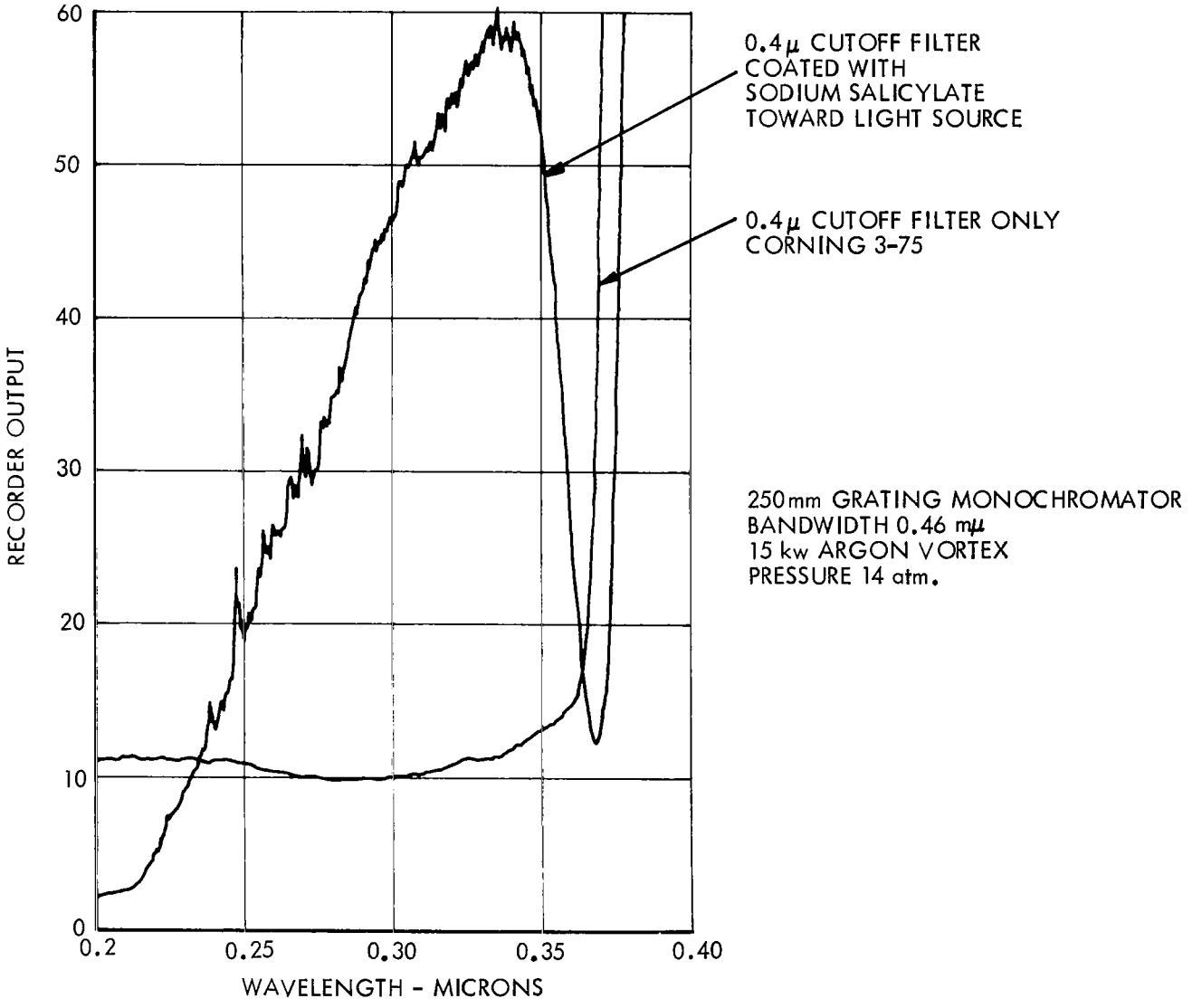

FIGURE 2.4.2 - SODIUM SALICYLATE + 1P28 RESPONSE

of the filter, the wavelengths transmitted by the monochromator as it scans from 0.2μ to 0.34μ appear as longer wavelengths between 0.36μ and 0.48μ with a constant quantum efficiency. These wavelengths pass the filter and cause a response in the S-5 (1P28) detector. The sodium salicylate detector and the lead sulfide give a complete coverage of wavelengths between 0.2μ and 1.4μ with detectors of nearly constant quantum efficiency. The only other factors affecting the monochromator system spectral response are atmospheric transmission, mirror reflectivity and monochromator transmission itself.

The problem of scattered light within a monochromator must be considered, particularly in the ultraviolet. Figure 2.4.3 traces the recorder output with and without a glass slide before a 1P28 detector. These curves indicate that scattered light is not important when observing a 15 kw argon plasma.

Monochromator systems are often calibrated by use of a standard tungsten ribbon filament. The spectral radiance of such a source is typically 250 mμ - 1.3×10^{-2}, 350 mμ - 1.53, 450 mμ - 13.5; 550 mμ - 44.1; and 1000 mμ - 152 in microwatts per steradian-millimicron-mm^2. The use of such a sharply sloping distribution for the determination of the spectral distribution of radiation from a high powered arc which must have very large spectral radiances in the blue and ultraviolet is difficult. As an alternate approach we divided the spectrum into three intervals, 0.2μ to 0.5μ, 0.5μ to 0.9μ and 0.9μ to 2.6μ. The dividing wavelengths were selected to avoid argon line emissions and to use available short wave cutoff filters, Corning 3-70 and 7-56. The transmission of these filters can be checked by use of the radiation of a vortex source or a tungsten filament and the monochromator. They can also be used to filter out higher orders. The radiant power of the source may then be measured at any desired angle without optics other than water-cooled apertures designed to prevent unwanted infrared or reflected radiation from entering a calibrated thermopile placed at a known distance. Similar measurements taken with the 3-70 filter and 7-56 filter before the thermopile yield data which can be reduced to radiant power within the wide intervals selected. Unfortunately, the cutoff of absorption filters is not precise and the radiant power within these three spectral intervals cannot be considered accurate to better than $\pm$10%.

The monochromator was calibrated by observation of a tungsten filament and the transmission computed as an average for each of the three wide intervals. The transmissions observed were as would be expected within the intervals when grating and mirror reflectivity, and ozone and quartz transmission were considered. However, the average transmission for the 0.2μ to 0.5μ interval was not consistent

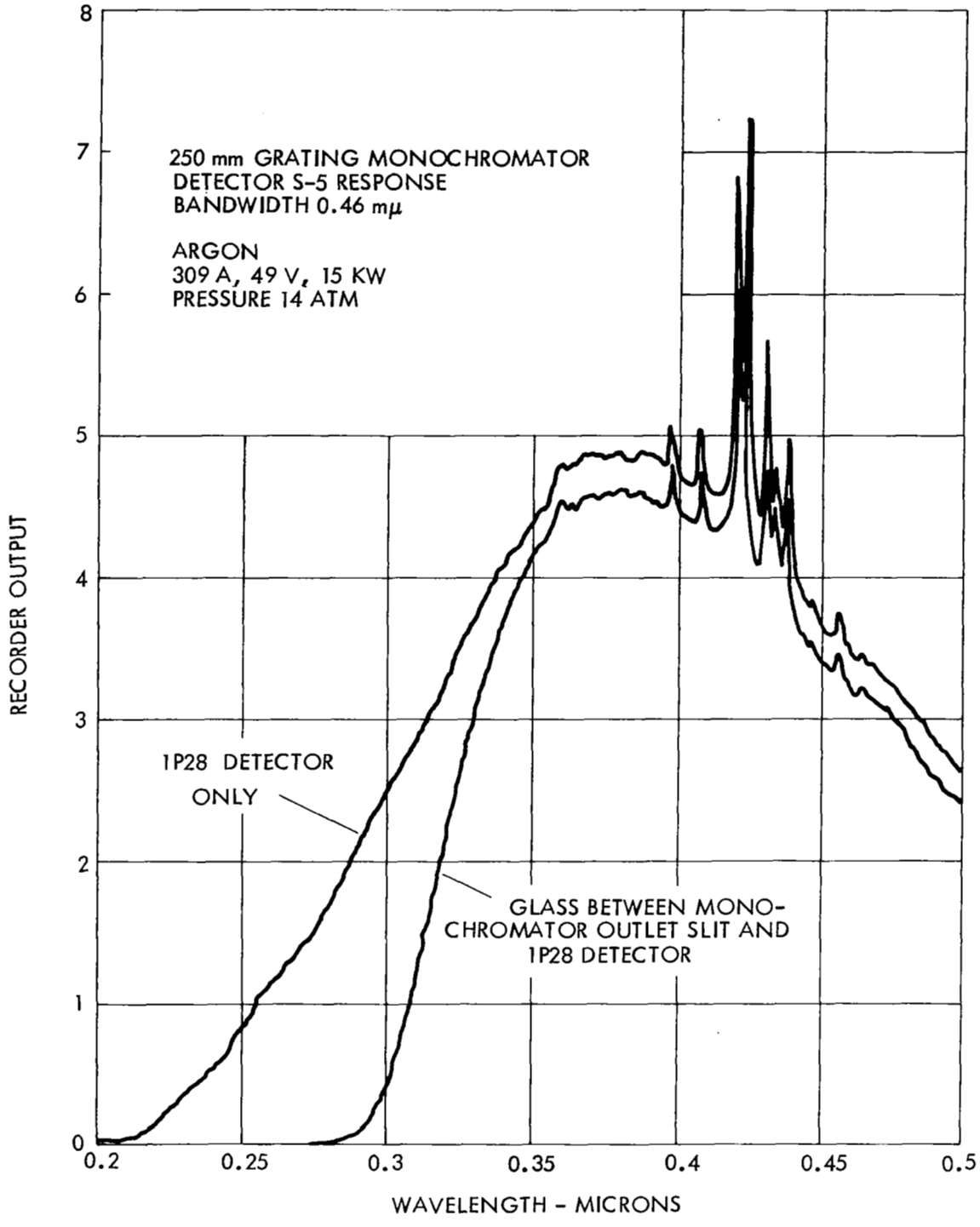

FIGURE 2.4.3 - ARGON INTERMEDIATE ULTRAVIOLET

with the transmissions for intervals 0.5μ to 0.9μ and 0.9μ and 2.6μ. It is believed that while instrument scatter is not significant for high spectral powers, it may well be important and difficult to properly assess when viewing a tungsten ribbon filament. Partially corrected spectral distribution for an unknown source can be plotted from the basic monochromator data. Then adjustment in spectral power per unit wavelength can be made so that the integrated radiant power in intervals 0.2μ to 0.5μ and 0.5μ to 0.9μ equals that computed from the thermopile data. The spectral distributions so obtained should be accurate within 10% if fairly wide bandwidths, 50mμ to 100mμ, are used.

3.0 ARGON PLASMA STUDIES

The work with additives accomplished during the course of the project used argon as the majority gas. The additive's atomic number density was in almost all cases less than 10% of the argon density. It was important therefore to determine as closely as possible the argon plasma composition before attempting to understand the spectral output observed when a given additive was present. Hydrogen as an additive was used in a somewhat different sense, since its Stark broadening has been carefully studied by others and its use in small percentages as a diagnostic tool is recorded in the literature (Ref. 3.0).

3.1 Temperature Determination

Four methods of determining plasma temperatures were studied by obtaining experimental data and evaluating. They were based on slope of the continuum intensity in the ultraviolet, the absolute determination of continuum emissivity in the visible, inference from hydrogen's Balmer α Stark broadening measurements and the ratio of Balmer α radiation to the nearby continuum.

3.1.1 Ultraviolet Continuum Slope

The Kramers-Unsold theory develops a theoretical expression for the sum of free-free and electron-ion recombination radiation. The theory leads to a continuum which is frequency independent up to a cutoff frequency where the assumption of sufficiently dense atomic energy levels is not feasible. With argon a free electron with zero speed which radiatively recombines to the 4s level can not radiate a photon of wavelength shorter than 0.295μ. This is true since, while microfield effects may lower the ionization potential normally at 127, 110 cm^{-1}, the resulting radiation of a zero speed electron recombining at the 4s level (93,144 cm^{-1}) can only be less energetic. As discussed by Olsen (Ref. 3.1.1) and Mies (Ref. 1.5), radiation intensity over the range of $h\nu$ where no new quantum levels make a

contribution will vary as exp (-h ν/kT). This condition is met in the argon ultraviolet at wavelengths shorter than 0.3μ (.295μ). Several spectral measurements were taken to determine relative spectral intensities in the intermediate ultraviolet. The experimental vortex arc of Figure 2.1 was used with argon at 14 atm. Considering that the observations were taken in air and the obvious presence of ozone, the wavelength interval between 0.28μ and 0.30μ was selected for measurement. The monochromator in use has a grating with a nominal 0.30μ blaze and transmission at 0.28μ is slightly better than at .30μ. In contrast the fused silica, water and aluminum mirrors in the optical path from the arc plasma to the detector have a slightly better transmission at 0.30μ than at 0.28μ. It was therefore estimated that the actual transmission at these wavelengths is essentially constant.

The problem of known detector response then remains. The calibration of a detector or monochromator-detector system against a standard tungsten filament is apparently a recognized technique. The calibrated response is then used to determine spectral intensities in the 0.25μ vicinity. This amounts, however, to comparing intensities differing by many orders of magnitude and expecting to achieve 5 to 10% accuracy. The procedure does not seem likely to result in the required accuracy.

Instead, recognizing the sharply peaked response of photoemission (photomultiplier) devices, the constant quantum efficiency of sodium salicylate was exploited. The monochromator setup of Figure 2.4.1 was used. The exit slit radiation was passed through a relatively thick white layer of sodium salicylate coated on a Corning 3-75 filter with short wave cutoff near 0.40μ. This technique is described in section 2.4. Figure 3.1.1 is a trace of recordings obtained at three power levels. The intensity curve from 0.22μ to 0.34μ from sodium salicylate fluorescence is quite distinct from the direct transmission response beginning at 0.37μ. These runs show some tungsten lines and at these power levels ozone absorption is known to modify the transmission through the monochromator system. Also, a small correction for stray light should be made. The ozone concentration is unknown, so the wavelengths chosen for temperature determination were 0.28μ and 0.30μ ($\nu_1 = 1.07 \times 10^{15}$ and $\nu_2 = 1.00 \times 10^{15}$) using the relation

$$I_{\nu_2}/I_{\nu_1} = \exp (h\nu_1 - h\nu_2)/kT \qquad (3.1.1)$$

The 16.4 kw argon plasma temperature by this criteria is 13,300°K, the 13 kw is 12,900°K and 10 kw arc is 11,900. The accuracy of the technique is limited as a 10% error in experimental determination of the ratio of I_{ν_2}/I_{ν_1} means a change of 1,000°K in temperature.

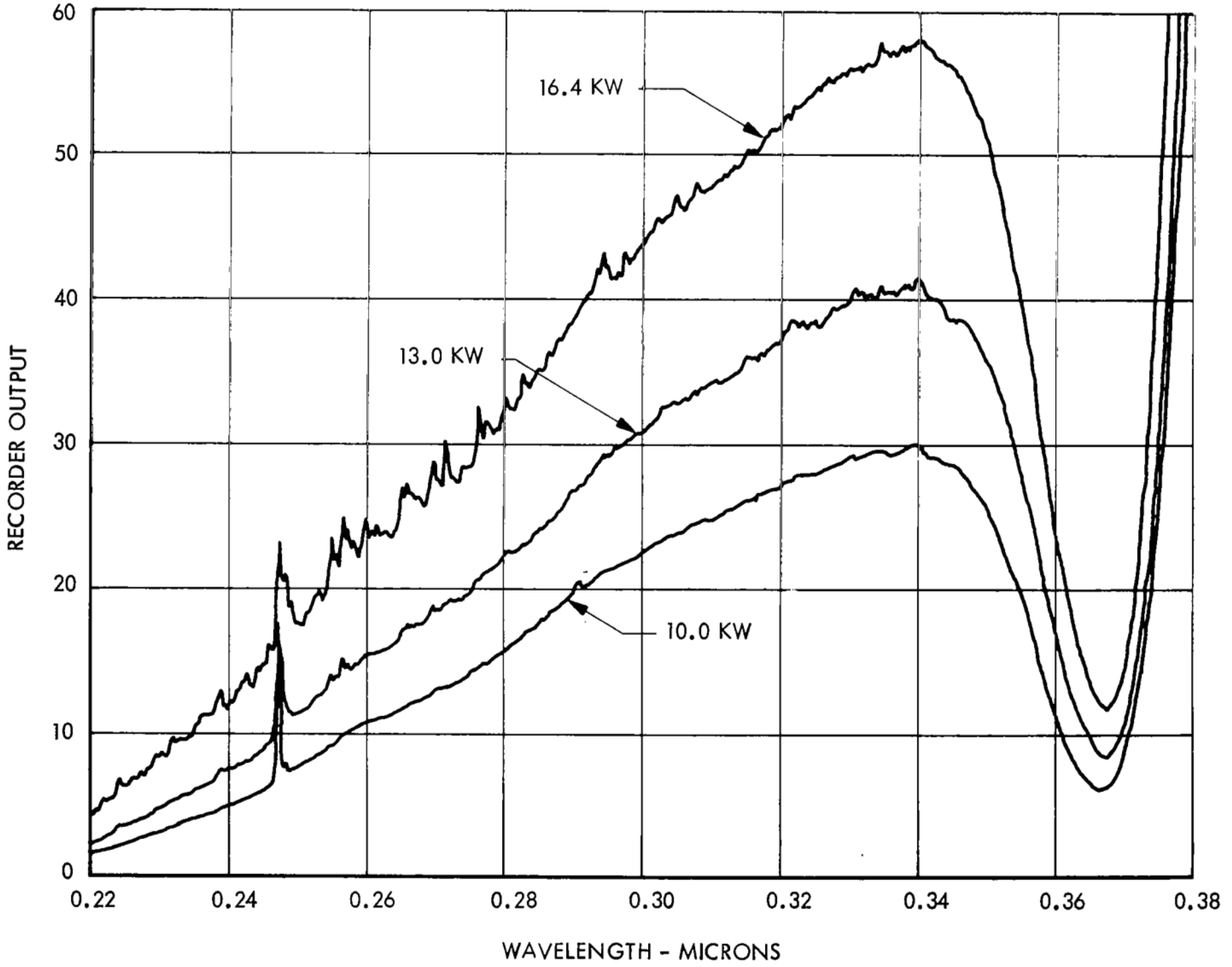

FIGURE 3.1.1 - SPECTRAL DISTRIBUTION USING SODIUM SALICYLATE

3.1.2 Continuum Emissivity

The continuum emissivity, defined as radiant power per unit plasma volume and unit solid angle, can be used for determination of temperature. The Kramers-Unsold relation gives the absolute emission coefficient as

$$Sc(T) = 5.41 \times 10^{-46} \bar{g} Z^2 \frac{n_i n_e}{T^{0.5}} \qquad (3.1.2)$$

where Sc(T) is in watts cm^{-3} str^{-1} per unit frequency. Z^2 in the plasmas being studied equals 1 and the ion density, $n_i = n_e$, the electron number density. T is the plasma temperature in degrees Kelvin and $\bar{g}$ is a quantum mechanical correction factor found experimentally to be 2.3. It is evident in the actual study of spectral distributions however, that g is frequency dependent.

Figure 3.1.2 Spectral Power Comparison: Sun vs Argon VSRS Ref. 3.1.2, was determined by correcting spectral distributions obtained by grating monochromator by data indicated in Figure 3.1.3 from observation of the output radiation by a calibrated thermopile and short wave cutoff filters. This technique is discussed in Section 2.4. The spectral radiant power between 0.45μ and 0.55μ (67 w str^{-1}) was used for computation of temperature by Equation 3.1.2. The wavelength band selected avoids the line radiation peaks as well as the low radiance zone around 0.7μ. Such an "average" position should reduce the error in using $\bar{g}$ as a constant. The frequency difference between 0.45μ and 0.55μ is 1.212×10^{14} cps and the arc volume is approximately 0.096 cm^3 at a pressure of 14.2 atmospheres. Equation 3.1.2 then reduces to

$$\frac{n_e^2}{T^{0.5}} = 4.63 \times 10^{33} \qquad (3.1.3)$$

Temperature and electron density are closely related at a given plasma pressure. As stated by Olsen (Ref. 3.1.3) "under the assumption of local temperature equilibrium, quasi-neutrality, and the application of Dalton's Law, the system of equations to be solved may be written with all of the corrections required for high density plasmas." Olsen has computed a particle number density table for argon at 1.1 atmosphere pressure. It is believed that these data can be converted to 14 atmospheres by a proportional increase in density for a given temperature. The errors introduced at temperatures under say 15,000°K should be small. Solving Equation 3.1.3 by these proportionally revised tables gives a temperature 12,000°K and $n_e = 9 \times 10^{17}$ cm^{-3}. This technique appears to be quite accurate as

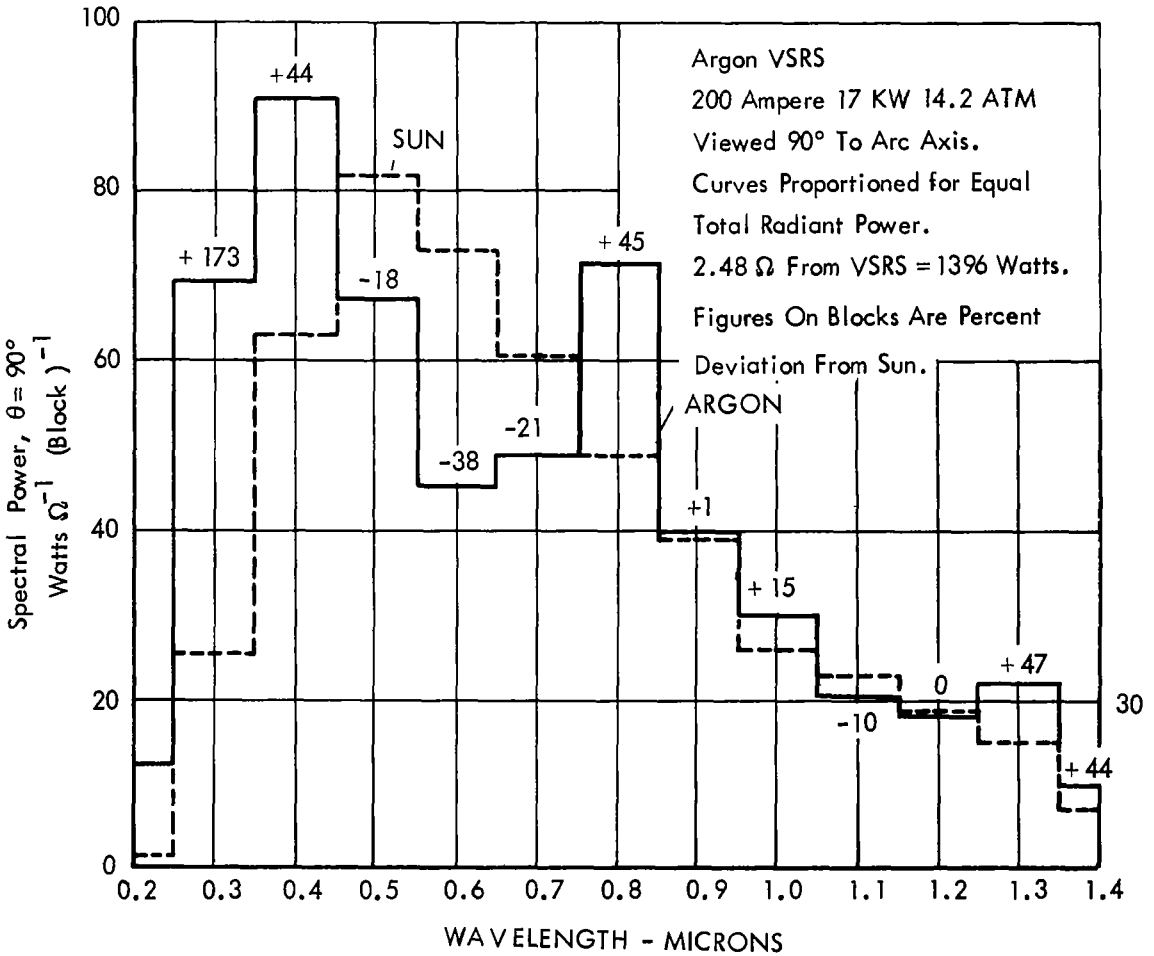

FIGURE 3.1.2 - SPECTRAL POWER COMPARISON: SUN VS ARGON VSRS

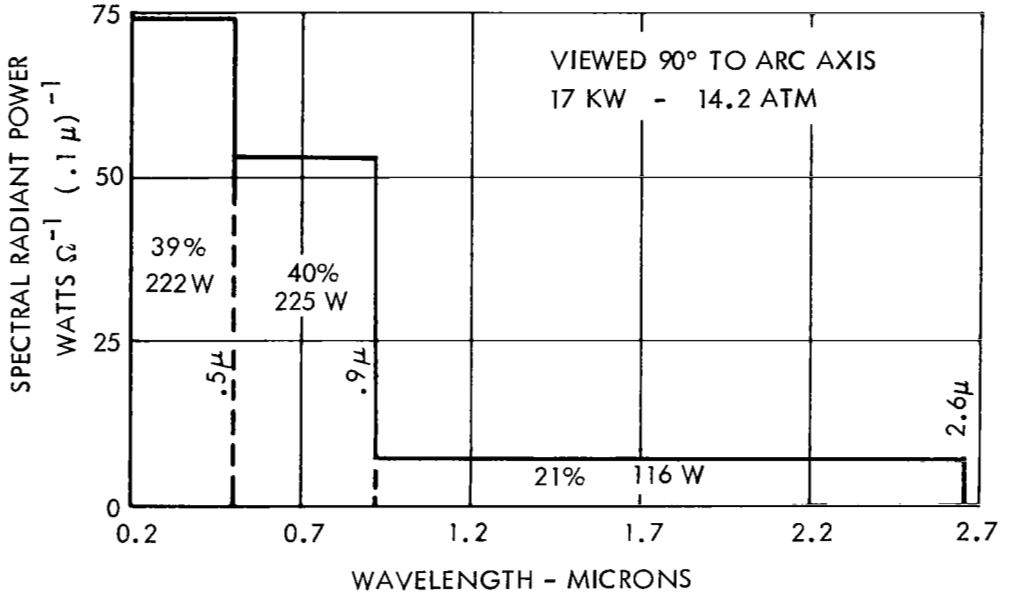

FIGURE 3.1.3 - SPECTRAL RADIANT POWER 200 A. ARGON VSRS

a 10% error in determining the spectral radiance and radiating volume makes less than a 100°K error in temperature. The difficulty here is in knowing the correct value for $\bar{g}$ and perhaps Z^2.

The change in argon plasma composition with temperature will be of concern later on in this paper. The following table has been prepared for reference:

Table 3.1 Particle Number Densities cm^{-3}
Argon p = 14 atm

T°K	neutral n_n		$n_i = n_e$		doubly ionized	
	n_1		n_2		n_3	
10,000	9.86	18	2.02	17	1.28	9
10,500	9.16	18	3.13	17	6.48	9
11,000	8.42	18	4.63	17	2.85	10
11,500	7.63	18	6.58	17	1.10	11
12,000	6.79	18	8.95	17	3.82	11
12,500	5.91	18	1.17	18	1.21	12
13,000	5.00	18	1.47	18	3.48	12

n_1, n_2 and n_3 are number densities using subscripts consistent with spectroscopic notation. For the purpose of this paper n_n for neutral, n_i and n_e for first ion and electron densities are used on occasion. The tabulated values are to be multiplied by ten to the power indicated by the integer following the decimal number.

3.1.3 Hydrogen Stark Broadening

The addition of a small percentage of hydrogen to the argon gas being recirculated in the vortex makes it possible to measure Stark broadening of a suitable hydrogen line and from this to determine electron and ion number densities. Using this information, temperature may be inferred since the plasma pressure is fairly well known. Figure 3.1.4, Spectral Distribution: Vortex Arc Near Hα, was observed while operating a vortex arc with a mixture of 98% argon and 2% hydrogen at 17.1 kw and a pressure of 14 atmospheres. The Balmer α line, Hα, is quite distinct and well broadened as compared to most argon lines. The estimated continuum line was constructed from the tangent point at the short wavelength side and sloped slightly upward toward the longer wavelength. There is some argon line contribution in the longer

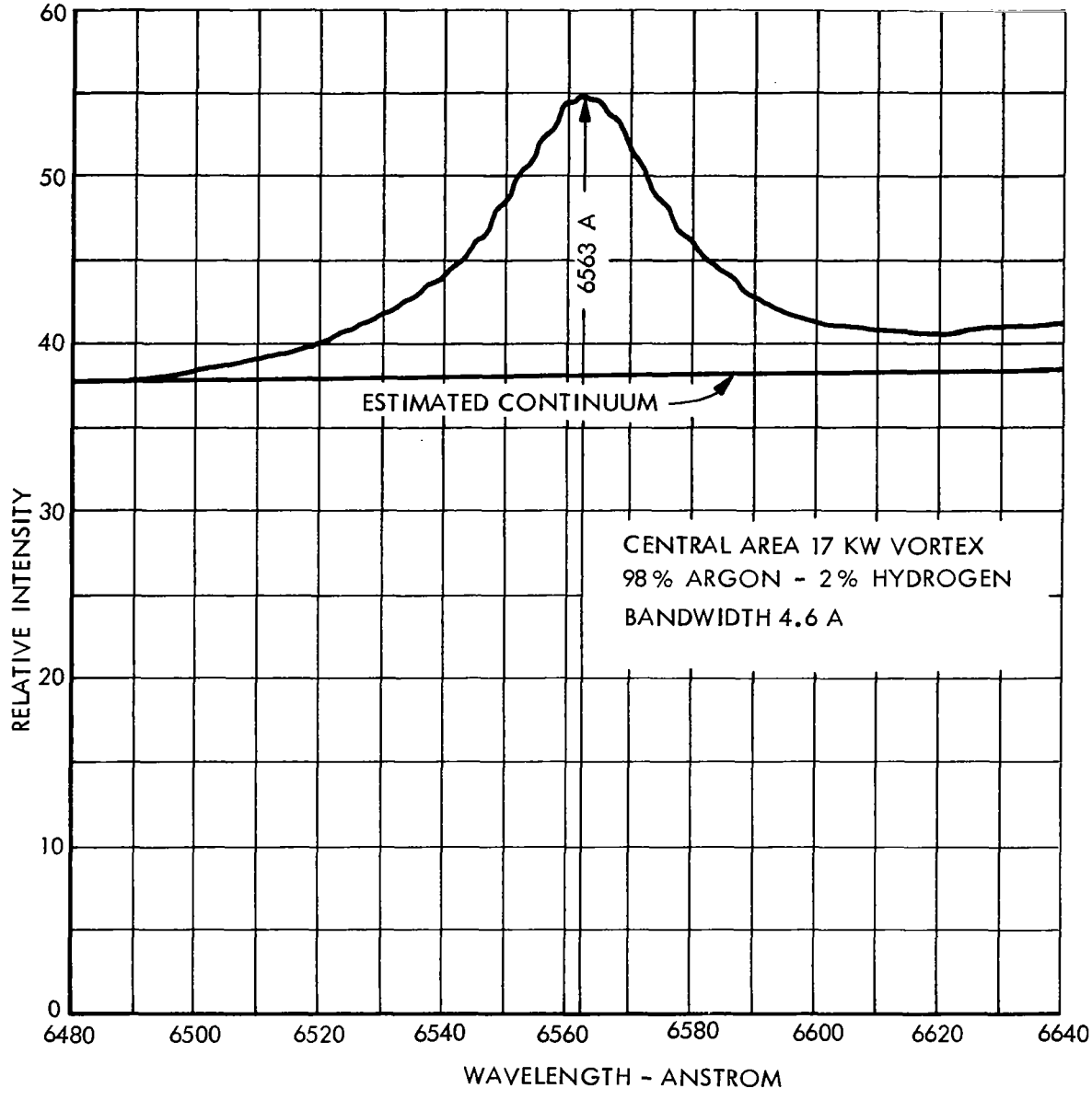

FIGURE 3.1.4 - SPECTRAL DISTRIBUTION: VORTEX ARC NEAR Hα

wavelengths, particularly around 6605 angstroms.

Figure 3.1.5, Hα Profiles: 2% H_2, 98% A Vortex Arc vs Theoretical, was constructed using the observed data. The theoretical curves were calculated using the technique and tables developed by Griem (Ref. 3.1.4). The observed curve falls between the Stark profiles for ion densities of 10^{18} and 5×10^{17} cm^{-3}. The actual ion density was taken as 7×10^{17} cm^{-3}. Using the plasma pressure of 14 atmospheres and evaluating by Table 3.1, the computed temperature is near 11,600°K.

3.1.4 Comparison of Results

The temperatures obtained by the three techniques discussed are tabled below:

Table 3.2 Vortex Plasma Temperatures

Technique	Input Power kw	Temperature °K
UV Continuum Slope	16.4	13,300
Continuum Emissivity	17.0	12,000
Hydrogen Stark Broadening	17.1	11,600

The agreement is only approximate, but considering the possible errors the actual plasma temperature is very likely within the range indicated. The addition of 2% hydrogen may easily result in a somewhat colder plasma due to power loss by dissociated hydrogen. The high value obtained by study of the ultraviolet slope may be erroneous since the accuracy of this technique is less than that of the others. The 12,000°K temperature seems most likely. This temperature indicates that the argon plasmas being studied are around 12% ionized when operating at 17 kw input power and 14 atmospheres pressure.

3.1.5 Ratio Balmer α to Continuum

The computation of temperature should be possible by determining the ratio of line radiant power to the underlying continuum. Examination of the high pressure argon spectrum shows a pronounced merging of broadened lines, which makes separation of continuum and line radiation difficult. The separation of line from line is also difficult. An additional source of error may arise from self-absorption, particularly with the infrared lines. The 2% hydrogen spectrum at Hα should not be subject to these difficulties. Referring to Figure 3.1.4, the

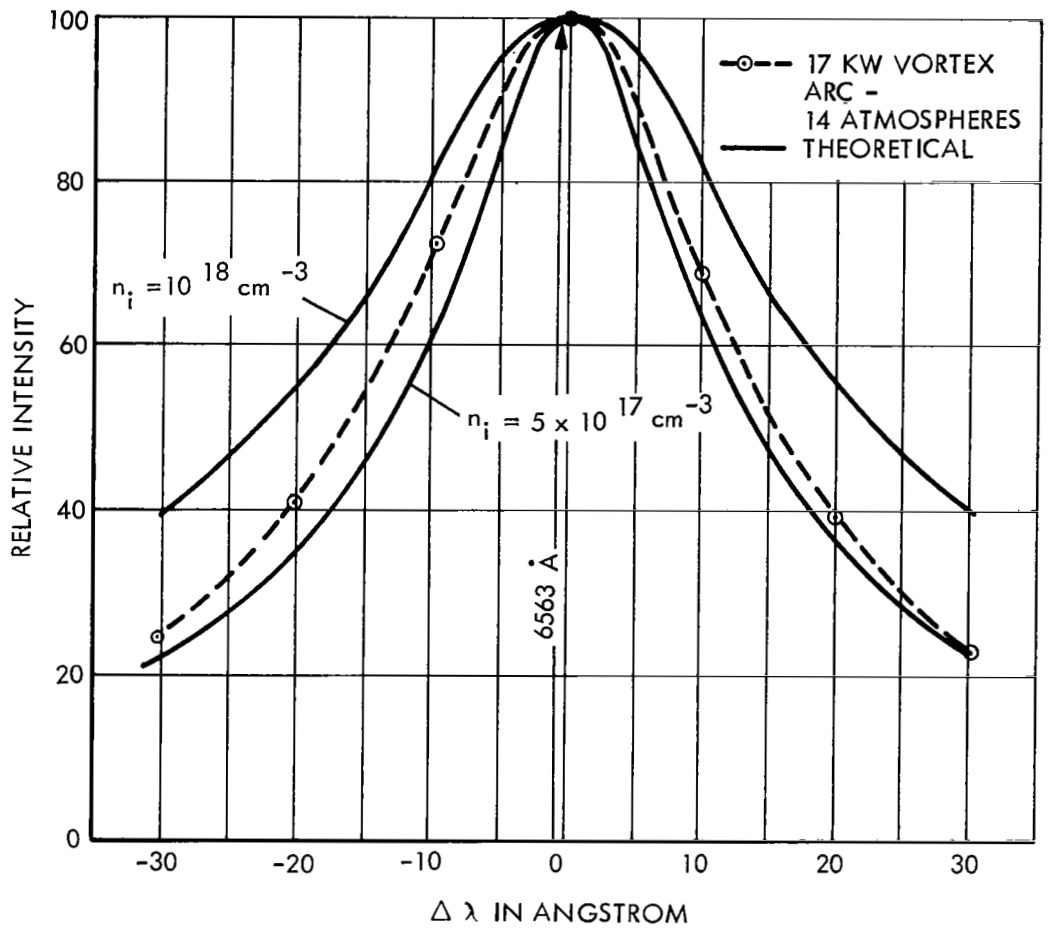

FIGURE 3.1.5 - Hα PROFILES: 2% H_2, 98% A VORTEX ARC VS THEORETICAL

wavelengths between 6480 A and 6563 A should have half of the $H\alpha$ line radiation at the existing temperature. This same temperature applied to the Kramers-Unsold equation (Equation 3.1.2) should yield the total continuum radiation between these two wavelengths. Integration of the area under the two curves, $H\alpha$ and continuum shows that $H\alpha$ radiation is 0.123 times the continuum.

The continuum by theory should be that occurring over the difference in frequency between $\lambda_1 = 6480$ A or $\nu_1 = 4.630 \times 10^{14}$ and $\lambda_2 = 6563$ A or 4.571×10^{14} which is 5.9×10^{12} cps. The absolute continuum emission coefficient should then be

$$S_c = 7.33 \times 10^{-33} \frac{n_e^2}{T^{0.5}} \text{ w cm}^{-3} \text{ str}^{-1} \qquad (3.1.4)$$

The emission coefficient for 1/2 of the $H\alpha$ line can be written as

$$S_{1/2\,H\alpha} = \frac{1}{2} A_{32} \quad 1.58 \times 10^{-24} \frac{n_1 \quad g_3}{\lambda_{32} \quad g_1} \exp\left(-\frac{E_3}{kT}\right) \qquad (3.1.5)$$

where n_1 is the atomic hydrogen ground state number density, g_1 and g_3 are statistical weights for ground state and third quantum level, E_3 is energy of third level with reference to ground state, λ_{32} is the Balmer α wavelength, and A_{32} the total transition probability. Evaluating Equation 3.1.5

$$S_{1/2\,H\alpha} = 4.77 \times 10^{-12} n_1 \exp\left(-\frac{12.1}{kT}\right) \text{ w cm}^{-3} \text{ str}^{-1} \qquad (3.1.6)$$

These equations may be solved for T by using Table 3.1 and the assumption that with a 2% hydrogen mixture $n_1 = .04 n_n$ where n_n is neutral argon's number density. The temperature required to achieve the observed ratio of line radiation to continuum is somewhat over 13,000°K. In effect the hydrogen radiation is less than would be expected under the assumptions made. Taking 12,000°K as the correct temperature, the continuum emission coefficient would be 53.6 w cm^{-3} str^{-1}. This gives a theoretical ratio of 0.196 to be compared with the observed ratio of 0.123. It is likely that this discrepancy is due to a greater percent ionization of atomic hydrogen than argon. The observed ratio implies that the atomic hydrogen is about 45% ionized.

Explanation of this discrepancy was attempted by use of several forms of the Saha equation. Following Olsen's treatment (Ref. 3.1.3) and expressing the ionization in terms of partial pressures,

$$\frac{P_i P_e}{P_n} = \frac{2u_i}{u_n}\left(\frac{2\pi m}{h^2}\right)^{3/2} (kT)^{5/2} \exp\left(\Delta E_i - E_i\right)/kT$$

$$= \frac{u_i}{u_n} 6.518 \times 10^{-7} T^{2.5} \exp\left(\Delta E_i - E_i\right)/kT \qquad (3.1.7)$$

where we are concerned only with the neutral and singly ionized atom. E_i is ionization energy. u_i and u_n are partition functions for the ion and the neutral atom; for hydrogen the ratio is taken as 1/2. Equation 3.1.7 was evaluated for $T = 12,000°K$, and $P_e = 1.46$ atmospheres from an electron density of 8.95×10^{17} cm^{-3} and an ionization potential lowering ΔE_i of 0.74 volts. The hydrogen ionization percentage indicated was around 2%. It may well be that the lowering of hydrogen's ionization potential is much more extreme than estimated. This process could explain the relatively low line emissivity observed.

3.2 Maxwellian Electron Speed Distribution

The Maxwellian distribution of speeds in a gas follows from the kinetic theory of gases. In a plasma the electrons may be treated as one of the constituents of the gas. The temperature of the electron gas is assumed to be close enough to the atomic gas to make Maxwell's law for speed valid.

$$n(v)\,dv = 4\pi n\left(\frac{m}{2\pi kT}\right)^{3/2} v^2 \exp\left(-mv^2/2kT\right) dv \qquad (3.2.1)$$

where n(v) is number density of electrons with speed v, n is total electron number density and m is mass of the electron. This relation reduces to a more useful form

$$\frac{n(v)}{n(\alpha)} = \frac{v^2}{\alpha^2} \exp\left(1 - \frac{v^2}{\alpha^2}\right) \qquad (3.2.2)$$

where α is the most probable speed and $n(\alpha)$ is the number density at this speed. If we wish to plot the Maxwellian distribution in terms of electron energy the relation becomes

$$\frac{n_{(E)}}{n_{(kT)}} = \frac{E}{kT} \exp\left(1 - \frac{E}{kT}\right) \qquad (3.2.3)$$

where kT is the energy of the electron with the most probable speed. E is the electron energy. Figure 3.2 sketches $n_{(E)}/n_{(kT)}$ vs. electron energy for temperatures of 16,000°K and 11,600°K. As temperature increases the relative density of electrons with energy greater than say 2 kT increases much more rapidly. The total electron density also increases as is shown in Table 3.1.

To aid in the understanding of argon plasma phenomena, the cross sections for elastic collision, excitation and ionization (Ref. 3.2.1) were plotted beneath the Maxwellian distribution. Also, some information on the radiative electron ion recombination was plotted. (Ref. 1.4). For comparison, a geometric cross section of 10^{-16} cm^2 was indicated for the argon atom. The elastic collision cross section is larger than any of the others and for most electron energies it is the only one of significance. At very low energies recombination is important. At energies above 11 ev excitation and then ionization become significant. However, it is clear that elastic collisions are by far the most likely. This fact assures that the Maxwellian distribution is valid for study of the argon plasma. The addition of additives with large cross sections for dissociation, excitation and ionization at lower electron energies will cause some distortion of the distribution but if the additive density is kept to a small percentage of the argon density, then the effect is probably more like a lowering of temperature.

It is interesting to compare the rate of ionization to the rate of recombination. For plasma equilibrium, the rate of recombination must equal the rate of ionization. This means that the product $n_i n_e v_s q_s$ for recombination will equal the equivalent product for ionization, $n_n n_e v_f q_f$. The number density of argon ions, n_i, is about 1/10 the neutral, n_n, the electron density of slow electrons is $\approx 10^4$ times the ionizing electron density. The velocity of the slow recombining electrons, v_s, is $\sim$ 1/10 that of fast ionizing electrons, v_f. The cross section for recombination, q_s, is no less than 1/10 the cross section for ionization, q_f. Comparison of products suggest that the rate of recombination assuming an exact Maxwellian distribution would be something like ten times the rate of ionization. It is likely that the number density of slow electrons in the argon plasma is actually less than the

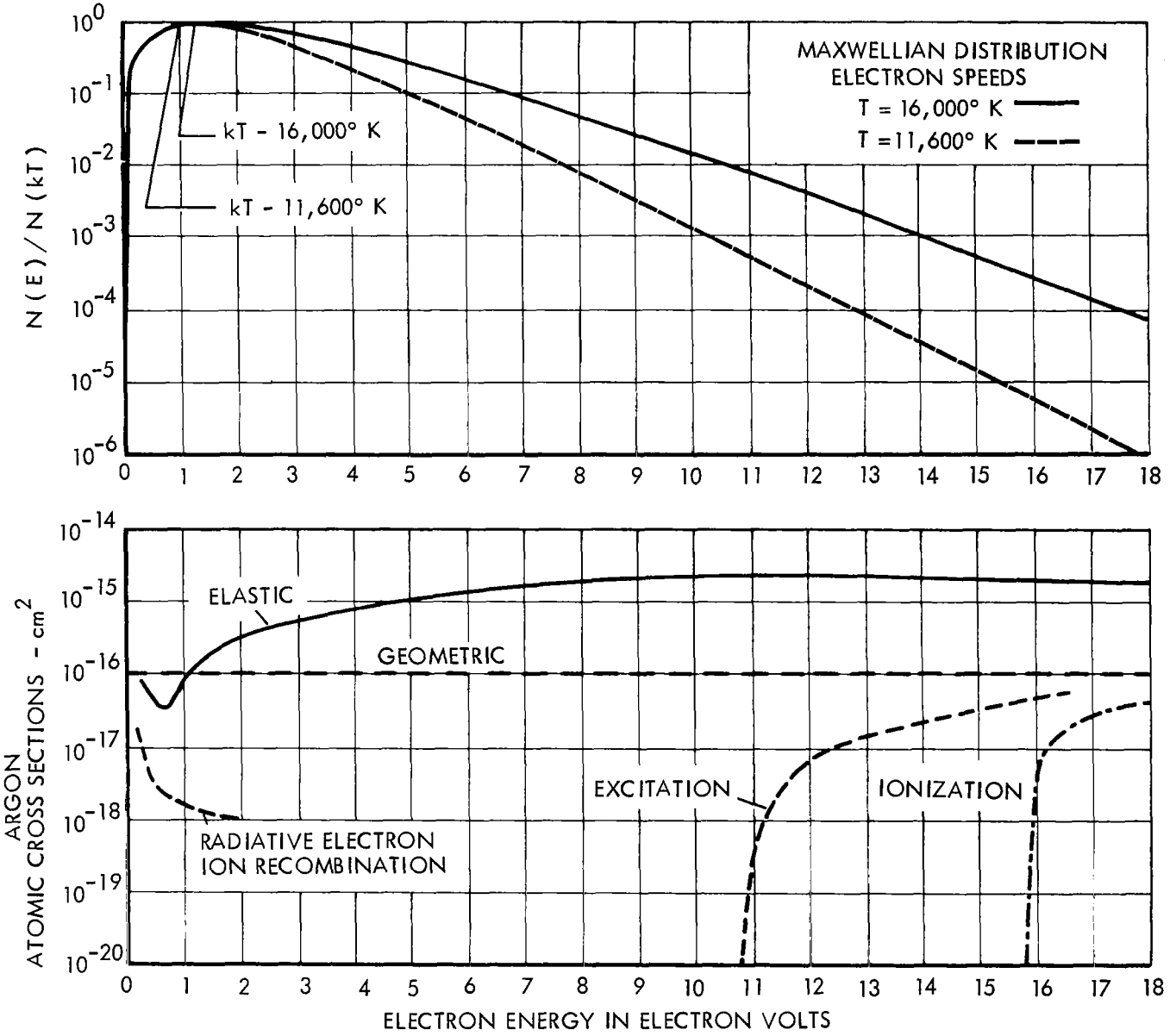

FIGURE 3.2 - ELECTRON ENERGIES AT 16,000° K & 11.600° K vs ARGON CROSS SECTIONS

theoretical number. Similar deviations from theory will undoubtedly occur near excitation energy levels. However, for most electron energies Maxwell's law for speed distribution must be valid. This assumption allows use of the plasma temperature concept as a means of conveniently describing the speed distribution of the electrons and atoms making up a plasma.

3.3 Electron Drift Velocity and Density

The concept of temperature as related to Maxwell's speed distribution allows calculation of a number of plasma parameters. Operating data on a typical argon vortex arc are as follows:

p_a = 10^4 mm Hg, pressure in arc column

D = 3.5 mm, diameter arc column

L = 10 mm, length of arc column

I = 300 amp, arc current

E = 70 volts, voltage, cathode to anode

Gas = argon

Electrodes = 2% thoriated tungsten

The average plasma temperature derived in Section 3.1 is taken as 12,000°K and allows computation of the electron mean free path, l_e.

$$l_e = (p_a\, p_c)^{-1} \text{ cm} \qquad (3.2.4)$$

where p_c is the probability of collision at unit pressure measured in mm Hg. Assuming that the electrons are in thermal equilibrium with the gas atoms, the electron with the most probable speed has an energy of 1.03 ev. The p_c for such an electron is ≈ 5 judging from the curves of Brode (Ref. 3.2.2). The mean free path l_e is then 2.0×10^{-5} cm. The root mean square thermal velocity, V_e, of electrons can then be determined from the relation

$$mV_e^2 = 3\,kT \qquad (3.2.5)$$

and for the stated vortex arc conditions $V_e = 4.8 \times 10^7$ cm sec^{-1}.

The electron mobility can be evaluated using the relation (Ref. 1.1).

$$b^- = e\, l_e\, (m_e V_e)^{-1} \qquad (3.2.6)$$

$$= 7.3 \times 10^2 \text{ cm sec}^{-1}/\text{volt cm}^{-1}$$

Estimating the field intensity of the vortex arc column of E = 50 volts cm^{-1}, this results in a drift velocity V^- equal to:

$$V^- = b^- E \qquad (3.2.7)$$

$$= 3.65 \times 10^4 \text{ cm sec}^{-1}$$

Due to the fact that the electron drift velocity, V^-, is much greater than the ion velocity the total arc current, J, must be equal the product

$$J = n_e A e V^- \qquad (3.2.8)$$

$$= 300 \text{ amperes}$$

where n_e is electron density, A is arc cross section area = 0.096 cm^2, $e = 1.602 \times 10^{-19}$ coulombs and V^- is given by Equation (3.2.7). Then for the typical argon vortex arc

$$n_e = 5.4 \times 10^{17}$$

This figure is of course an average and depends on the assumption of 12,000°K as an average temperature for the vortex arc column. It is interesting to note that the result is very close to the conclusions reached in Section 3.1.

The vortex gas flow has a very strong influence on the shape of the arc column. Figure 3.3.1 shows the characteristic radial profile of pressure within a vortex. The change of pressure with radius is greatest at radii from 1/2 to 2/3 of the exit orifice radius. This profile appears to occur even with the low pressure drop vortex used in the vortex arc. Figure 3.3.2, an observation of hydrogen Stark broadening as a measure of temperature, clearly indicates a sharp

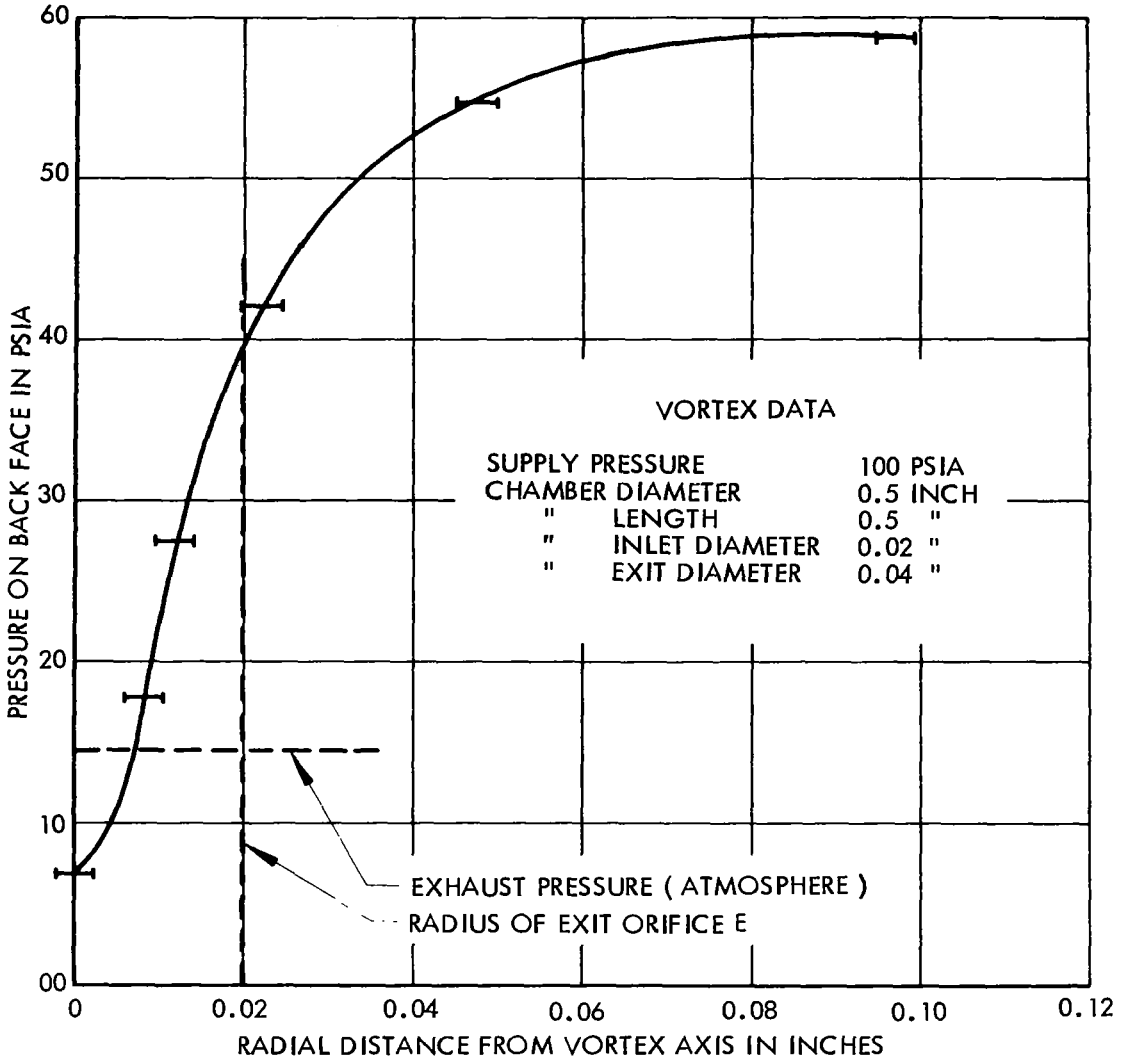

FIGURE 3.3.1 - RADIAL PRESSURE MEASUREMENT

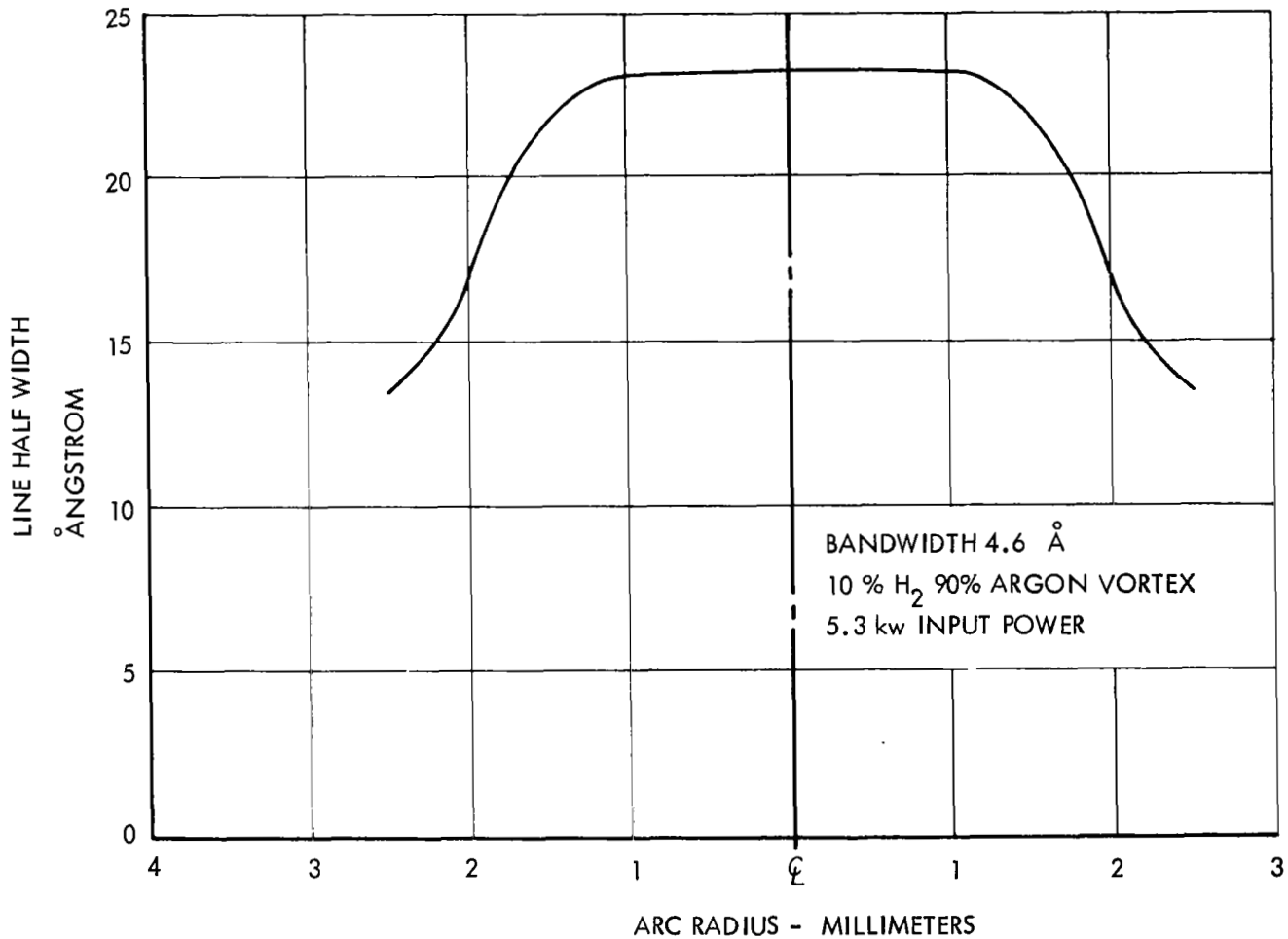

FIGURE 3.3.2 - 0.6563μ HYDROGEN LINE BROADENING

drop in temperature at a radius of ≈ 2 mm. The exhaust orifice in this case had a radius of 3.2 mm. This is a typical confirmation of the control of arc dimensions by vortex flow.

The vortex arc then tends to be a cylindrical column of uniform temperature and electron density in cross section. In the axial direction the cathode jet has a somewhat higher temperature, while the sections ahead of the anode are slightly colder than the middle cross section. However, in every cross section the boundary between the arc column and cold vortex gas is very thin, perhaps 0.5 mm due to the low thermal conductivity of the inert gases and also to the rapid ventilation caused by vortex flow.

3.4 Argon Line Radiation

The important argon lines were measured using the monochromator system described in Section 2.4 before proceeding to a study of additive line radiations. The argon line structure is relatively minor in total power and is superimposed upon the continuum. Study of the line radiation showed in addition that radiation from the higher term energy levels was either weak or absent. The spectral measurements were made with a bandwidth of 0.46 mμ. Figure 1.4, Energy Level Diagram of Argon I, sketches the excitation energy required for the various energy levels. Figure 3.4.1 gives a spectral distribution for argon in the wavelength interval 0.35μ to 0.44μ. The continuum is dominant but several broadened lines can be identified. The 4s - 6p transition at 0.3607μ has the highest excitation energy, about 15 ev, but is very weak. The 4s - 5p transitions around 0.42μ to 0.34μ are excited at lower energies and occur more frequently. Figure 3.4.2 gives the vortex argon spectrum between 0.60μ and 0.69μ. First, the 0.6032μ line for a 4p - 5d transition with E_n = 15.13 ev does not appear. However, a number of lines with upper levels at 5d', 5d, 6s and 7s levels are evident although not very strong. In contrast, Figure 3.4.3 gives argon vortex lines for the wavelengths between 0.75μ and 0.84μ. The continuum here contributes roughly one half of the radiant power with broadened line radiation related to 4s - 4p transitions making up the remainder. The excitation energy for these transitions is around 13.0 ev to 13.5 ev. It is apparent that in an argon vortex operating at the low power level of 4.4 kw very little radiation occurs from transitions originating at energy levels above 15 ev or 121,000 cm^{-1}. As the input power is increased the upper energy level of observed lines tends to lower even more. This observation is consistent with the lowering of ionization potential expected in high density plasmas.

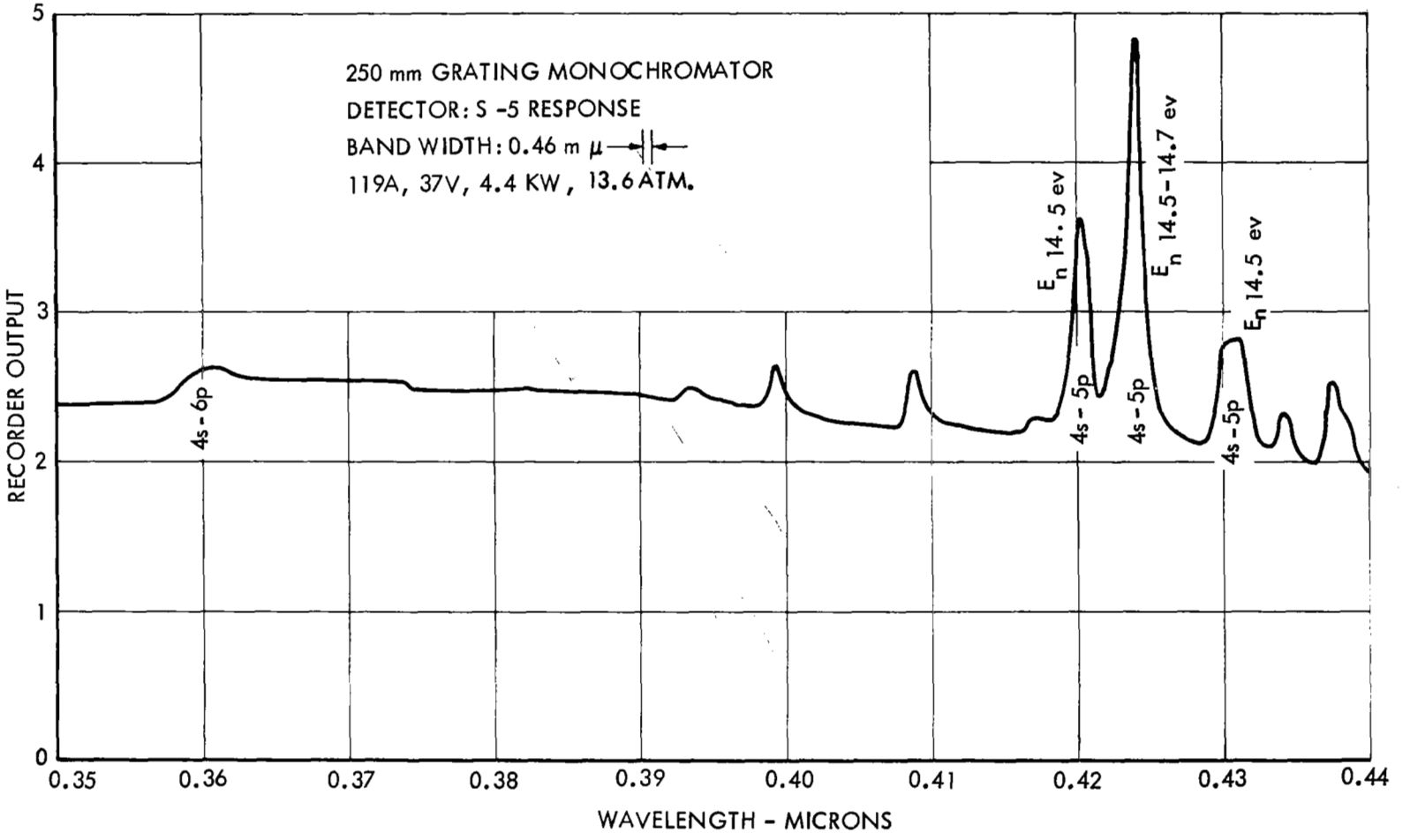

FIGURE 3.4.1 - SPECTRAL DISTRIBUTION: ARGON VORTEX, 0.35μ to 0.44μ

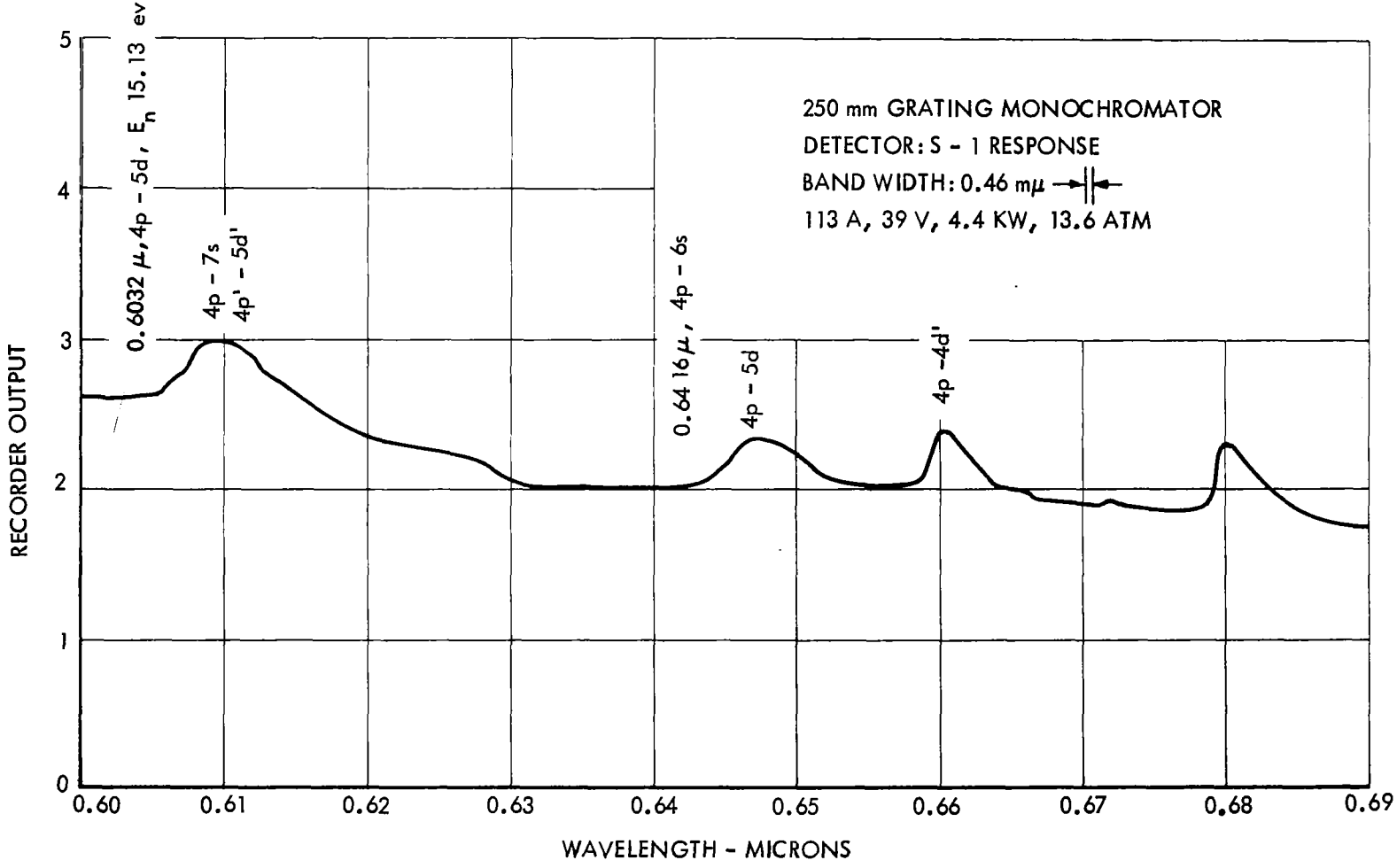

FIGURE 3.4.2 - SPECTRAL DISTRIBUTION: ARGON VORTEX, 0.60μ to 0.69μ

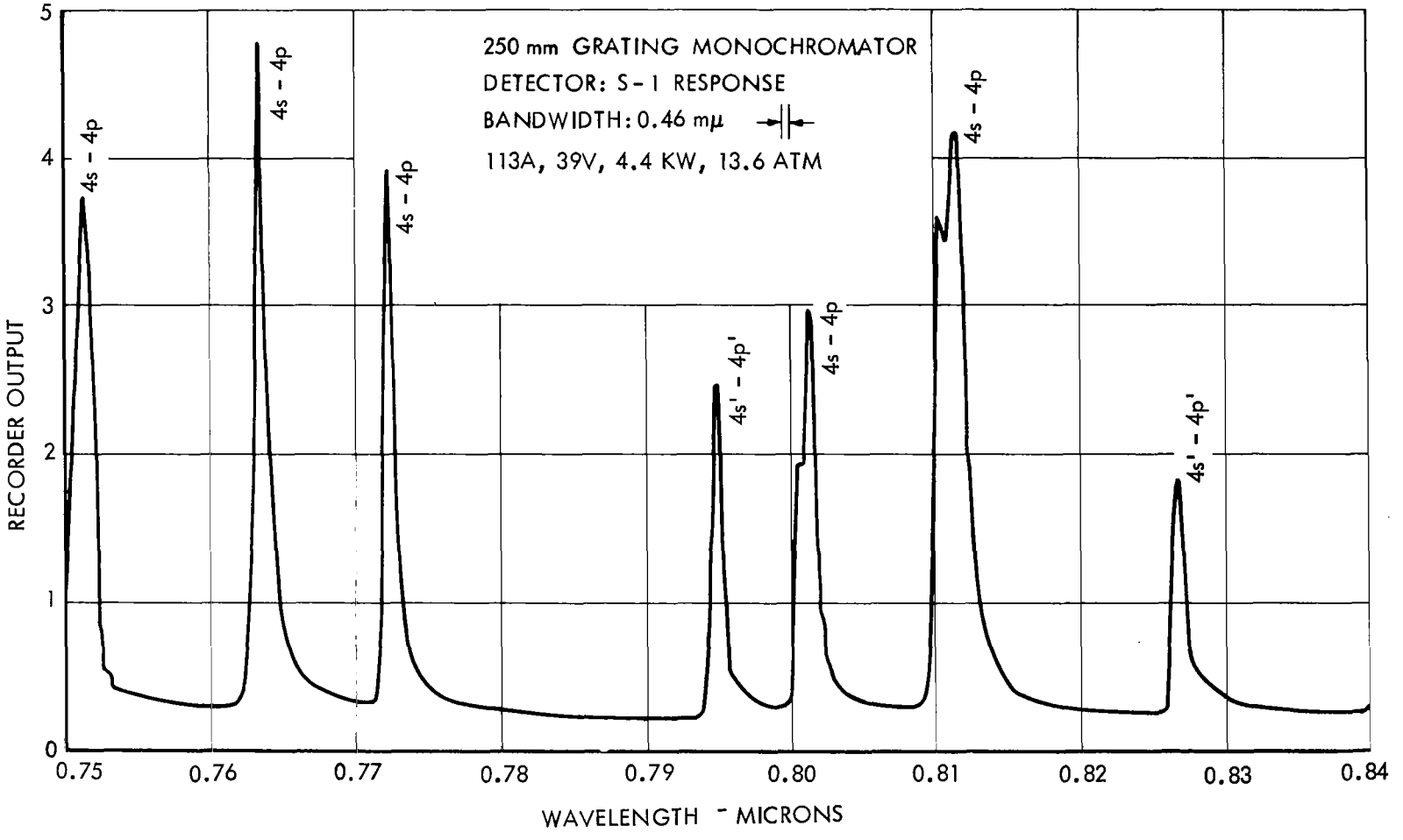

FIGURE 3.4.3 - SPECTRAL DISTRIBUTION: ARGON VORTEX, 0.75μ to 0.84μ

4.0 ADDITIVE STUDIES

The additives selected were studied both theoretically and experimentally. First, an estimate of electron density and temperature was made. Then the technique of Aller (Ref. 4.0) based on Menzel's work was employed to determine the degree of ionization of the additive. The following equation is in convenient form for computation.

$$\frac{n_{s+1}P_e}{n_s} = \frac{(2\pi m)^{1.5}}{h_3} (kT)^{2.5} \frac{2u_{s+1}(T)}{u_s(T)} \exp(-E/kT) \qquad (4.0)$$

where subscript s stands for the lower level and E stands for its ionization energy, and P_e is electron pressure. u is the partition function and while u itself is difficult to obtain, the ration u_{s+1}/u_s can be estimated.

The number of possible additives is quite large and the Menzel equation 4.0, can be used to determine those which might be useful. If we assume an argon plasma temperature of 10,000°K to 12,000°K and electron densities between 2×10^{17} cm^{-3} and 9×10^{17} cm^{-3}, then the degree of ionization may be roughly estimated by referring to ionization potentials. Any atom with an ionization potential of less than 9 volts is very likely to be highly ionized. At the other extreme an atom with an ionization potential greater than 14 volts is very likely to radiate most effectively in the vacuum ultraviolet. It is then possible to list the atoms which might be of interest in the additive studies.

Table 4.0 Ionization Potentials of Additives - Volts

	I	II	Strong Lines - μ	
Hydrogen	13.6		0.122	0.656
Beryllium	9.32	18.2	0.455	0.235
Carbon	11.3	24.4	0.297	0.166
Oxygen	13.6	35.1	0.136	0.130
Phosphorus	10.6	19.7	0.179	0.254
Sulfur	10.4	23.4	0.190	0.181
Chlorine	13.1	23.8	0.139	0.135
Calcium	6.11	11.9	0.393	0.397
Scandium	6.56	12.8	0.361	0.363
Titanium	6.83	13.6	0.335	0.336
Zinc	9.39	18.0	0.308	0.214
Arsenic	9.81	20.2	0.197	0.189
Selenium	9.75	21.5	0.207	0.196
Bromine	11.9	21.6	0.158	0.149
Strontium	5.69	11.0	0.408	0.422
Yittrium	6.38	12.2	0.371	0.360
Zirconium	6.84	12.9	0.339	0.344
Niobium	6.88	13.9	0.309	0.323
Cadmium	9.00	16.9	0.326	0.229
Tellurium	9.01	21.5	0.226I	0.116II
Iodine	10.4	19.0	0.206	0.183
Barium	5.21	10.0	0.455	0.493
Lanthanum	5.61	11.4	0.395	0.408
Samarium	5.60	11.2	0.357	0.442
Europium	5.67	11.2	0.421	0.413
Gadolinium	6.16	12.0	0.342	0.365
Yitterbium	6.22	12.1	0.369	0.329
Mercury	10.4	18.8	0.254	0.185
Radium	5.28	10.1	0.381	0.468

The underlined ionization potential indicates the atom referred to in the strong line column. These wavelengths include resonance lines and strongest lines as tabulated in the American Institute of Physics Handbook (Ref. 4.1). For example, the strong lines for calcium II are 0.393μ and 0.397μ and would be dominant if calcium were added to the argon vortex. Study of the table indicates that barium II should be the most efficient additive element in meeting the objective of shifting the peak of the argon plasma radiation toward longer wavelengths. Unfortunately, even barium peaks at shorter wavelengths than are actually required. The following sections give the experimental data obtained by actual injection of various additives to the argon plasma. The strongest lines produced were as indicated by Table 4.0.

4.1 Titanium

The titanium additive experiments were made at relatively low power and pressure, around 3 kw and 8 atmospheres. The plasma temperature was estimated at 10,000°K and electron density at 1×10^{17} cm^{-3}. The electron pressure was calculated to be 1.4×10^{5} dynes cm^{-2}. Using equation 4.0 titanium should exist in the argon plasma with the following proportion; the neutral atom 3.5% and the singly ionized atom 96.5%.

Figure 4.1.1 gives the energy levels of titanium I and II arranged one above the other merely to indicate that electrons exciting the argon energy levels displayed to the left have sufficient energy to excite neutral titanium to excited ionized states. In the argon plasma, however, very little titanium I (neutral) exists and the dominant radiation should be from titanium II and should be seen at wavelengths related to the dominant and numerous 4p - 4s transitions.

One of the first materials to be successfully introduced into the arc was titanium nitride. Spectral distribution is shown in Figure 4.1.2. The titanium I resonance line, 0.5174μ, or the strongest line, 0.4982μ, of the neutral atom make a very weak contribution to the radiation observed. Instead, line radiation from singly ionized titanium is very strong showing a peak around TiII 0.3349μ. No radiation relating to nitrogen is evident. The titanium ionization potentials are 6.83v for the neutral atom and 13.57 volts for the singly ionized atom. It is very apparent that titanium in the vortex arc exists as the singly ionized atom as was indicated by solution of Menzel's equation, equation 4.0. Actually the neutral atom density will be even less as the first ionization potential must be lower than 6.83 volts due to microfield effects.

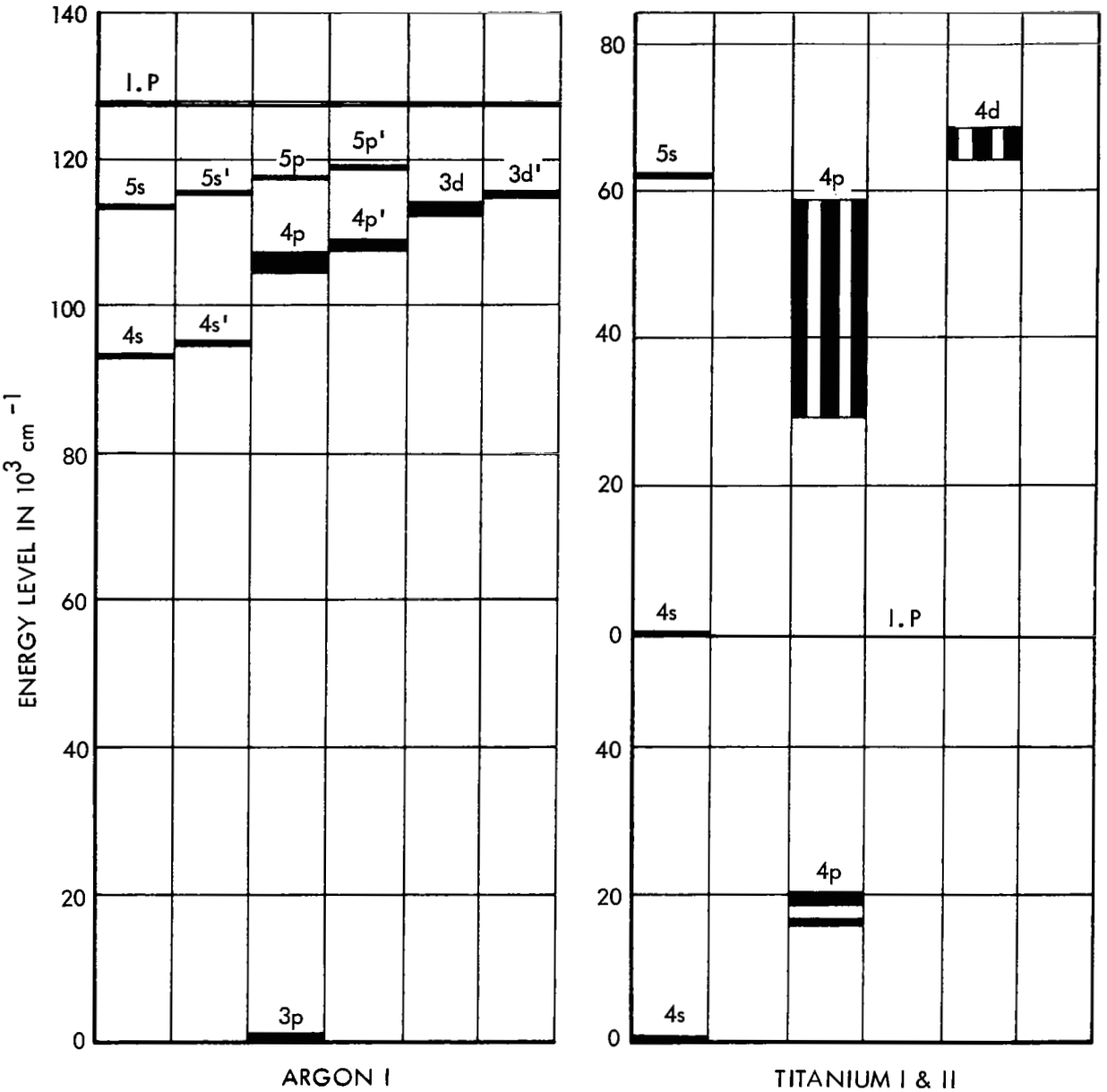

FIGURE 4.1.1 - ENERGY LEVELS - ARGON VS TITANIUM

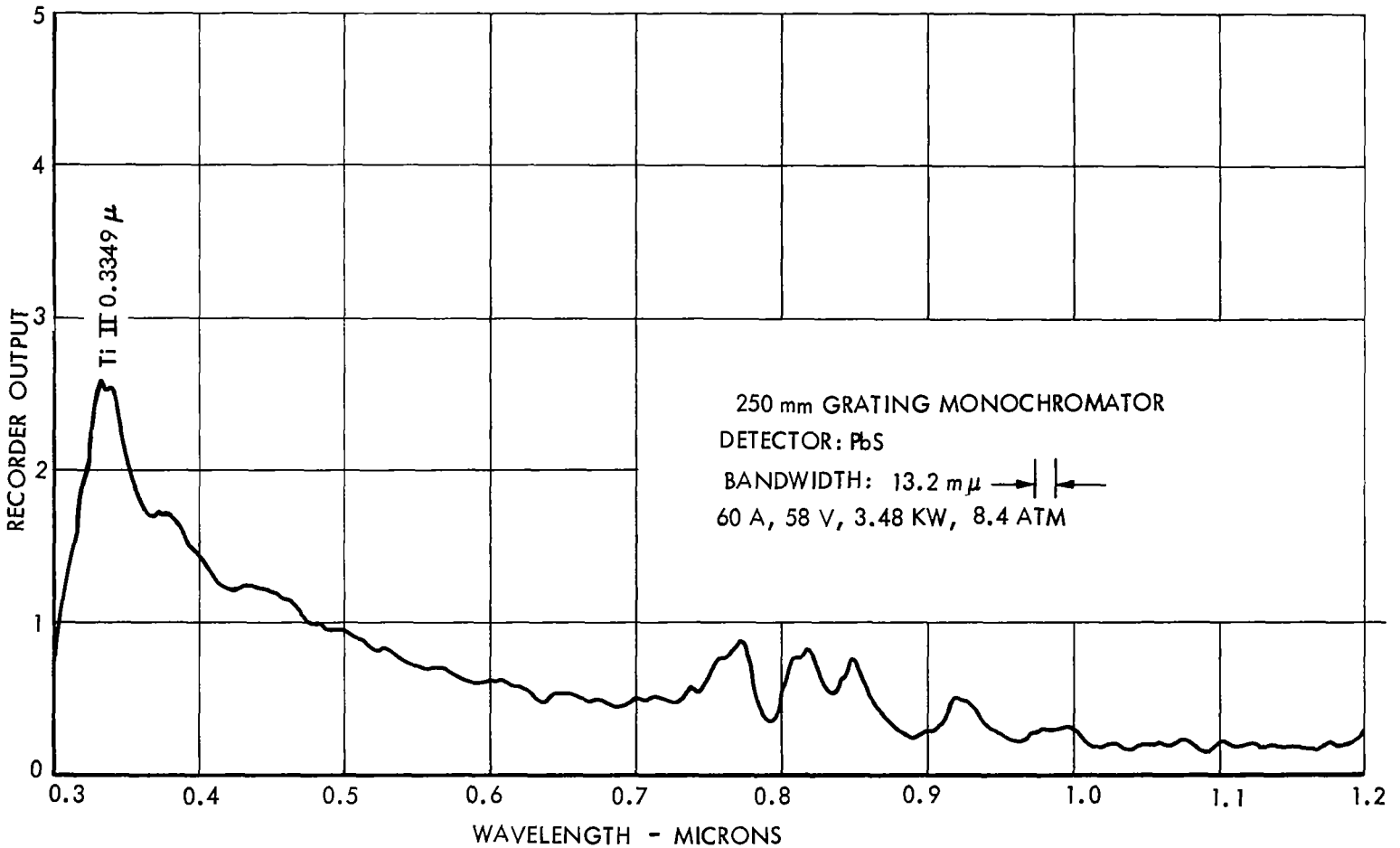

FIGURE 4.1.2 - SPECTRAL DISTRIBUTION: TITANIUM NITRIDE IN ARGON VORTEX

One of the next powders used was barium titanate. Its spectral distribution as excited in the argon vortex is given in Figure 4.1.3. Once again the strong ultraviolet lines of titanium II are evident around 0.335μ. However, added to this and the usual argon lines are barium lines. These lines are also related to the singly ionized atom. The argon-titanium vortex is then a strong source of near ultraviolet and while not pertinent to the solar simulation problem it offers insight as to the plasma physics of additives to the argon vortex.

4.2 Barium

Barium as indicated in Figure 4.1.3 produces radiation in wavelengths which could be useful in improving the spectral match of argon plasma radiation to the desired solar spectrum. Most data taken with barium were at about 14 atmospheres and an estimated temperature of 10,000°K. These estimates are compatible with an electron density of 2×10^{17} cm^{-3} and an electron pressure of 2.8×10^{5} dynes cm^{-2}. Applying Equation 4.0 we find that the barium atom would exist as follows:

1.7%	Neutral, Ba I
95.3%	Singly Ionized, Ba II
3.0%	Doubly Ionized, Ba III

It is very likely that if lowering of ionization potentials could be taken into account the Ba III percentage would rise appreciably.

The spectral distribution of the argon vortex with barium as an additive shows in Figure 4.1.3. The energy level diagram, Figure 4.2.1 can be used to explain the peaks observed. The strongest lines are around 0.455μ, 0.493μ, 0.413μ, and 0.389μ. These lines are indicated on the energy diagram. Neutral barium is ionized at 5.21 volts and the singly ionized atom is again ionized at 10.0 volts. It is clear that barium II is the important radiating atom. As stated in the previous paragraph barium III must also exist, however, as neutral barium has two electrons above a closed "O" shell similar to xenon the resonance radiation of the third electron is in the vacuum ultraviolet and has not been observed.

The radiation of barium in the vortex arc is quite different from its emission in mercury vapor-metallic iodide arc lamps as reported by Reiling (Ref. 4.2.1). In a 400 watt lamp with barium iodide as an additive the strongest barium lines are 0.5535μ, 0.6142μ, 0.6498μ, 0.6595μ, 0.7059μ, 0.7280μ, 0.7673μ, and 0.8560μ, all from barium I. The lowest energy level barium II line

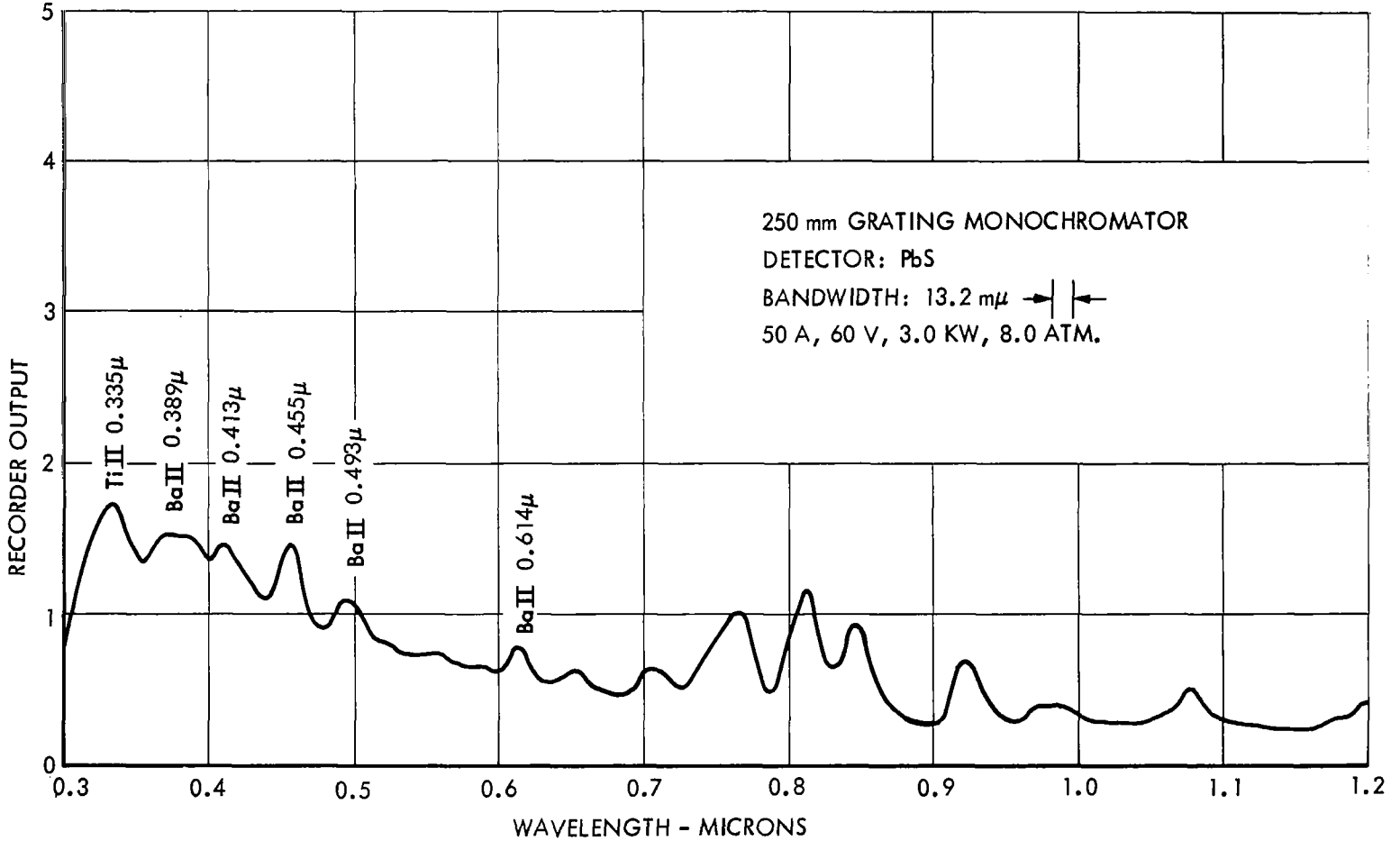

FIGURE 4.1.3 - SPECTRAL DISTRIBUTION: BARIUM TITANATE IN ARGON VORTEX

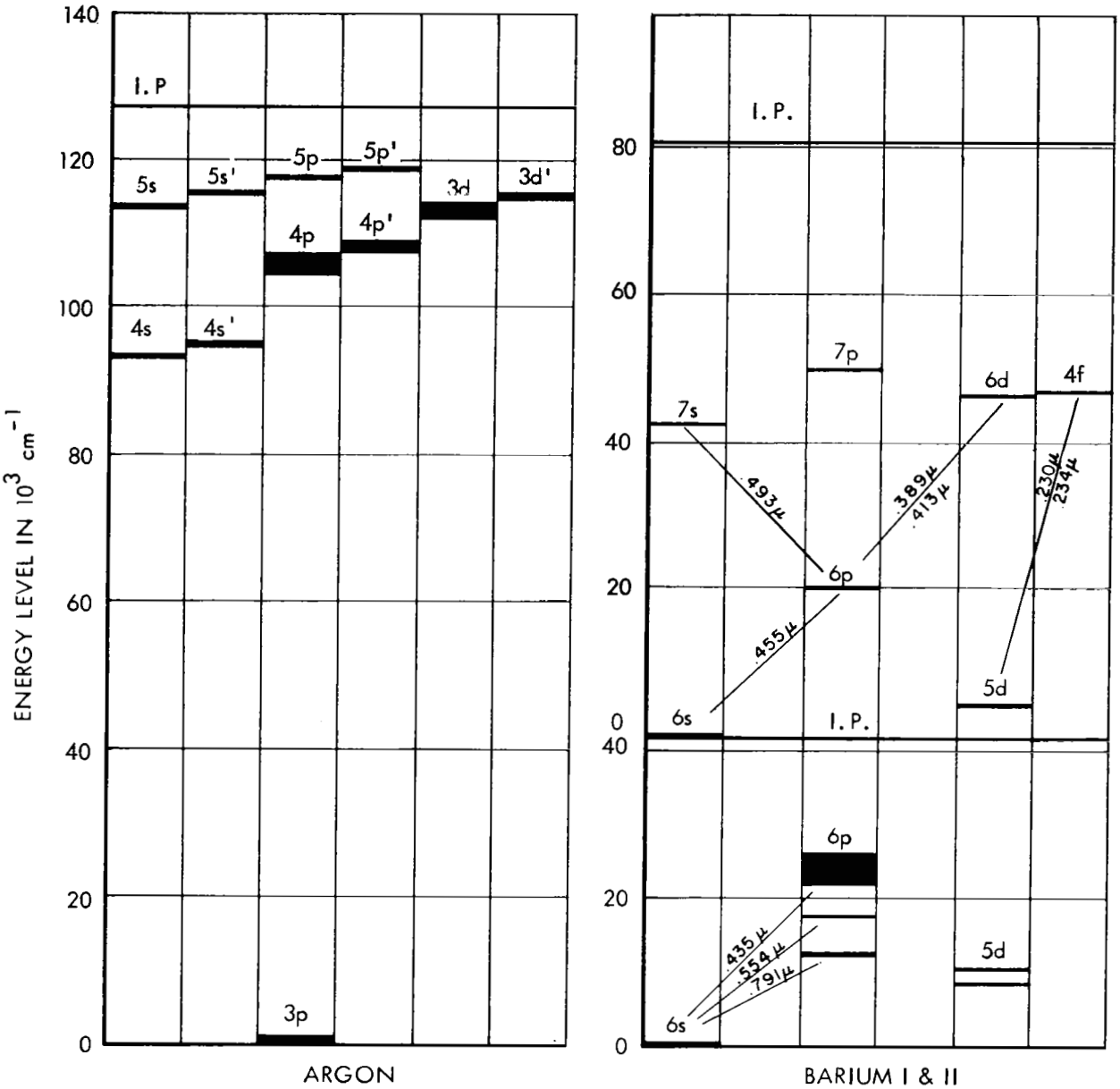

FIGURE 4.2.1 - ENERGY LEVELS - ARGON VS BARIUM

at 0.4554μ is also present. It is very clear that the excitation energies prevailing in the argon vortex arc are far higher than in the mercury arc lamp.

Figures 4.2.2, 4.2.3, and 4.2.4 show the line structure of barium II as observed with the addition of barium bromide to the argon vortex while operating at 8.6 kw. The 0.46 mμ bandwidth does not completely resolve the line structure, but does indicate a large line intensity relative to the continuum. The table of line strengths listed below were taken from "Tables of Spectral Line Intensities" NBS No. 32. (Ref. 4.2.2)

Table 4.2 Barium II Line Intensities

Wavelength Microns	Intensity NBS No. 32
0.2304	28
0.2335	55
0.2634	10
0.3892	140
0.4131	150
0.4166	20
0.4525	13
0.4554	6500
0.4900	40
0.4934	2000

The recorded data is qualitatively compatible with these intensities. There is no evidence of any important barium I emission.

Microradiance measurements using Ba Br_2 as an additive to the argon vortex were made with the set up described in Section 2.0. These tests were conducted with an additive feed rate of 1.0 mg sec^{-1}. The microradiance contours of the Ba Br_2 additive arc and a pure argon arc are shown in Figures 4.2.5 and 4.2.6. Comparing the two it can be seen that the additive (Ba Br_2) decreases the peak radiation intensities at the axis of the arc, and causes the arc to increase in diameter.

Broadband (.05μ) spectral distribution curves were run with barium bromide (at a flow rate of 1.0 mg sec^{-1}) in the argon vortex arc. Figure 4.2.7 shows the Ba Br_2 argon spectral distribution with direct comparison to pure argon

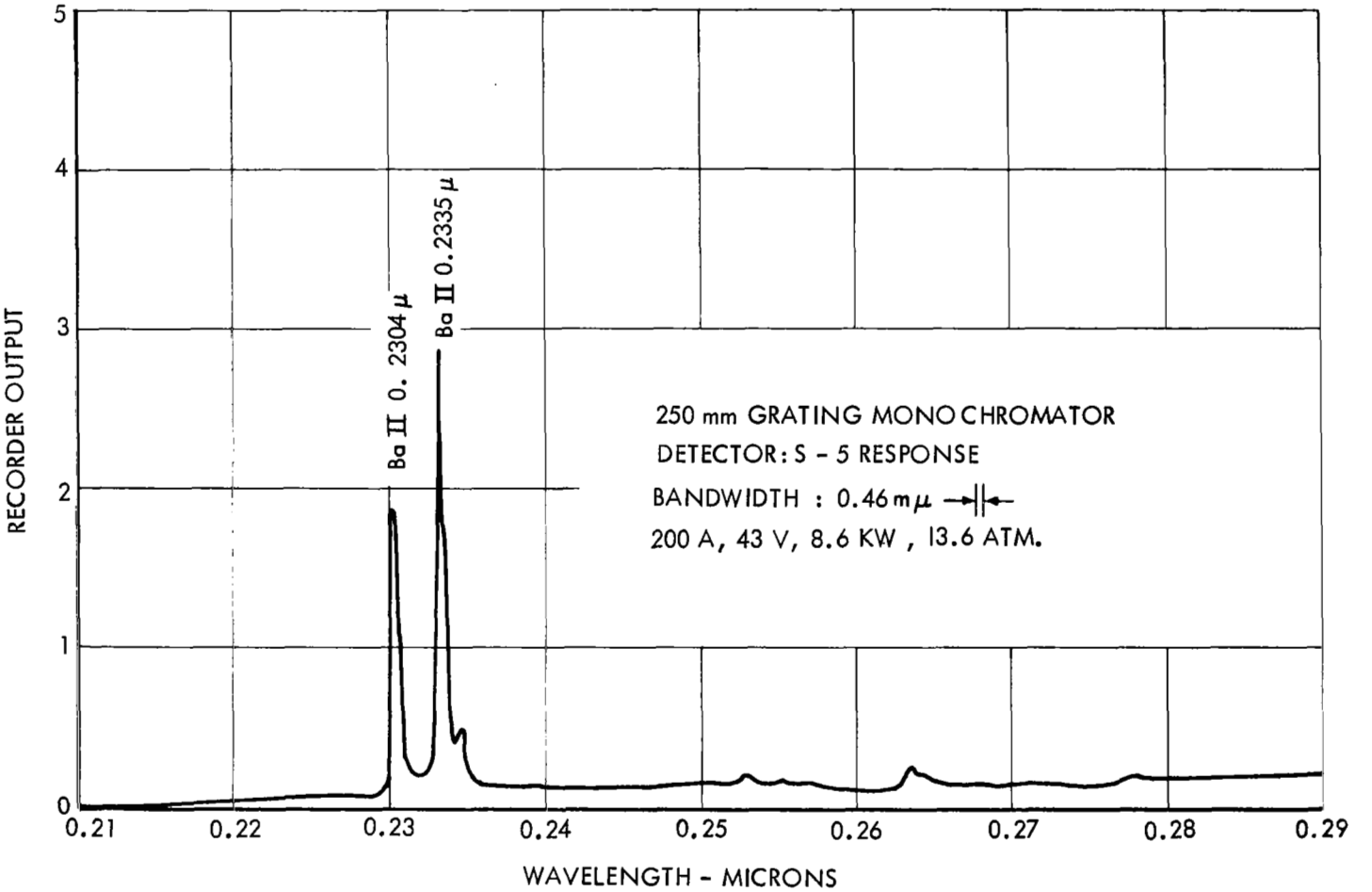

FIGURE 4.2.2 - SPECTRAL DISTRIBUTION: ARGON + BARIUM BROMIDE, 0.21μ to 0.29μ

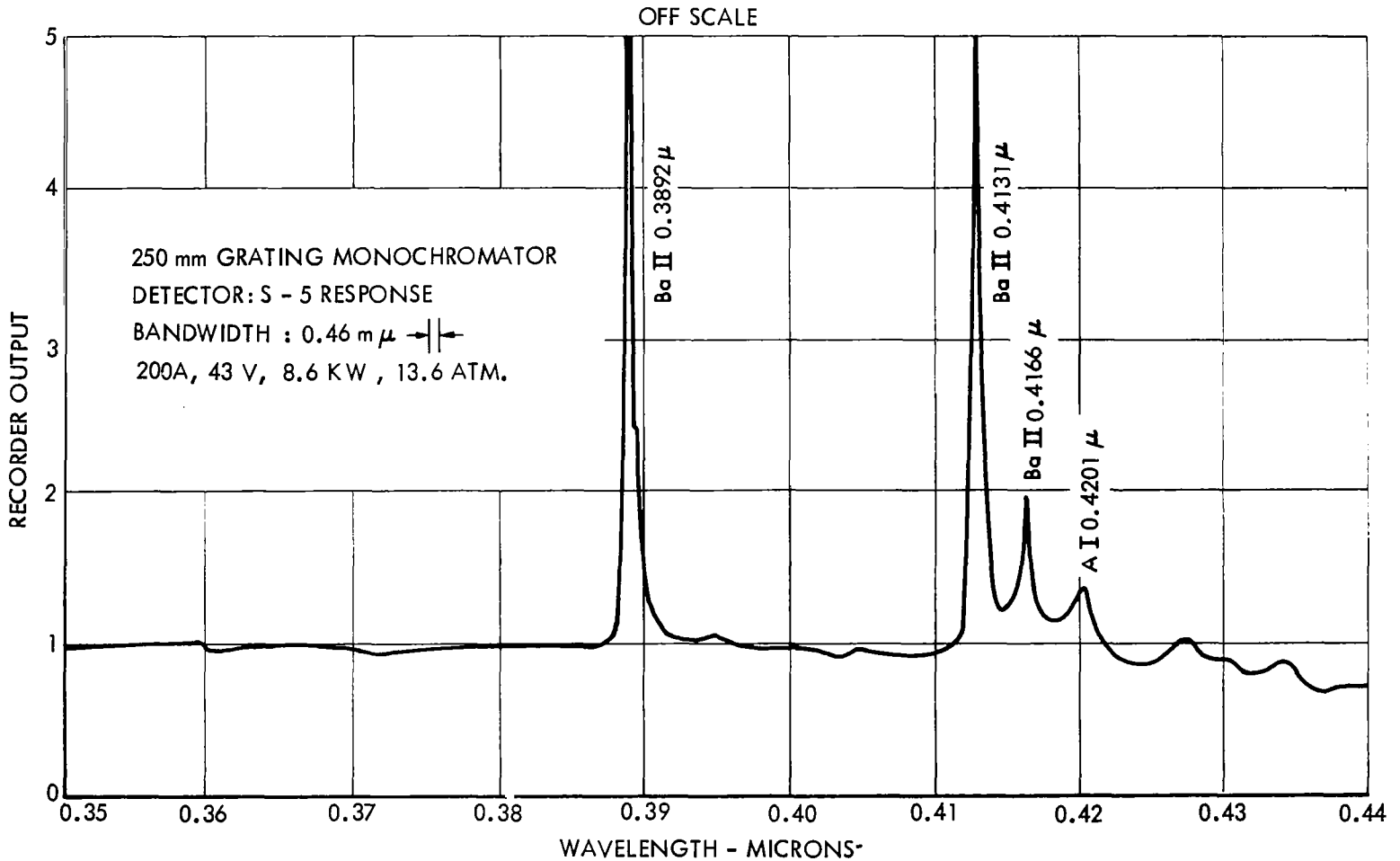

FIGURE 4.2.3 - SPECTRAL DISTRIBUTION: ARGON + BARIUM BROMIDE, 0.35μ to 0.44μ

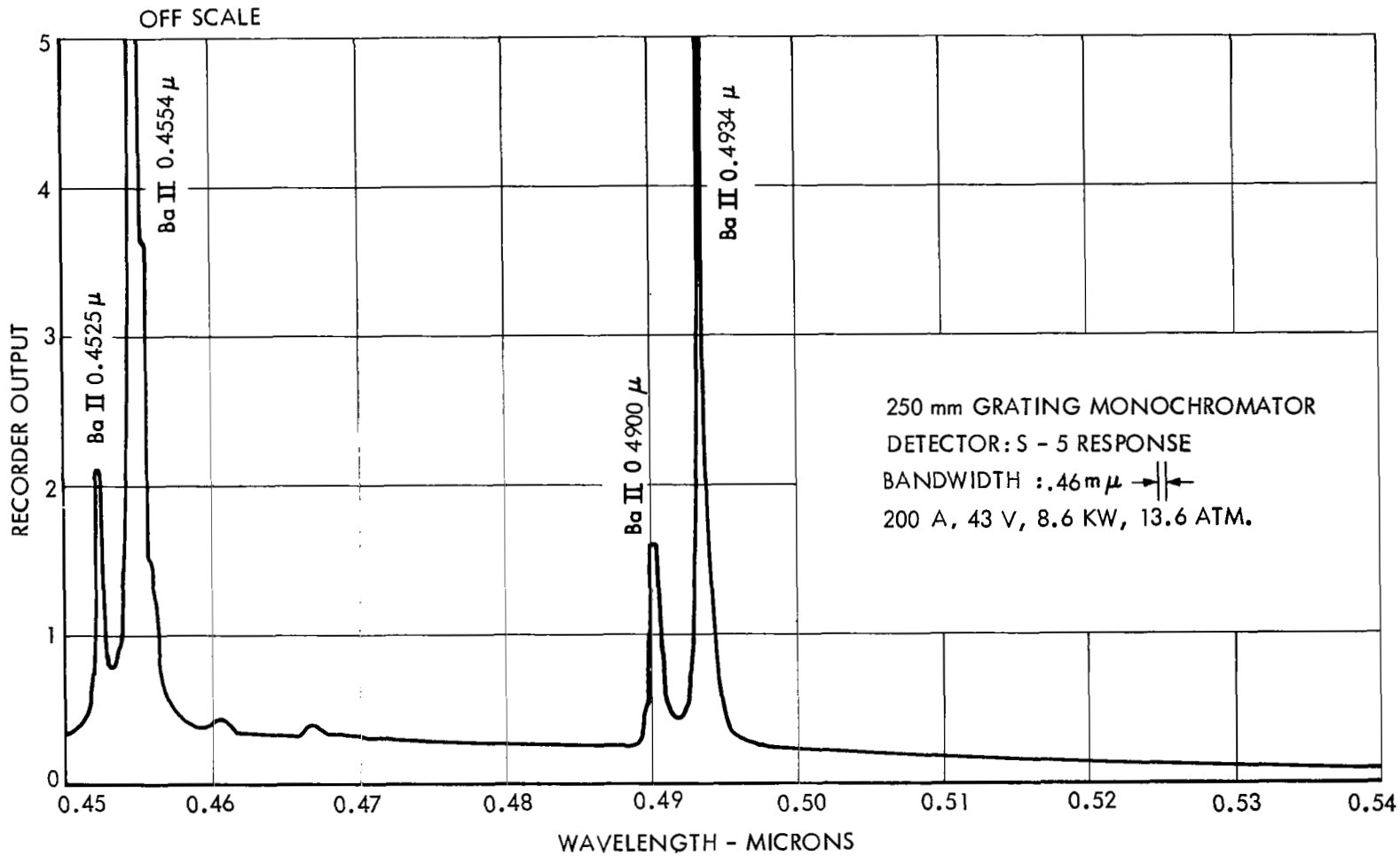

FIGURE 4.2.4 - SPECTRAL DISTRIBUTION: ARGON + BARIUM BROMIDE, 0.45μ to 0.54μ

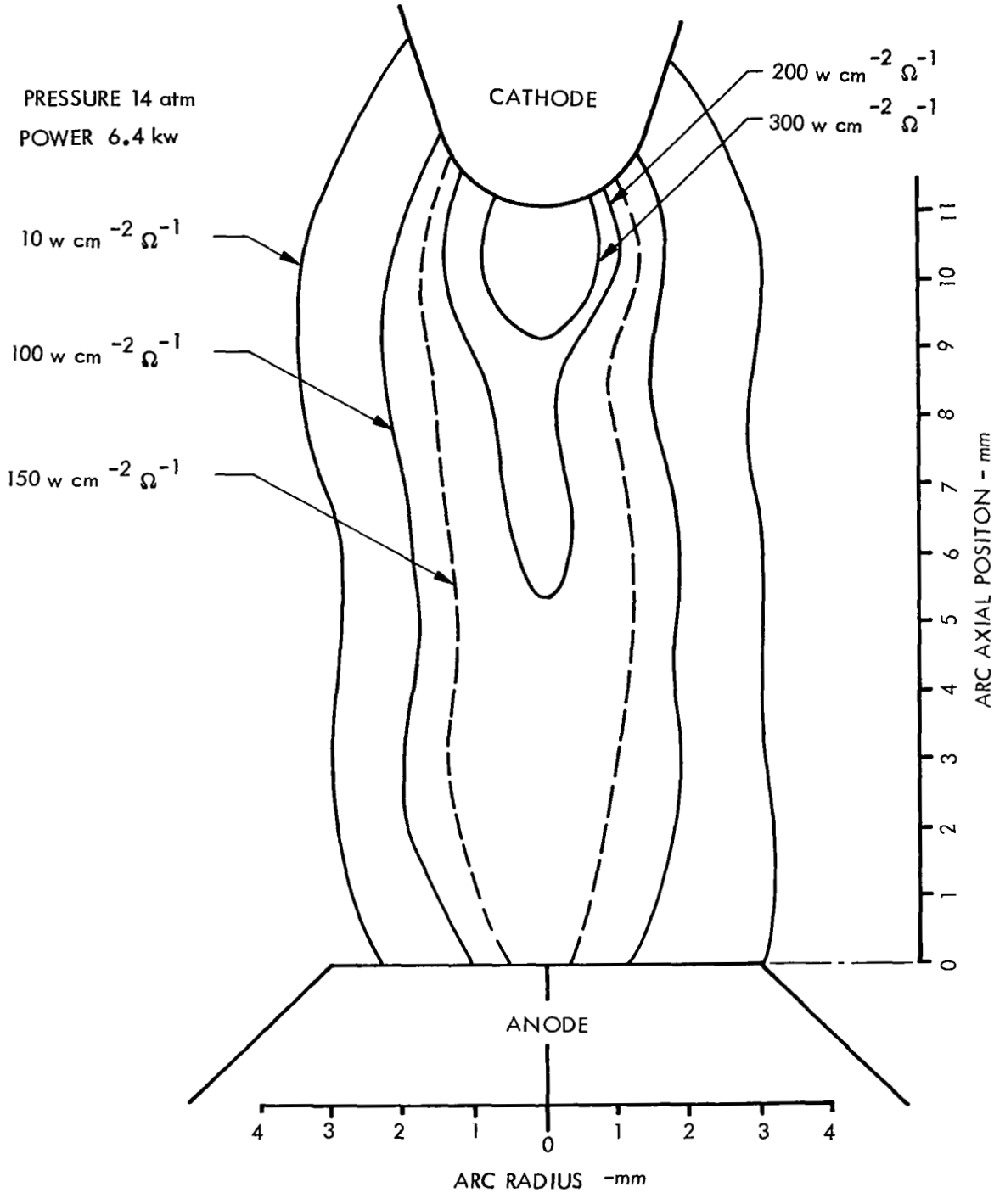

FIGURE 4.2.5 - RADIANCE CONTOURS - BARIUM BROMIDE

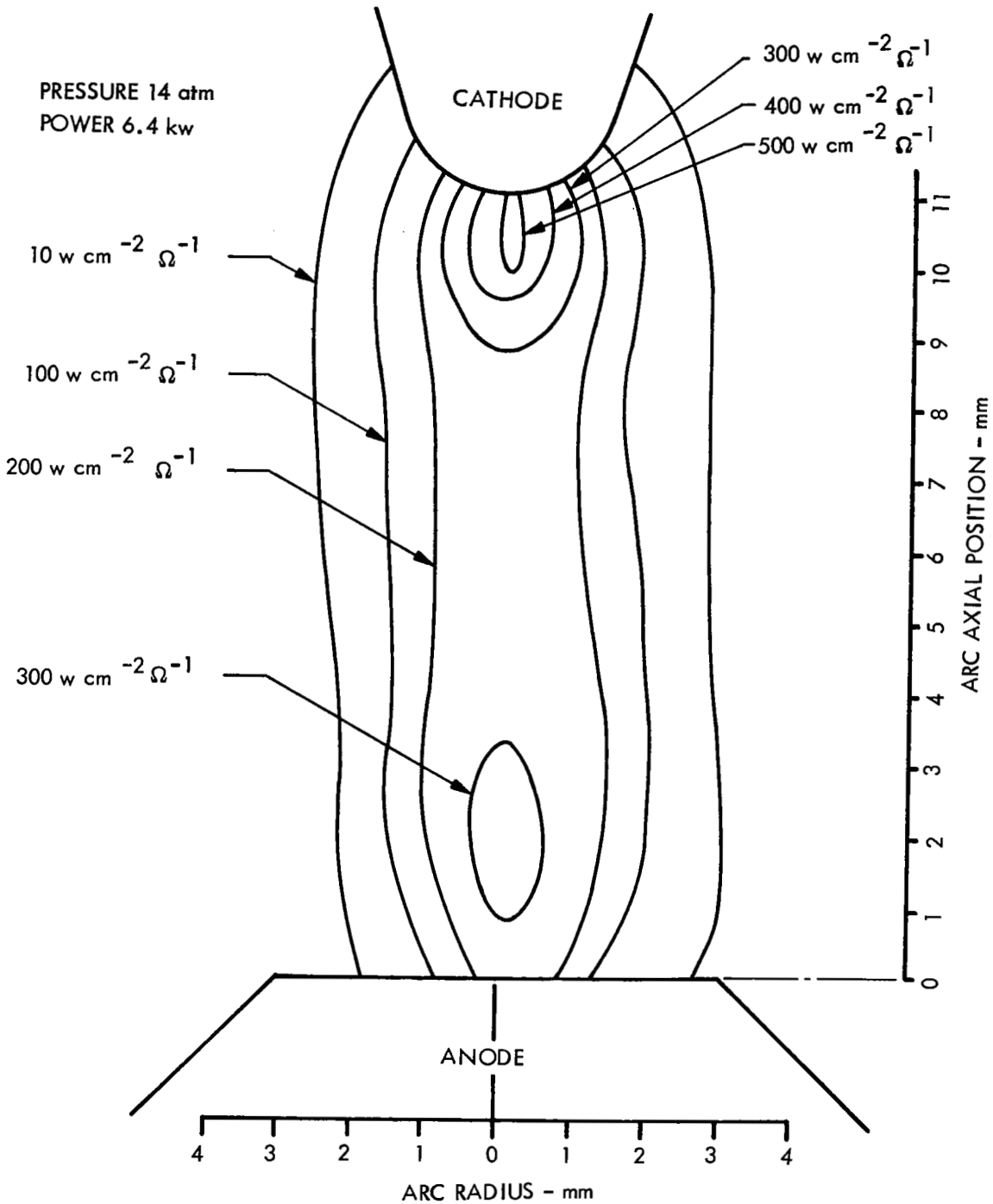

FIGURE 4.2.6 - RADIANCE CONTOURS - ARGON

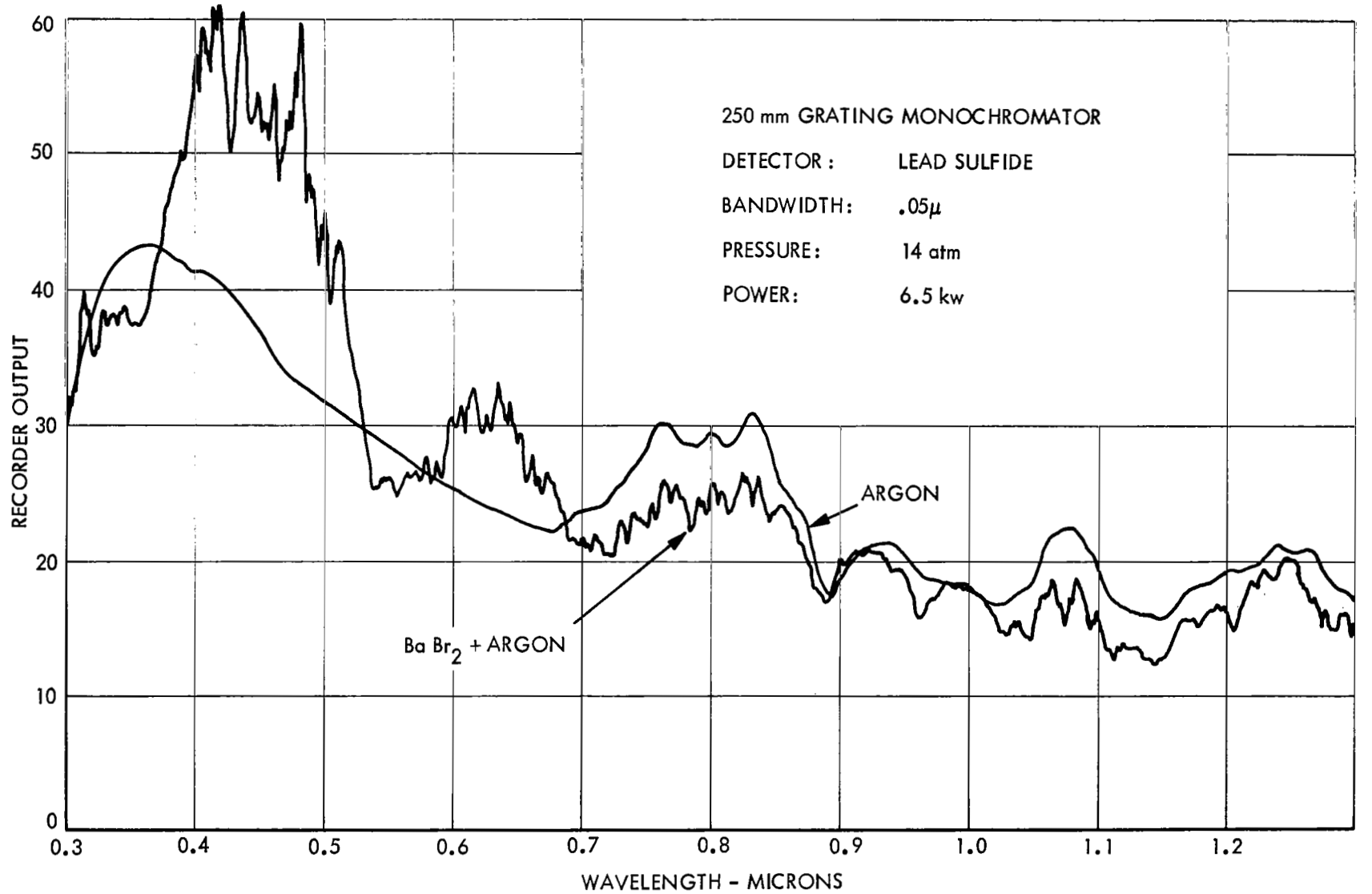

FIGURE 4.2.7 - SPECTRAL DISTRIBUTION: BARIUM BROMIDE & ARGON

for wavelengths between 0.3μ and 1.2μ. It can be seen from this curve that barium gives a pronounced increase in radiation from 0.4μ to 0.5μ and from 0.6μ - .65μ, with respect to argon. This is due to the very strong barium II lines which occur in these areas. Of minor interest is the increase in lumens per watt of input power with the barium additive over lumens per watt with pure argon. This increase amounted to 12%.

4.3 Sodium

An excellent check on the phenomena being observed is provided by Figure 4.3.1 giving the spectral distribution of an equal mixture of sodium and barium chlorides. Barium II lines are dominant but sodium I lines at 0.330μ, 0.589μ, 0.819μ, and 1.140μ are evident. Sodium II lines are not observed. Both barium and titanium have two electrons above a closed shell while sodium has one, apparently when these elements are excited within the argon vortex the line radiations observed are related to transitions of the electron just above this shell. Sodium is a less efficient radiator than titanium or barium as its neutral atom ionizes at 5.10 volts with a second ionization at 47.3 volts. The sodium electron can contribute to the electron population but has much less chance of dropping to the neutral ground state than barium or titanium electrons have of returning the singly ionized ground state.

Equation 4.0 may be evaluated for sodium using the assumptions that the plasma temperature is 10,000°K, electron density 2×10^{17} cm^{-3} and electron pressure 2.8×10^{5} dynes cm^{-2}. The ionization of the neutral sodium atom is 95.4%. The first or resonant atomic energy level of Na II occurs at 264,928 cm^{-1} above its ground state with a corresponding photon wavelength of 0.0378μ. Such an energetic radiation can not be excited in the high pressure vortex arc. It is interesting to note that even though sodium I has a lower ionization potential than either barium or titanium, it is less ionized under equal conditions of plasma temperature and electron pressure. This effect is due to the ratio of partition functions. The magnitude of the evaluated partition function for singly ionized sodium is much less than that of Ti II or Ba II. The spectral distribution of Figure 4.3.1 confirms this estimate as Na I lines are observed while Ba I and Ti I lines are essentially missing. The ionization of the neutral atom is determined approximately by the Menzel equation (4.0) as no correction is made for lowering of the ionization potential. In any case, as Na I does exist in a small percentage in the plasma arc core we can expect a shell with a much higher number density of Na I at some radius around the vortex axis. However if a radius is selected

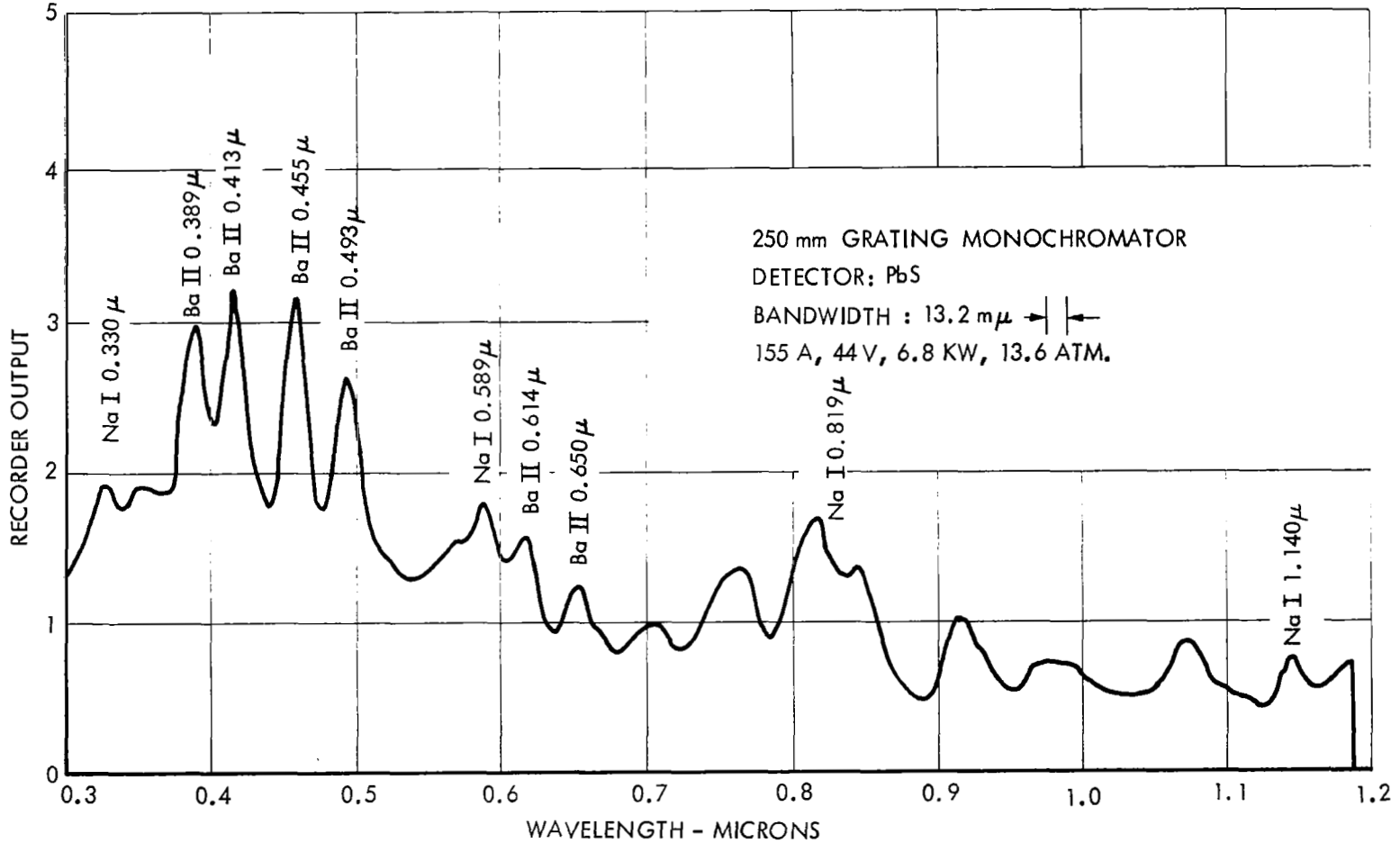

FIGURE 4.3.1 - SPECTRAL DISTRIBUTION: SODIUM AND BARIUM CHLORIDES

with a temperature of 9000°K, electron number density of 7×10^{16} cm^{-3} and electron pressure of 8.7×10^{4} dynes cm^{-2} the Na I is 96.4% ionized. This effect is due to the fact that the reduction in electron pressure in the essentially argon plasma slows the rate of recombination more than the rate of ionization decreases with reduction in temperature. If we move out to a very cold shell at a temperature of 4000°K, electron density of 1.7×10^{11} and an electron pressure of 0.094 dynes cm^{-2} the ionization of Na I increases to over 99%. The conclusion must be that sodium remains highly ionized within the argon plasma itself. However, neutral sodium vapor does surround the arc column and can be excited by the strong radiation flux emitted by the argon plasma. Such a sodium halo is in fact observed as a brilliant yellow cylindrical shell completely surrounding the central arc column.

Figure 4.3.2, Radial Profile of Na Cl + Argon Arc Radiation at 0.589μ, compares the radial profile of argon radiation at the sodium resonance line with the profile while injecting Na Cl. The arc column is known to become slightly larger as additives are injected but the increased radiation at radii from 2 mm to 4 mm is much greater than this effect. Figure 4.3.3 estimates the relative contribution of sodium as a function of radius.

The sodium halo at a zone 3.5 mm from the arc axis was studied by monochromator and the spectral distribution is shown in Figure 4.3.4. This position at 3.5 mm is well outside the usual vortex arc. Some radiation is undoubtedly scatter from the fused silica tube walls but the essential features must be as emitted from the halo. The sodium resonance lines are dominant but other lines are also evident. The lines around 0.42μ are from argon. The conclusion must be that most excitation this far from the arc axis is by photons emitted from the central argon plasma.

4.4 Hydrogen

Hydrogen is particularly interesting as can be seen from Figure 4.4.1 "Energy Levels - Argon vs Hydrogen". All energy levels of hydrogen up to the lowered ionization level should be highly excited. Radiation from the 3 to 2 transitions, Balmer α, at 0.6563μ would be particularly useful in filling the relatively low spectral energy region in the argon spectrum at near this wavelength. Figures 4.4.2 and 4.4.3 "Spectral Distribution: Hydrogen - Argon Vortex" taken using 10% hydrogen at 11 kw input power and 11 atmospheres pressure are quite instructive. Balmer α line radiation is much more intense than that of nearby argon transitions and shows a large amount of broadening. The half intensity line width is about 9 mμ. The line shape is then fairly well resolved by the 0.46mμ bandwidth used. The Balmer β line, 0.486μ is also strong and broad. However, the Balmer γ line

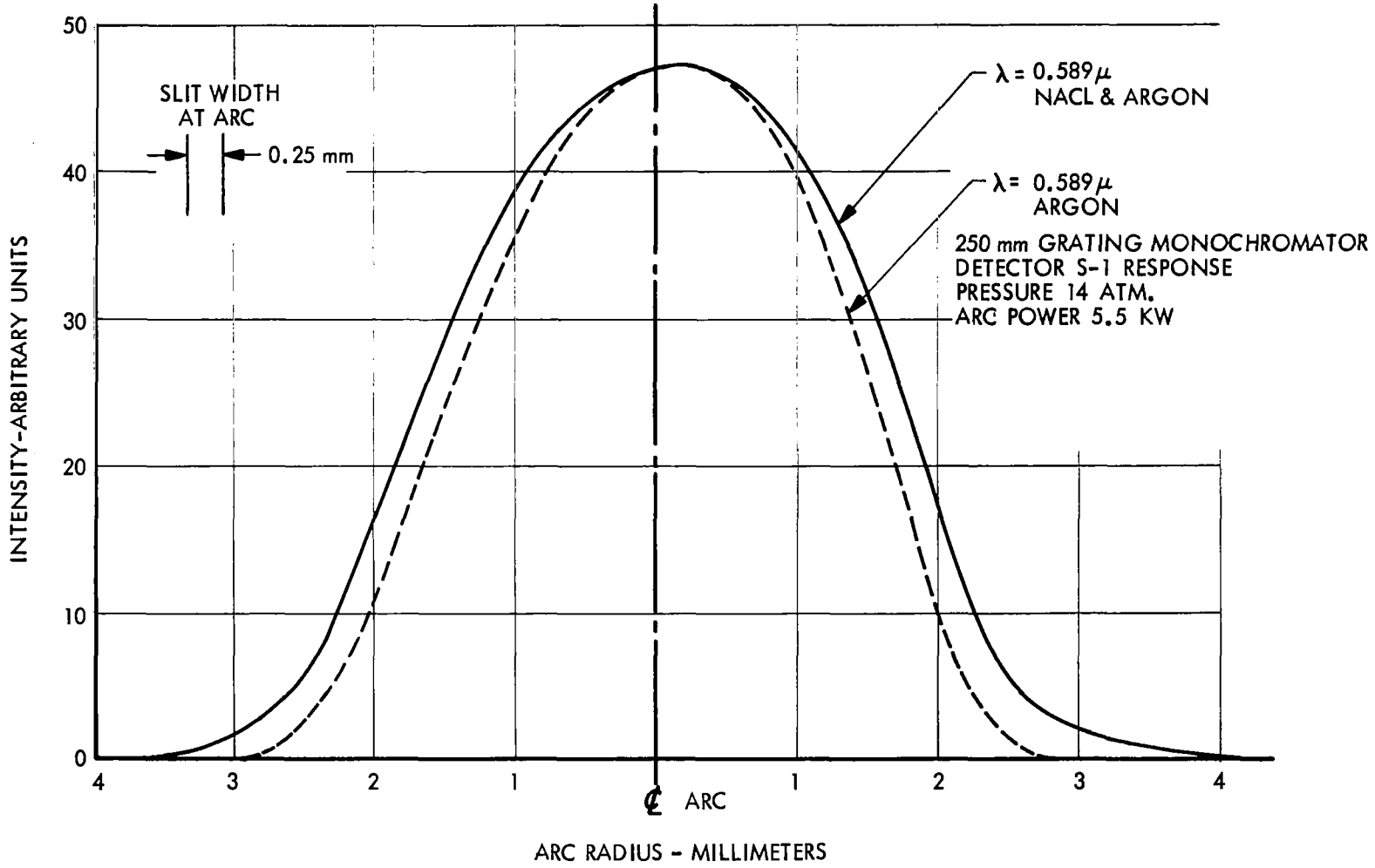

FIGURE 4.3.2 - RADIAL PROFILE OF NACL+ARGON ARC RADIATION AT 0.589μ

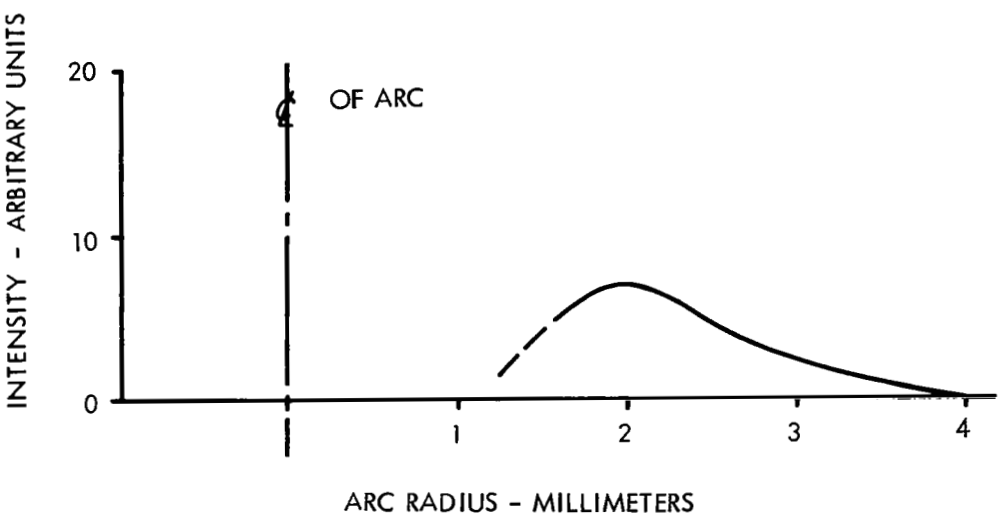

FIGURE 4.3.3 - INTENSITY CONTRIBUTION OF SODIUM AT 0.589μ VS RADIUS

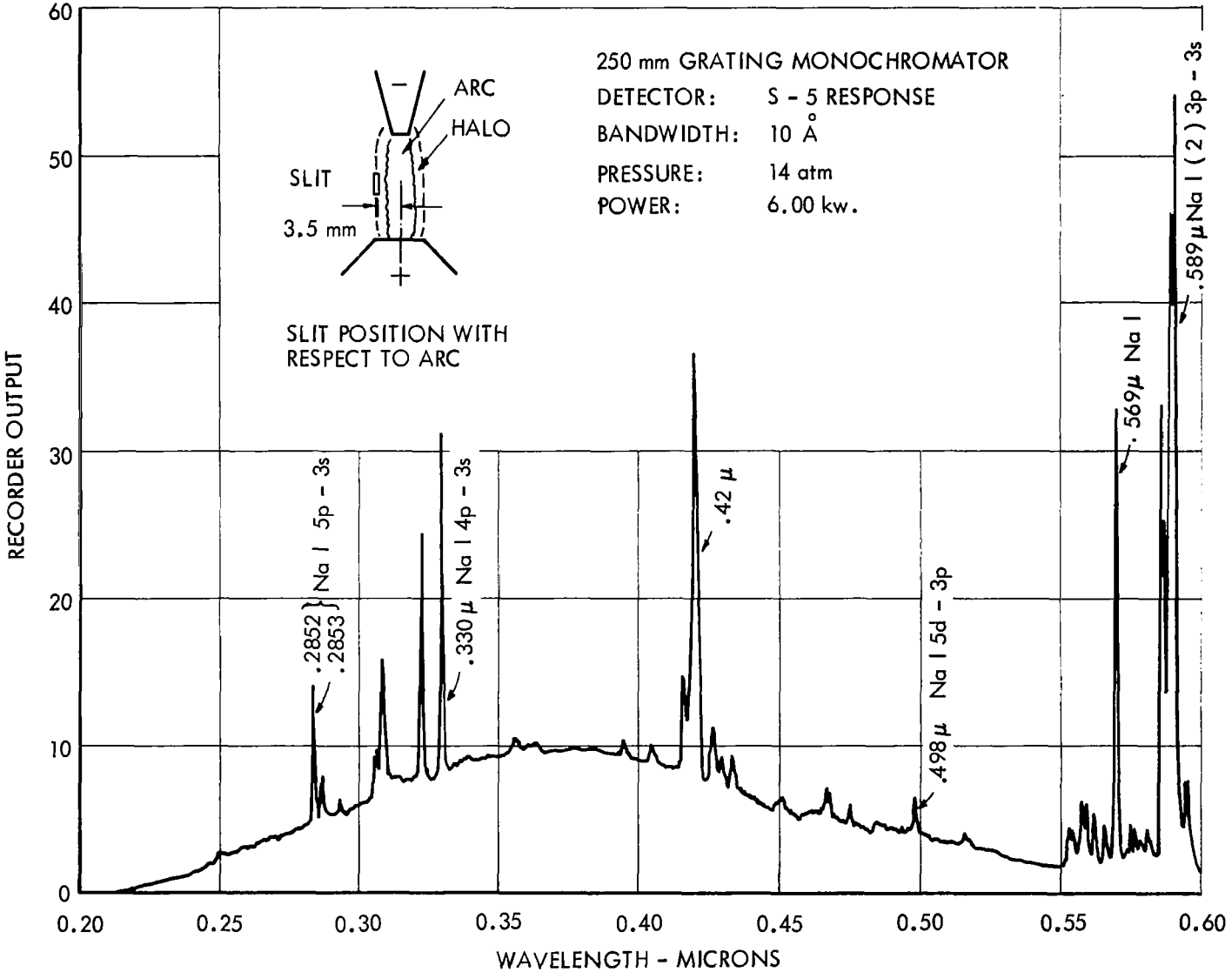

FIGURE 4.3.4 - SPECTRAL DISTRIBUTION OF SODIUM HALO

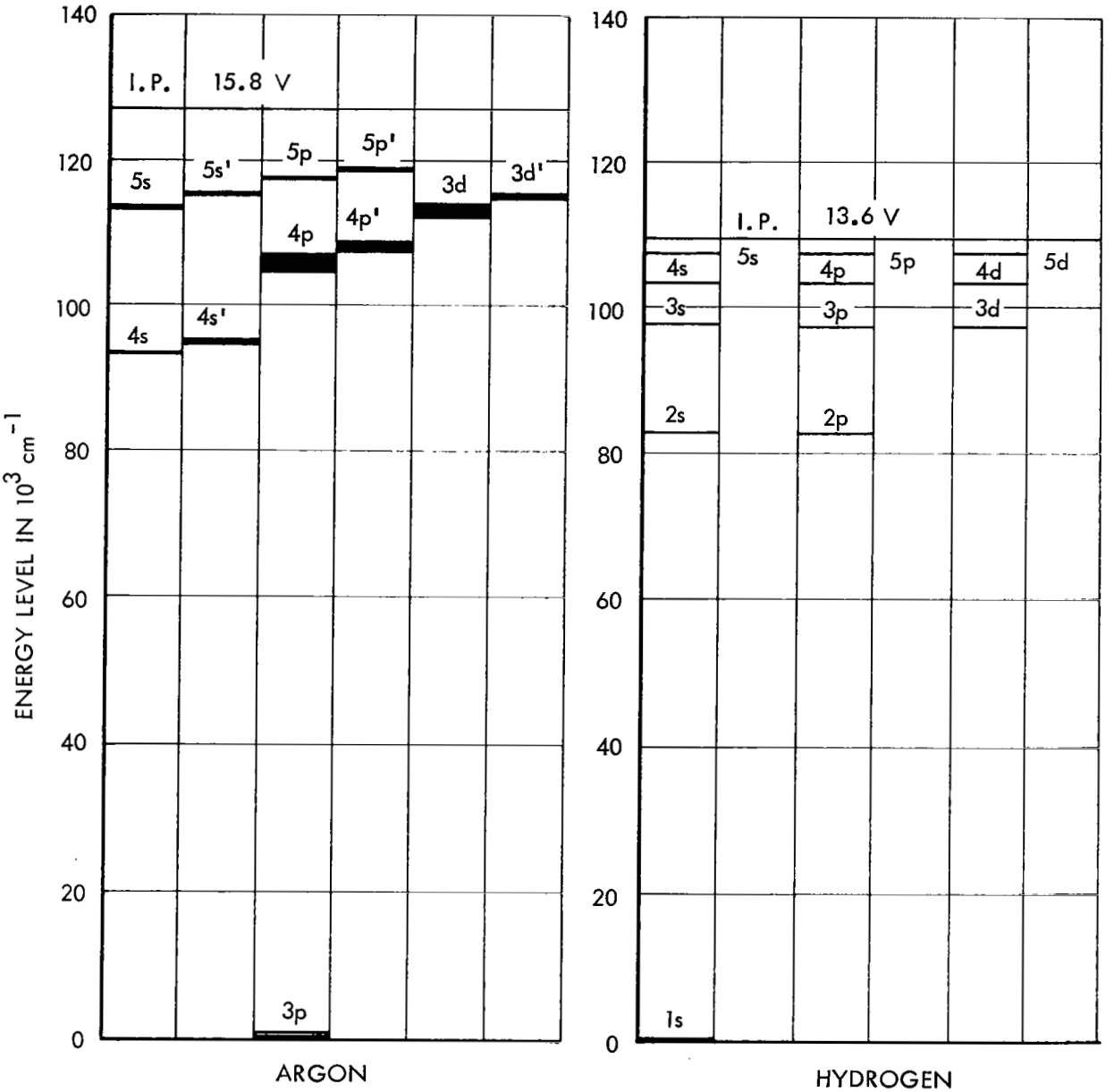

FIGURE 4.4.1 - ENERGY LEVELS - ARGON VS HYDROGEN

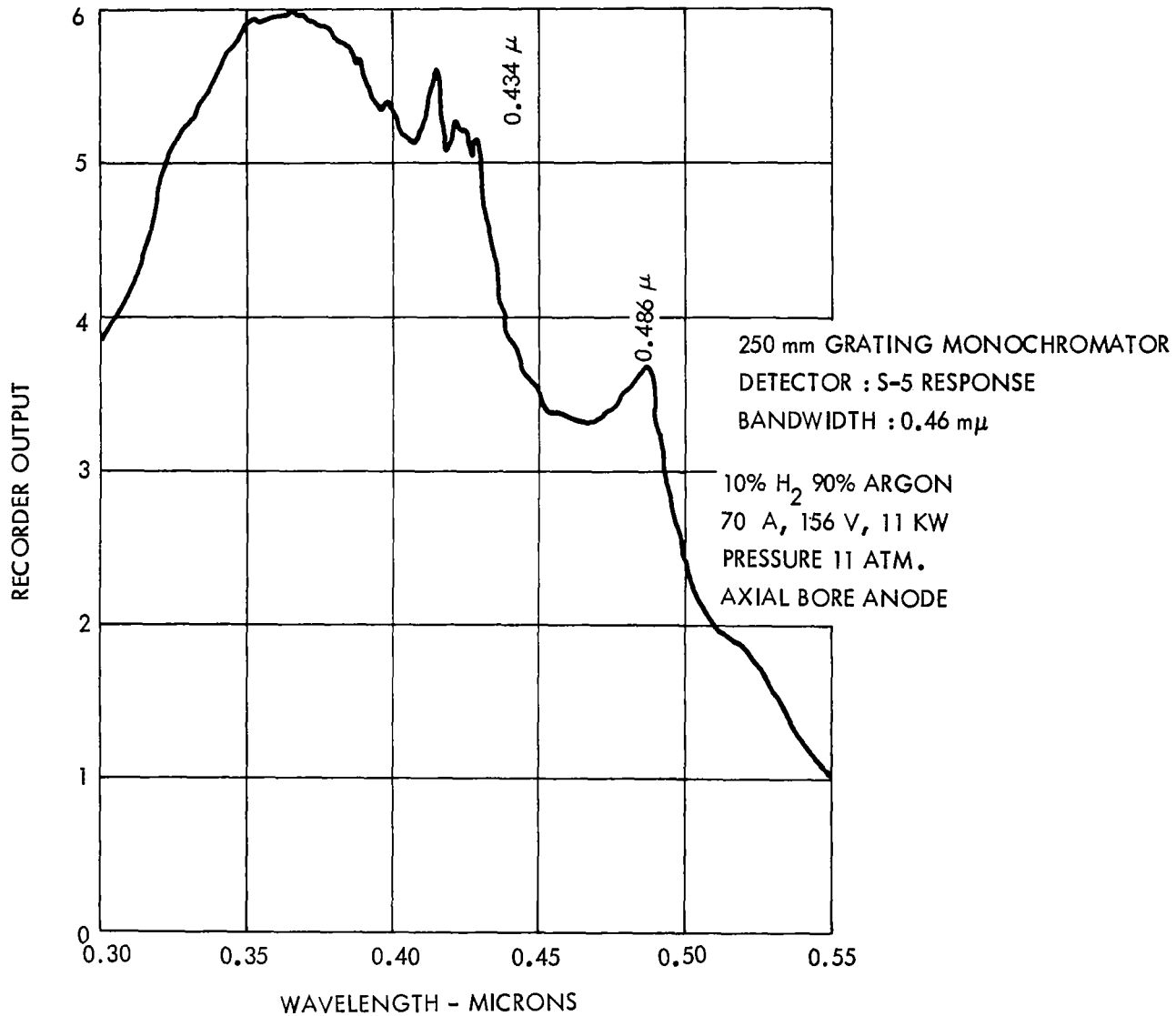

FIGURE 4.4.2 - SPECTRAL DISTRIBUTION: HYDROGEN - ARGON VORTEX - Hβ

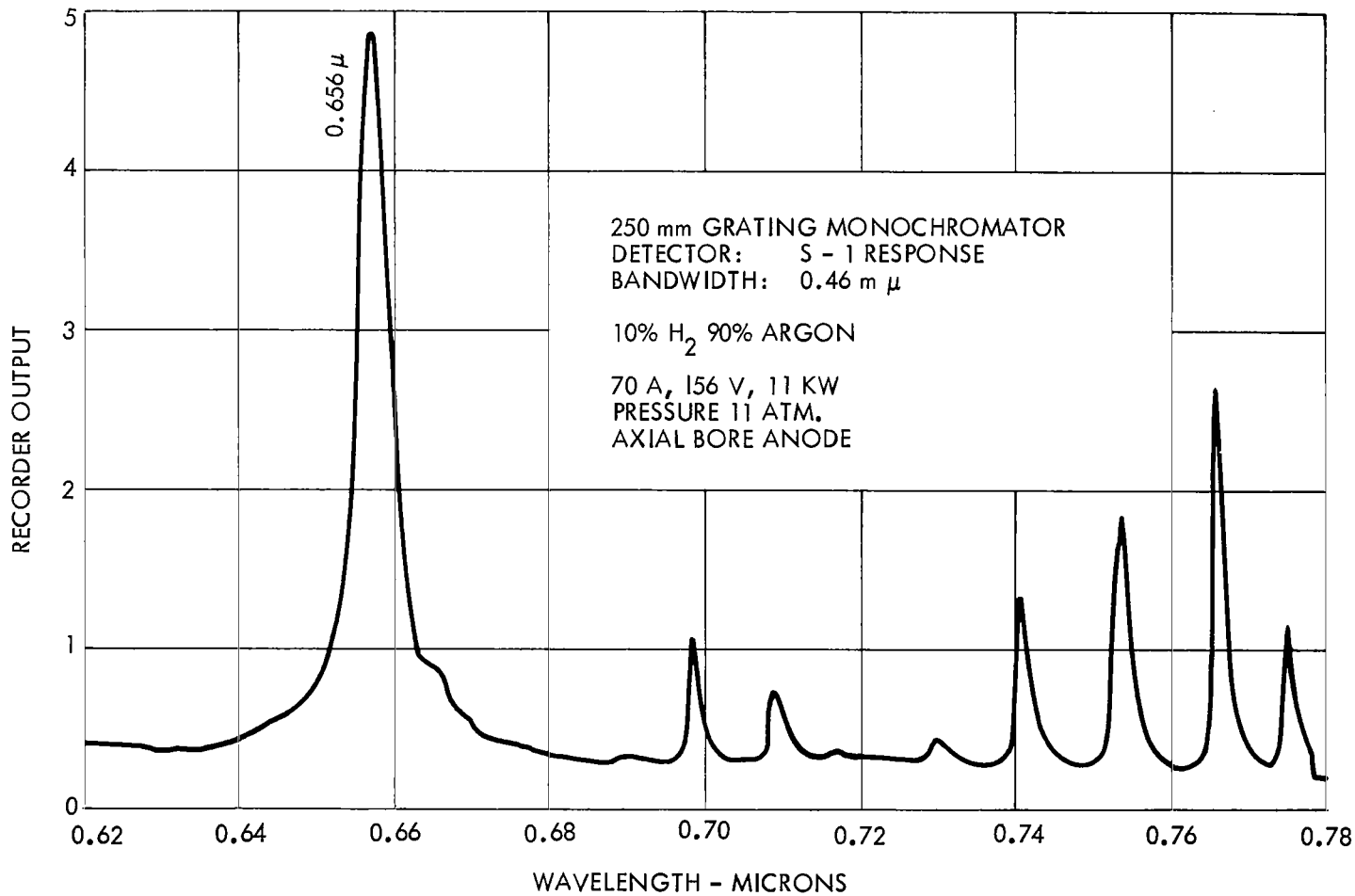

FIGURE 4.4.3 - SPECTRAL DISTRIBUTION: HYDROGEN - ARGON VORTEX - Hα

0.434μ is not evident. This is probably due to stripping of electrons from the higher term levels as has been noted with argon. The absence of Balmer γ radiation then confirms a lowering of the ionization potential. The results obtained were sufficiently interesting to justify a 25 kw run comparing argon and 5% H_2 + 95% argon vortex radiation. Figure 4.4.4 gives the results. The characteristic ultraviolet excess and visible deficiency of argon is clearly evident. 5% hydrogen causes a general decrease in radiative efficiency except around 0.656μ where the output increases. It can also be seen that near 0.486μ the 5% H_2 output is nearly equal to the original argon curve. The 5% H_2 - 95% argon curve is a better match of solar radiation than pure argon. It is likely that higher hydrogen percentages would produce an even better match but only with additional loss in total radiative efficiency. However, the evaluation of light source radiative efficiency must consider the spectral transmission of the solar simulation system. It is entirely possible that hydrogen-argon mixtures will have improved system efficiencies even though the total radiative efficiency of the source decreases.

The use of krypton instead of argon has been considered. Krypton has a 4p ground state, 5s resonance at 81,000 cm^{-1}, 5p levels from 91,000 cm^{-1} to 94,000 cm^{-1} and ionization potential at 14.0 volts. These levels are compatible with hydrogen and efficient excitation of Balmer α and possibly β lines is expected. The krypton-hydrogen mixtures should have less vacuum ultraviolet than argon. The atomic cross sections of krypton for electron collision are considerably greater than those of argon, and the radiation processes should be more efficient.

The use of xenon with hydrogen mixture has been studied by Thouret and Strauss (4.4) in compact arc lamps. They note that the excitation levels of hydrogen are higher than those of xenon. For example, the ionization potential of xenon is 12.1 volts or 97,800 cm^{-1} while the 3rd quantuum level of hydrogen is 97,500 cm^{-1} and the 4th at 102,800 cm^{-1}. Some Balmer α radiation can be expected but excitation can not approach the extent likely with argon and krypton. Although hydrogen does not substantially participate in the excitation and ionization processes of the short arc lamps, hydrogen-xenon mixtures merit study in the vortex arc with its higher excitation potentials if the addition of radiation at wavelengths near 0.656μ proves to be desirable.

The addition of hydrogen for the purpose of further constricting the inert gas vortex arcs would serve no useful purpose. Essentially, the radial dimension of an arc is controlled by the mean free path of electrons throughout the arc volume. The mean free path is inversely proportional to the product of the atomic number

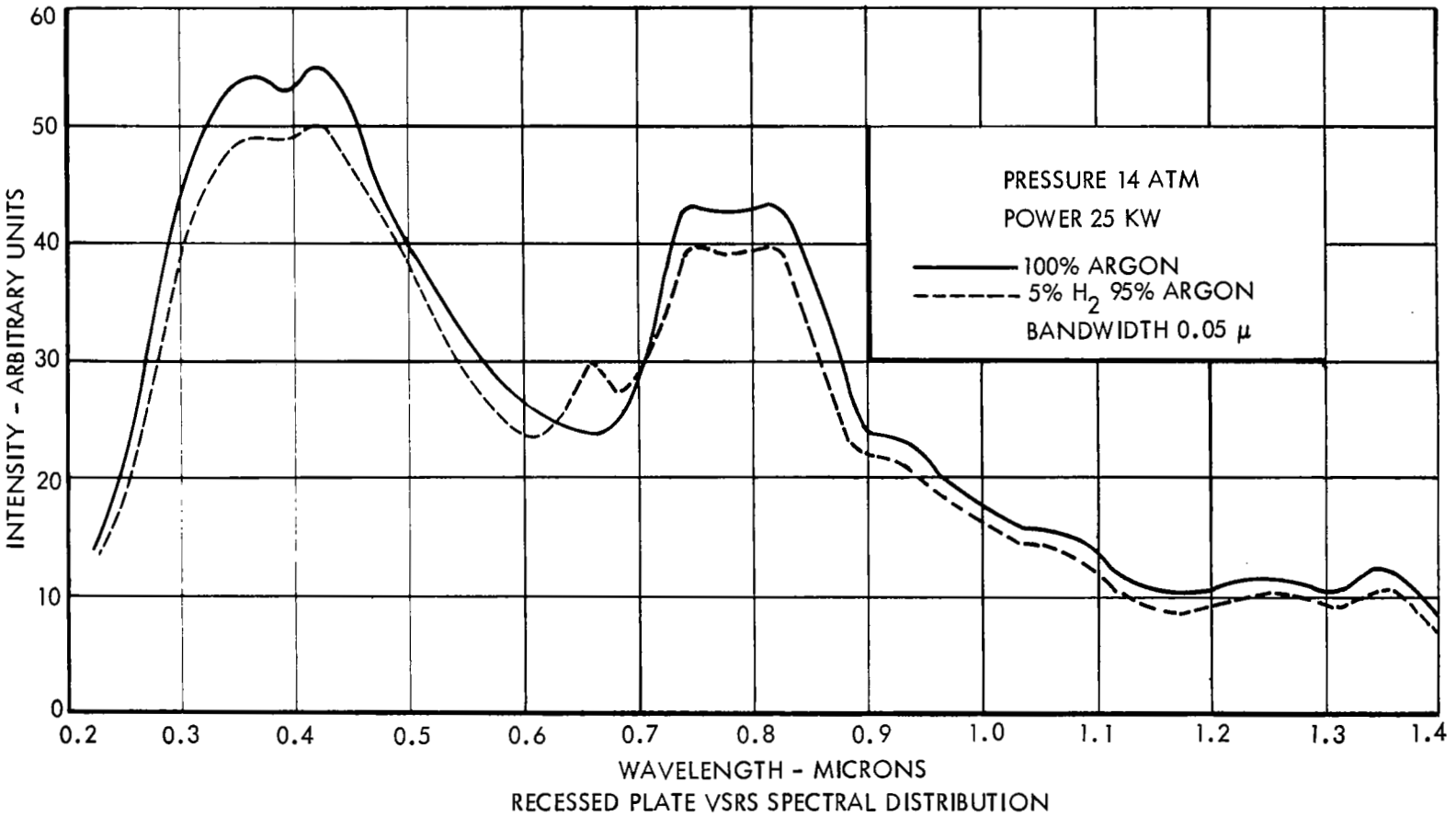

FIGURE 4.4.4 - SPECTRAL DISTRIBUTION: ARGON vs ARGON + 5% H_2

density of the arc gas and its electron collision cross section. As the vortex flow maintains a cool high density gas very close to the arc axis, electron mean free path decreases very rapidly as an electron moves out from the arc core. The addition of molecular hydrogen with its large cross section may have some effect but this was not apparent with the 25 kw run. The number density in a typical argon vortex at about 2 mm from the arc axis (just outside the arc) is believed to be $\approx 3.7 \times 10^{20}$ cm^{-3} operating with $\approx$ 14 atmospheres input pressure. At this same location the number density of 5% hydrogen would be 1.8×10^{19} cm^{-3}. Considering electrons of 4 ev energy argon's elastic collision cross section is 7.5×10^{-16} cm^2 while molecular hydrogen's is 14×10^{-16} cm^2. The product of number density times cross section or number of collisions per centimeter would then compare as 2.8×10^5 cm^{-1} for argon to 2.5×10^4 cm^{-1} for molecular hydrogen making argon the more important constricting gas. At lower energies the effect of 5% hydrogen becomes more important being about equal to argon at one electron volt and less. It is interesting to note that assuming an atomic temperature of argon at around 12,000°K (about 1.03 ev) in the arc core the atomic number density would be $\approx 7.8 \times 10^{18}$ cm^{-3} and the number of elastic collisions per centimeter for 4 ev electrons would be 5.7×10^3. This number would increase by a factor of 3 as electron energies continue to increase under the arc gradient to 12 - 14 ev where inelastic collisions become important. It is very evident that electron mean free path in the vortex arc is probably 50 times greater along the arc axis than it is approximately 2 mm from the axis in the cool vortex flow. The presence or absence of hydrogen does not appreciably change this condition.

4.5 Bromine

Figure 4.5 sketches the energy levels of bromine. This diagram is presented as the salts studied were often compounds of bromine. 6p - 5s and 5p - 5s transitions should produce observable radiation, however, bromine lines have not been noted. Assuming typical plasma conditions of T = 10,000°K, $n_e = 2 \times 10^{17}$ cm^{-3} and $P_e = 2.8 \times 10^5$ dynes cm^{-2}, Equation 4.0 can be evaluated to approximate the composition of bromine in the argon plasma. This turns out to be 3.7% singly ionized and 96.3% the neutral atom. Lowering of the ionization potential which is normally at 11.84 volts to 10.8 volts would increase ionization to 12% which is not enough to explain the absence of bromine lines. It appears possible that the ionization lowering is sufficient to reduce the number of bromine atoms excited to 6p levels. This process appears to occur with Hγ. The 5p - 5s lines are mostly infrared at wavelengths which were not carefully studied. The 5s - 4p lines are in the vacuum ultraviolet and were not measured. These factors may be sufficient to account for the lack of bromine radiation.

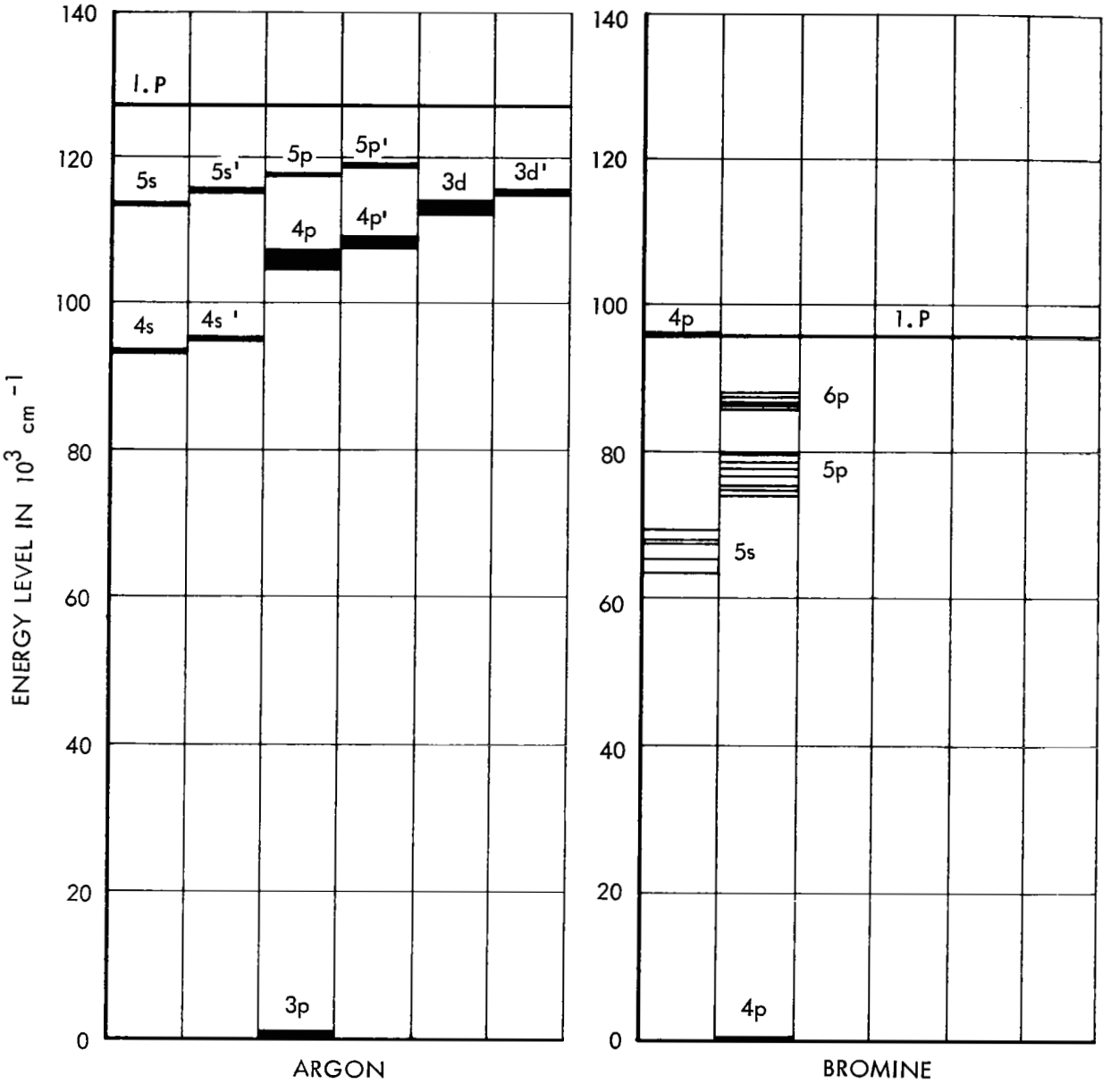

FIGURE 4.5 - ENERGY LEVELS - ARGON VS BROMINE

The compounds used as additives are easily dissociated in the plasma as is indicated by the following table:

Table 4.5 Dissociation Energy

Compound	Electron Volts
Na Cl	3.58
Na Br	3.85
Ba Cl	2.7
Ba Br	2.8
Ba O	4.7
Ti O	6.9
Hg Cl	1.0

This dissociation energy usually is returned to the electrodes as the atoms recombine mostly on the metallic surfaces.

4.6 Lanthanum

Lanthanum follows barium in the periodic table of elements. It has two electrons in the P shell as does barium but has an additional electron in the underlying O shell. Considering the excellent radiating properties of barium it appeared that lanthanum could be an improvement. Figure 4.6.1 sketches the atomic energy levels of La I and II. Comparison of these levels with those of barium, Figure 4.2.1 will show a general similarity. The 4f - 5d transitions should produce radiation in the visible where with barium similar transitions were in the intermediate ultraviolet. Unfortunately, the energy difference between 6p - 6s levels is greater than with barium. Quoting from Meggers (Ref. 4.2.2) "La II is the most completely developed example of a 2-electron spectrum which has yet been investigated." Large numbers of lines should be expected and would minimize problems rising from use of a strong line source in a solar radiation simulator.

Judging from Equation 4.0, the condition of lanthanum in a typical argon plasma with a temperature of 10,000°K, electron density of 2×10^{17} cm^{-3} and electron pressure of 2.8×10^{5} dynes cm^{-2} is as follows:

Neutral, La I	2.5%
Singly Ionized, La II	94.0%
Doubly Ionized, La III	3.5%

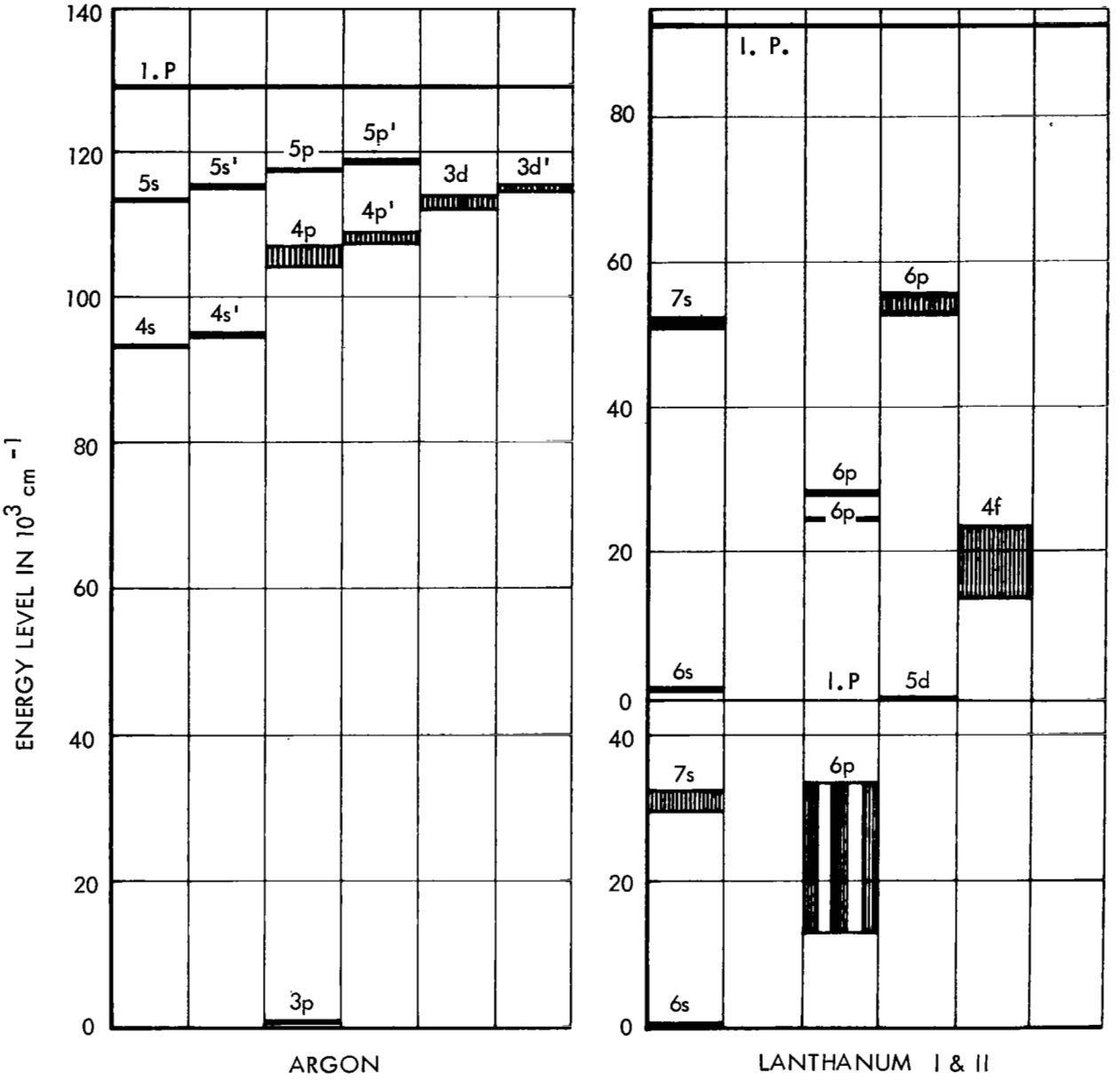

FIGURE 4.6.1 - ENERGY LEVELS - ARGON VS LANTHANUM

The important radiator then is La II.

Figure 4.6.2, Spectral Distribution - Lanthanum Chloride, was taken while injecting the lanthanum salt into a 6 kw argon plasma operating at a pressure of 14 atmospheres. Numerous lanthanum II lines are observed and the more important are indicated. Unfortunately, most of the lanthanum contribution is at wavelengths shorter than 0.45μ. This near ultraviolet radiant power does not improve the spectral match of the argon vortex to the sun.

4.7 Mercury

Mercury vapor is used in a number of successful light sources and partly for this reason its injection into the argon plasma was studied. Mercury erodes most metals used in fabrication of vortex arc devices making its use inconvenient. Experiment early in the program showed that liquid mercury could be introduced to an electrode and allowed to boil off into the plasma column. This feed technique proved to be erratic. Later on in the program powder feeding techniques improved and mercury was added to the arc as the bromide or chloride at flow rates of 1.0 mg sec^{-1}.

The typical argon plasma conditions were assumed to be those related to 10,000°K. With this assumption and by evaluating the Menzel equation, mercury is found to be 21% ionized. Correction for lowering of the ionization potential would increase the ionization percentage. In either case mercury in the argon vortex is more highly ionized than the argon.

Figure 4.7.1, Energy Levels - Argon vs Mercury, indicates that Hg I and lower level Hg II lines should be observed. Figure 4.7.2 is a trace of the monochromator recorder output between 0.20μ and 0.60μ. The strong Hg I lines are clearly evident. A few Hg II lines with lower energy levels at $6s^2$ are also in evidence. Figure 4.7.3 traces the spectral distribution between 0.21μ and 0.29μ in more detail. The cluster of Hg II lines in vicinity of 0.22μ to 0.23μ is clearly outlined.

The primary purpose for the addition of Hg was for decreasing the energy deficiency of the argon spectrum relative to the solar spectrum in the 0.5μ to 0.7μ region. Mercury has a number of strong lines in this region. The strongest line 5460 Å results from the 7s - 6p transition in the triplet levels. Unfortunately the addition of mercury also added a large amount of unwanted

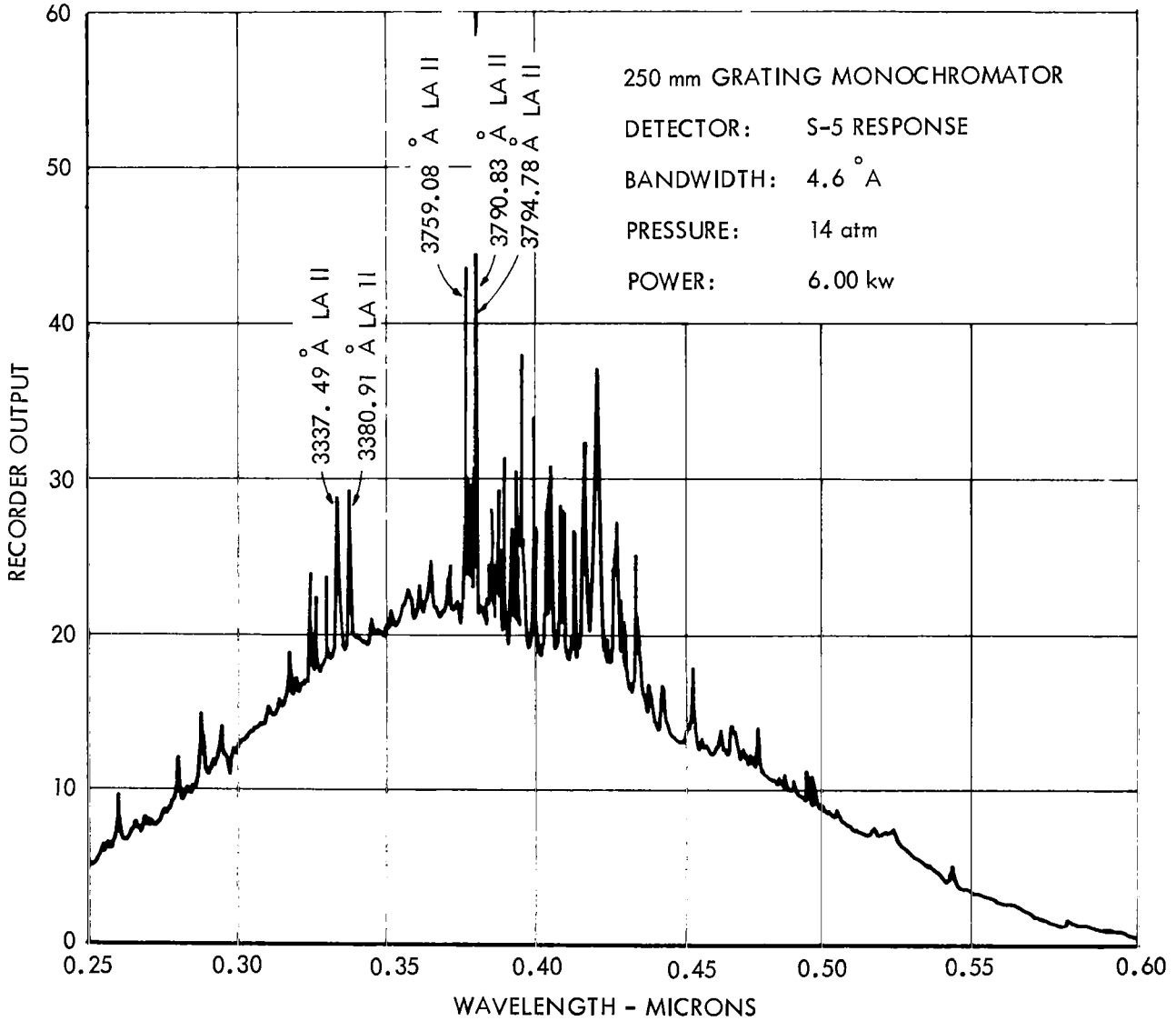

FIGURE 4.6.2 - SPECTRAL DISTRIBUTION: LANTHANUM CHLORIDE

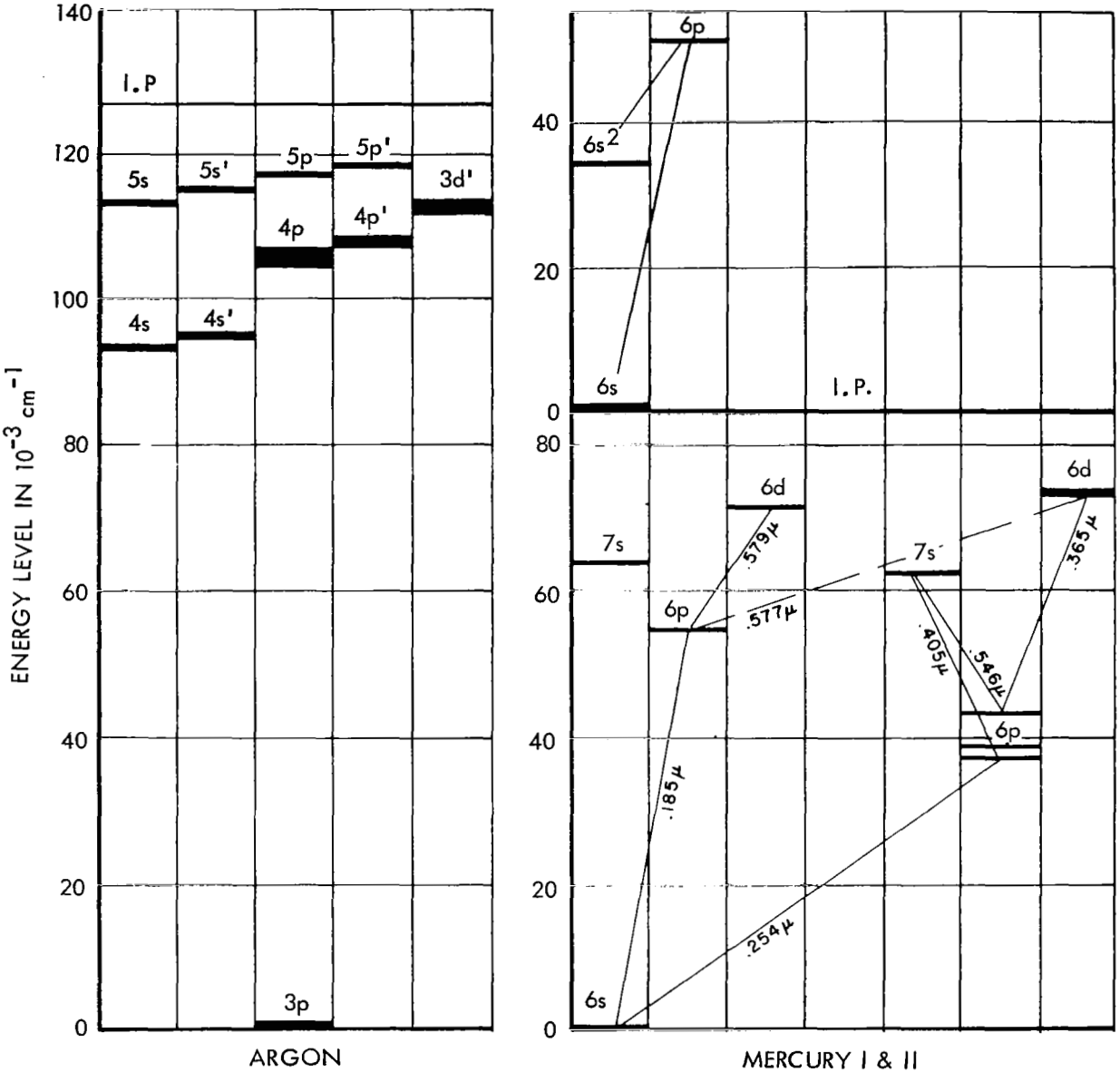

FIGURE 4.7.1 - ENERGY LEVELS - ARGON VS MERCURY

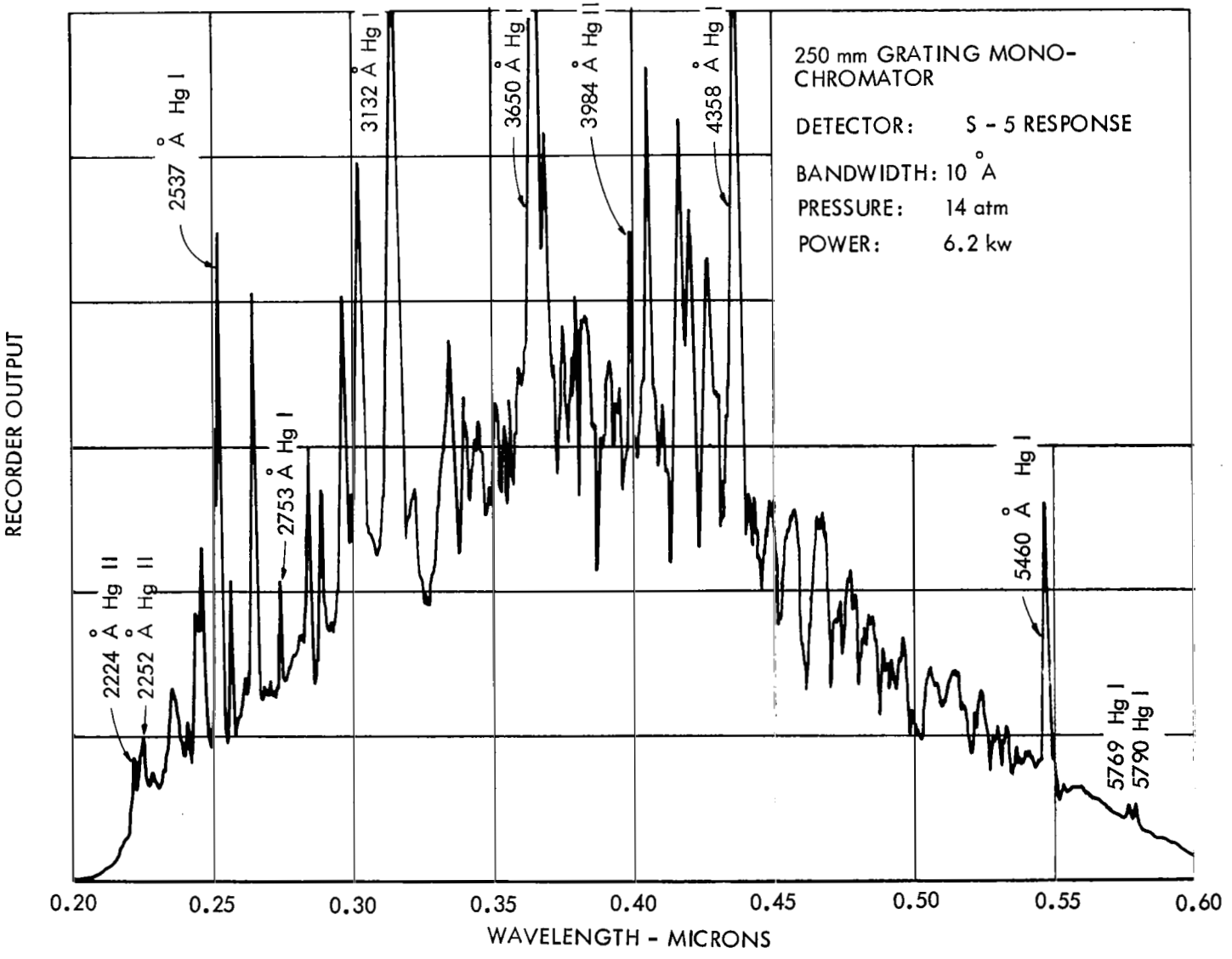

FIGURE 4.7.2 - SPECTRAL DISTRIBUTION: MERCURIC CHLORIDE

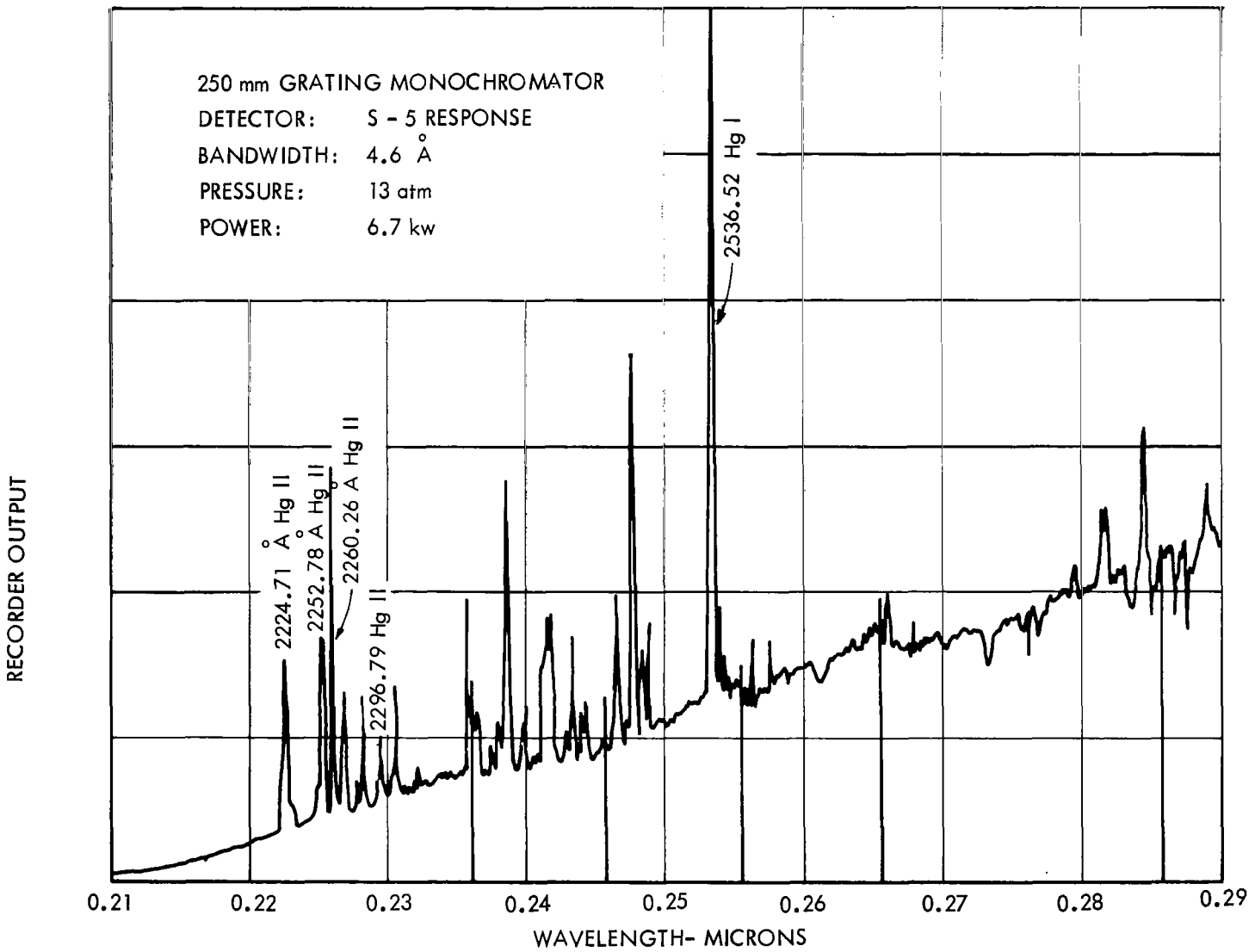

FIGURE 4.7.3 - SPECTRAL DISTRIBUTION: MERCURIC BROMIDE

ultraviolet radiation due to the strong resonance lines and the great number of UV triplet transitions.

5.0 CONTINUUM RADIATION

Much of the work on this contract was directed toward improving simulation of the solar spectrum as observed in space by injecting additives into an argon vortex arc with the purpose of modifying the argon spectrum. The theoretical work accompanying these experiments resulted in a better understanding of vortex arc physics. This improved physics was in turn applied toward solution of the fundamental problem, improvement of solar radiation simulation. The continuum radiation processes proved to be particularly important with a growing indication that xenon in the high pressure vortex arc would produce an excellent solar match.

The radiation resulting from the spontaneous recombination of an ion and an electron forms a continuum which in a high pressure plasma, proves to be more important than the line radiation process. As discussed by Mohler (Ref. 1.4) the rate of recombination, dn_i/dt, can be expressed by the relation

$$dn_i/dt = vq(v)n_i n_v \tag{5.1}$$

where q(v) is the recombination cross section for electrons of speed v, and n_i and n_v are number density of ions and electrons. The radiant energy emitted per unit volume per steradian, S_c, is then

$$S_c = (4\pi)^{-1} vq(v)n_i n_v h\nu \tag{5.2}$$

q(v) is large for electrons of $v = 0$ but in a given plasma very few electrons exist with zero speed. At higher electron speeds say comparable to 0.4 ev, $q = 5 \times 10^{-18}$. Mohler also points out that while the cross section is infinite for $v = 0$ it decreases as the reciprocal of the electron's kinetic energy or

$$q = \text{const}/E_e$$

or using our single data point

$$q = 2 \times 10^{-18}/E_e \tag{5.3}$$

Figure 3.2, Electron Energies at 16,000°K and 11,600°K vs Argon Cross Sections, gives a plot of the recombination cross section along with elastic, excitation and ionization cross sections. Above these curves is a Maxwellian distribution of electrons plotted as a relative number against electron energy. Comparing this distribution against the cross sections, it is clear that most electron collisions are elastic. Only at the extremes do radiative recombination and excitation and ionization become important.

The Kramers-Unsold theory (Ref. 3.1.1 and 3.1.4) simplifies the product of n_v and, q(v) and v to obtain

$$S_c(T) = \bar{g}\ 5.41 \times 10^{-46}\ Z^2\ n_i n_e\ T^{-0.5} \qquad (5.4)$$

$S_c(T)$ is in watts cm^{-3} str^{-1} per unit frequency. This equation was used in Section 3.1.2. The $T^{-.5}$ term corrects for the decrease in proportion of electrons of relatively slow velocity as temperature increases. These electrons are most effective in the recombination processes. The term $\bar{g}$ is considered as having an average value of 2.3, however it is actually wavelength dependent as the recombining electrons must move to the actual energy levels of the atom.

5.1 Argon

The energy level diagram of argon I, Figure 1.4, can be used to predict peaks in the argon continuum. As has been pointed out previously, the microfield effects in these high pressure plasmas lower the effective ionization potential of argon from 127,100 cm^{-1} to about 120,000 cm^{-1}. One continuum peak, therefore, should be caused by recombination from 120,000 cm^{-1} to the 4s and 4s' levels while another should occur on recombination to the 4p and 4p' levels. The corresponding wavelengths are .37μ to .41μ and .68μ to .88μ. The shorter wavelength peak should have a greater intensity in terms of power per unit wavelength as the recombination process is concerned with numbers of electrons while power involves $h\nu n_e$.

Referring to Figure 1.2, Spectral Distribution: Argon VSRS vs Sun, it can be seen that the argon peaks are quite well located. Also the peak near .4μ is nearly twice that at .8μ. If line radiation could be subtracted the relation might be quite close. The bulge in the spectral distribution at 1.2μ extending to the edge of the plot can be traced to recombination at the lower 3d levels. The interesting peaking of the high pressure argon spectrum at the wavelengths of 4s - 5p transitions around .40μ to .42μ in wavelength is probably due to a merging of Stark

broadening effects into continuum processes. In other words, the electron at 5p levels needs only a small additional energy to become free. The broadened 4s - 5p line radiation when added to the continuum then can determine the actual spectral peak.

5.2 Cesium

Mohler's work with cesium (Ref. 1.4) is of interest here as cesium's ground state is 6s and similar to the resonance level, also 6s, of xenon. Figure 5.1 gives the cesium continuum observed in a discharge tube at a region with an ion number density of 10^{12} to 10^{14} cm^{-3} and very low electron speeds. The lowering of ionization potential is quite small and it is assumed that free electrons recombine from very near this level at 31,407 cm^{-1}. Radiation wavelengths produced by recombination to the 6s, 6p and 5d levels are indicated by the dashed lines. In every case the actual measured peak is displaced toward longer wavelengths. This displacement indicates that the ionization potential was lowered ≈ 0.1 ev even with ion densities orders of magnitude lower than in a high pressure vortex arc. The difference in energy between the small peak observed near 0.33μ (6s) and 0.52μ (6p) is about 1.38 ev. Considering the similarity of the cesium and xenon atom a somewhat similar energy spacing is to be expected with xenon. The difference being that the xenon 6s peak will be much larger than the 6p peak.

5.3 Xenon

The Stark broadening coefficients for xenon are assumed to be larger by a factor of three than those of argon and similar to those of cesium. The merging of line broadening into the continuum should take place at relatively lower levels than in argon. In any case xenon's 6s - 7p lines (See Figure 5.2) similar to argon's 4s - 5p transitions should be well broadened and add sufficient energy to locate the spectral distribution peak near 0.47μ. This possibility should result in an excellent match with the solar spectrum in space as the peak here is also at 0.47μ.

The structure of the xenon energy levels, Figure 5.2, is quite similar to argon with the resonance level at 6s instead of 4s. One important difference is that the 6s' level is very close to the 6p level while with argon 4s' is just slightly higher than 4s. It is believed that in the vortex arc the lowering of xenon's ionization potential will be greater than that observed with argon. For first investigations the effective ionization potential was taken at 88,500 cm^{-1}. This assumption places a continuum peak between 0.46μ and $.49\mu$ for the 6s level, between $.81\mu$

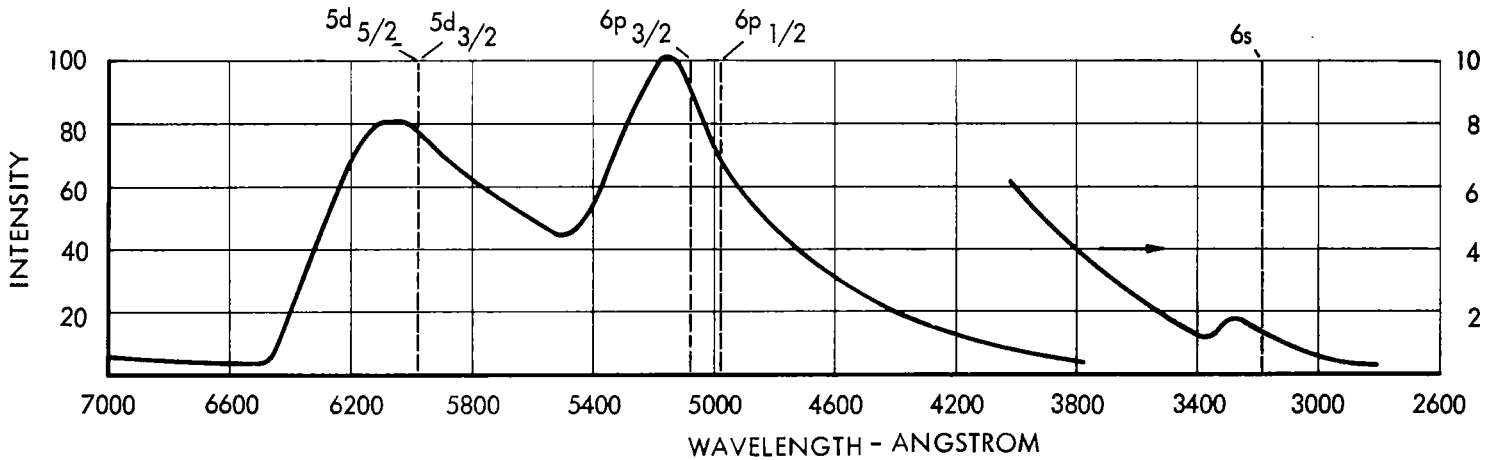

FIGURE 5.1 - INTENSITY DISTRIBUTION: CONTINUOUS EMISSION SPECTRUM OF CESIUM

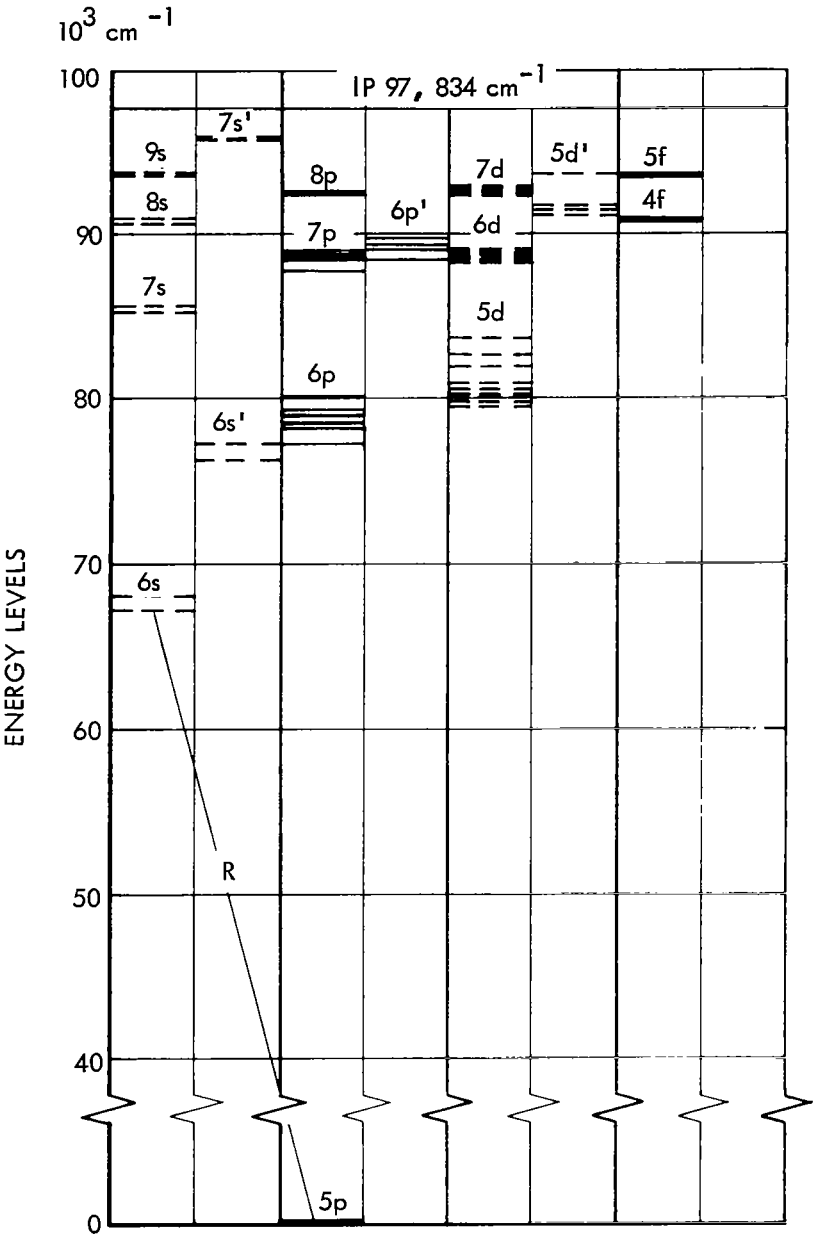

FIGURE 5.2 - ENERGY LEVEL DIAGRAM XENON I

and .89μ for 6s' and .89μ and longer wavelengths for 6p. A xenon vortex arc operating at 21.7 kw and 12.7 atmospheres was then observed at 90° to the plasma column using the techniques described in Section 2.4. The following table gives the three interval spectral distribution obtained by thermopile and short wavelength cutoff filters.

Table 5.0 21.7 kw, 12.7 atm. Xenon Spectrum

Wavelength Interval	Radiant Power Watts str^{-1}	Percent of Total
0.2μ to 0.5μ	293	35.9
0.5μ to 0.9μ	322	39.5
0.9μ to 2.6μ	200	24.6
Totals	815	100.0

A comparison with a similar observation of an argon vortex, Figure 3.1.3, will show that xenon has a proportionally smaller amount of radiation in the 0.2μ to 0.5μ interval. A similar distribution for solar radiation is of interest.

Table 5.1 Solar Irradiance (m = o)

Wavelength Interval	Irradiance Watts m^{-2}	Percent of Total
0.2μ to 0.5μ	327	24.1
0.5μ to 0.9μ	600	44.2
0.9μ to 2.6μ	428	31.7
Totals	1355	100.0

Essentially, the xenon vortex plasma at 12.7 atmospheres has an excess in the ultraviolet. However, the ratio of radiation in the 0.5μ to 0.9μ interval to the 0.9μ to 2.6μ interval is very close to that of sunlight in space.

The monochromator data obtained by using sodium salicylate with a 1P28 photomultiplier, a lead sulfide cell and adjusted to be consistent with Table 5.0 was prepared as Figure 5.3, Spectral Distribution: Xenon Vortex. The peaks caused by recombination to 6s, 6s' and 6p levels may be obscured by broadened line

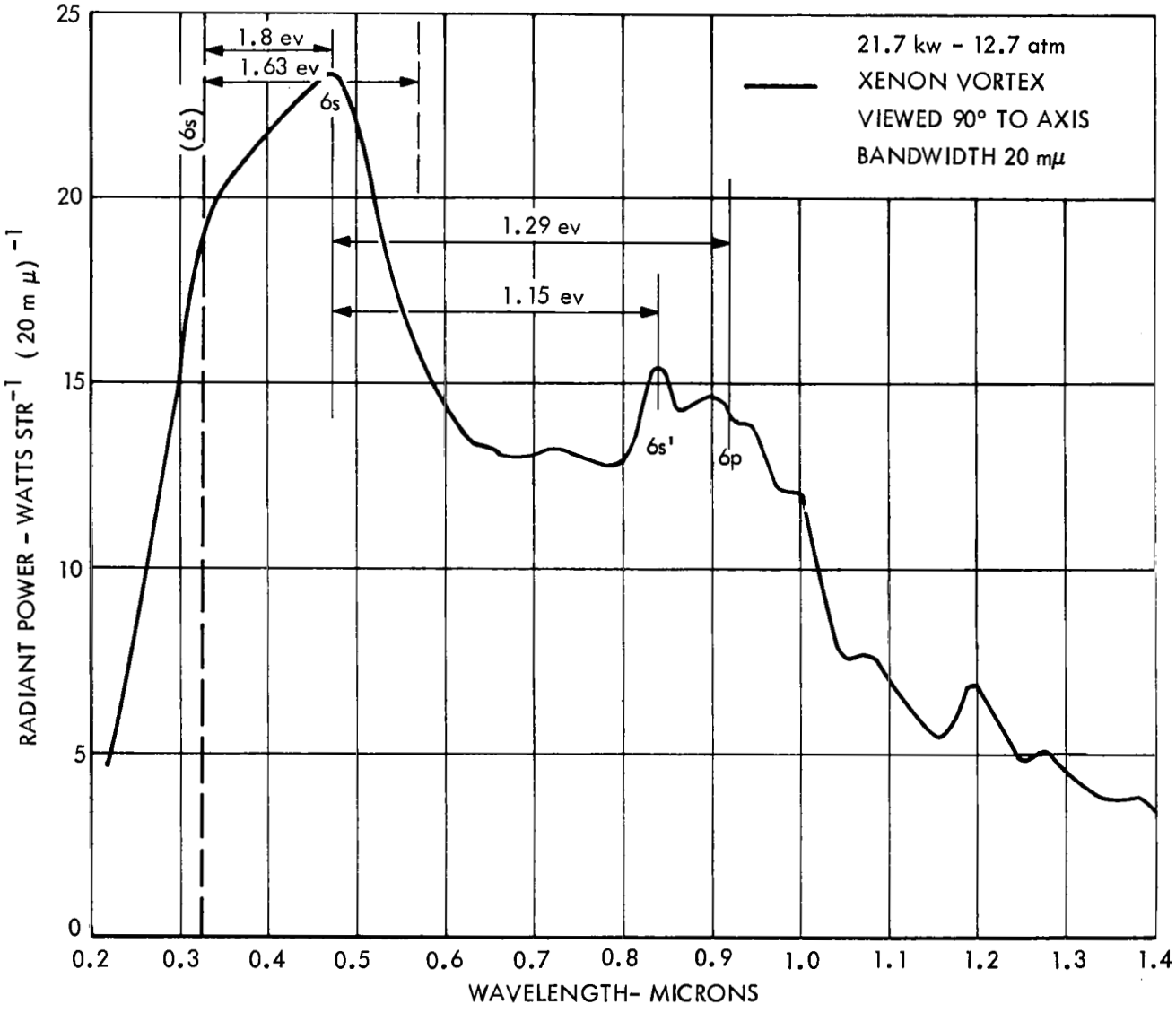

FIGURE 5.3 - SPECTRAL DISTRIBUTION: XENON VORTEX

radiation but should be somewhere near the indicated wavelengths. The 6s peak would have been located at 0.325μ if no lowering of ionization potential had occurred. However, this data indicates a lowering of 1.18 ev. The 6s' and 6p peaks are located at 1.15 ev and 1.29 ev from the actual 6p peak. These spacings are consistent with the atomic energy levels concerned and tend to confirm the importance of recombination radiation.

A very promising approach to improving the match of the xenon vortex spectrum to the sun is to increase operating pressure to around 20 atmospheres. At this pressure and a temperature of 12,000°k it is estimated that ion and electron number densities will approach 3×10^{18} cm^{-3}. Operating conditions can be adjusted to achieve a lowering of ionization potential by ≈ 1.63 ev. Such a lowering would minimize the ultraviolet excess and place the 6s continuum peak near 0.56μ as dashed in Figure 5.3. The peak would be broad on the short wave side for a good solar match. On the long wave side the 6p peak would shift to 1.38μ and be very broad, the 6s' peak should be evident at 1.2μ. All of these predicted changes appear to be favorable from the solar radiation simulation standpoint.

6.0 COMPARISON WITH SOLAR SPECTRUM

Comparisons with the solar spectrum have been made using the Johnson curve as the zero air mass spectral distribution. Due to instrumentation limitations the spectral measurements of radiation from the vortex arcs was accomplished between 0.2μ and 1.4μ. This interval accounts for 86.4% of the solar spectrum. The remaining 13.6% of longer infrared is not accurately known. The high density plasmas studied must radiate at all wavelengths due to free-free and some free-bound continuum. The only spectral gaps should be due to fused silica absorption at 2.7μ and at wavelengths longer than 4.0μ. The long infrared radiation of the vortex arcs is likely to be proportionally less than in solar radiation. This deficiency is not critical as surface heating and photochemical effects usually are not sensitive to wavelength or photon energy at wavelengths longer than 1.0μ. All of the radiation sources discussed in the paragraphs following could utilize a somewhat larger collection solid angle for the simulating beam to give equal total power. This change would increase the characteristic ultraviolet excess but would improve spectral match from 0.45μ to 0.8μ. The near infrared excess would be increased but would compensate for deficiencies in wavelengths longer than 1.4μ.

The specific intensity of the solar beam is 2060 w cm^{-2} str^{-1} assuming that solar irradiance at the earth's orbit is 1400 w m^{-2} and field angle is 32 minutes.

All of the vortex radiation sources tested can exceed this specific intensity or radiance. For example, the 21.7 kw, 12.7 atm xenon vortex plasma discussed in Section 5.3 has a cross section area of 33 mm^2 as observed from 90° to the long axis. The radiant power at this angle is 815 watts str^{-1}. This makes the average radiance 2500 watts cm^{-2} str^{-1} or sufficient to duplicate the specific intensity of the solar beam if an optical system with 82.5% transmission can be achieved.

The following paragraphs assume optical collection of source radiation to form a beam which equals solar radiant power between 0.2μ and 1.4μ. A linear scale is used so that the discrepancies will be immediately evident.

The 25 kw, 14 atm argon vortex spectrum is compared with the zero air mass solar spectrum in Figure 1.2. An excess of ultraviolet exists from 0.2μ to 0.4μ. At 0.3μ this amounts to 180% more than the solar intensity. A deficiency exists in the visible and amounts to 48% of the solar intensity at 0.6μ. There is an additional zone of excess in the infrared with 30% more than the solar intensity at 0.80μ.

Figure 6.1, Spectral Distribution: Barium, Hydrogen, Argon VSRS vs Sun, shows that the use of barium and hydrogen as additives has modified the argon deficiency zones but has not eliminated them. The short ultraviolet around 0.23μ is increased. At 0.3μ the excess is 165% of solar intensity for some improvement. While at 0.6μ very little change occurred. However, considerable reduction in the argon radiation deficiency can be noted at 0.5μ and 0.65μ. The remainder of the argon curve is essentially unchanged.

Hydrogen is the only additive which contributes in the argon visible deficient zone without adding to the ultraviolet excess (See Figure 6.2). Hβ radiation at 0.49μ and Hα at 0.66μ reduce the argon deficiency in these wavelengths. It is very likely that larger hydrogen percentages would cause even more improvement. Unfortunately hydrogen is diatomic and the dissociation and recombination processes taking place in a vortex arc result in transfer of large amounts of power to the anode.

The 21.7 kw, 12.7 atm xenon vortex arc has a better match to the solar spectrum than argon or any of the additive-argon mixtures tested. Figure 6.3, Spectral Distribution: Xenon Vortex vs Sun, indicates an excess in the ultraviolet with 140% more than solar intensity at 0.3μ decreasing to 40% at 0.35μ. The match at the solar peak is good, but a deficiency exists between 0.5μ and 0.82μ. At 0.6μ this amounts to 34% and at 0.7μ the deficiency is 30%. From 0.9μ to 1.4μ the

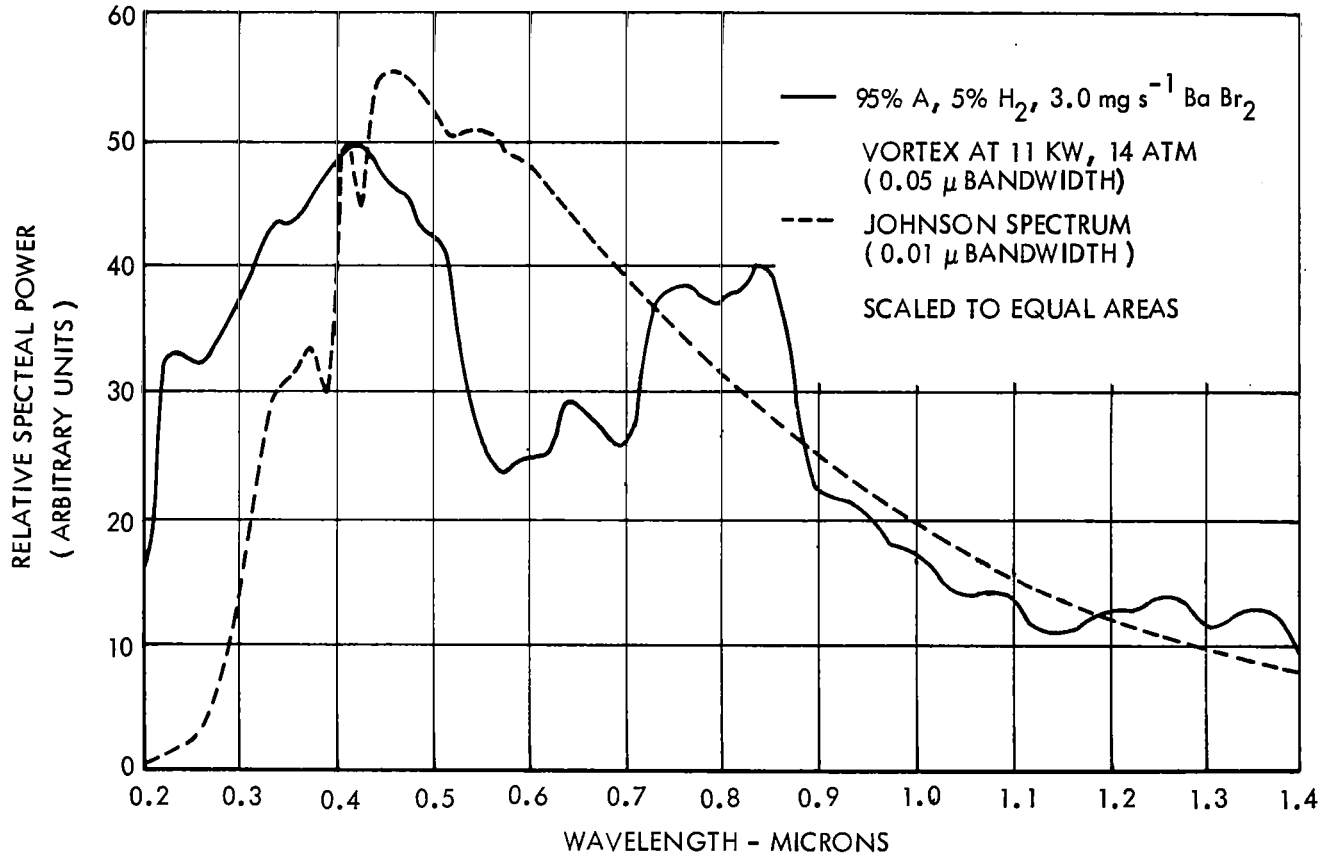

FIGURE 6.1 - SPECTRAL DISTRIBUTION: BARIUM, HYDROGEN, ARGON VSRS VS SUN

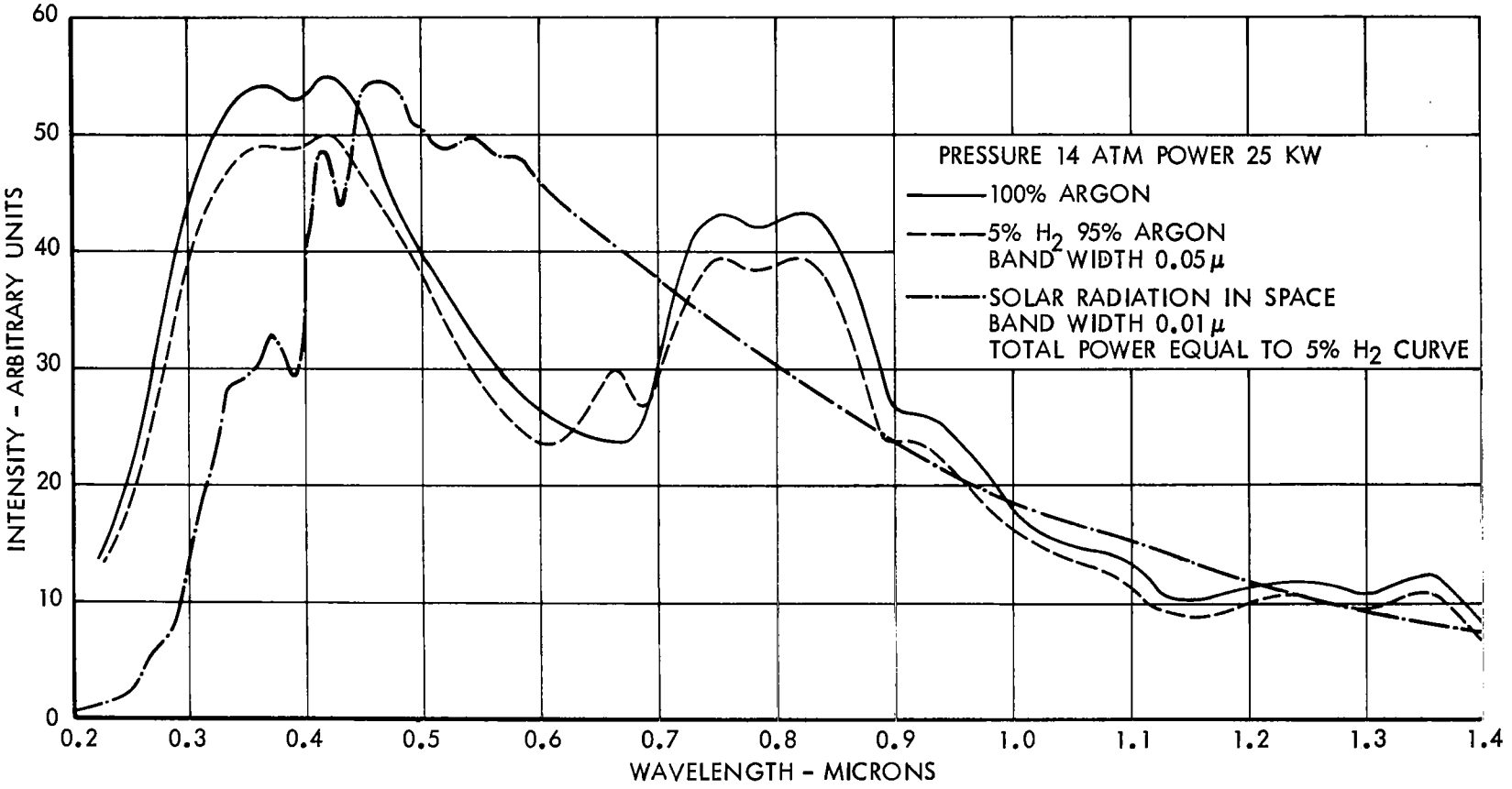

FIGURE 6.2 - SPECTRAL DISTRIBUTION: HYDROGEN ARGON VORTEX VS SUN

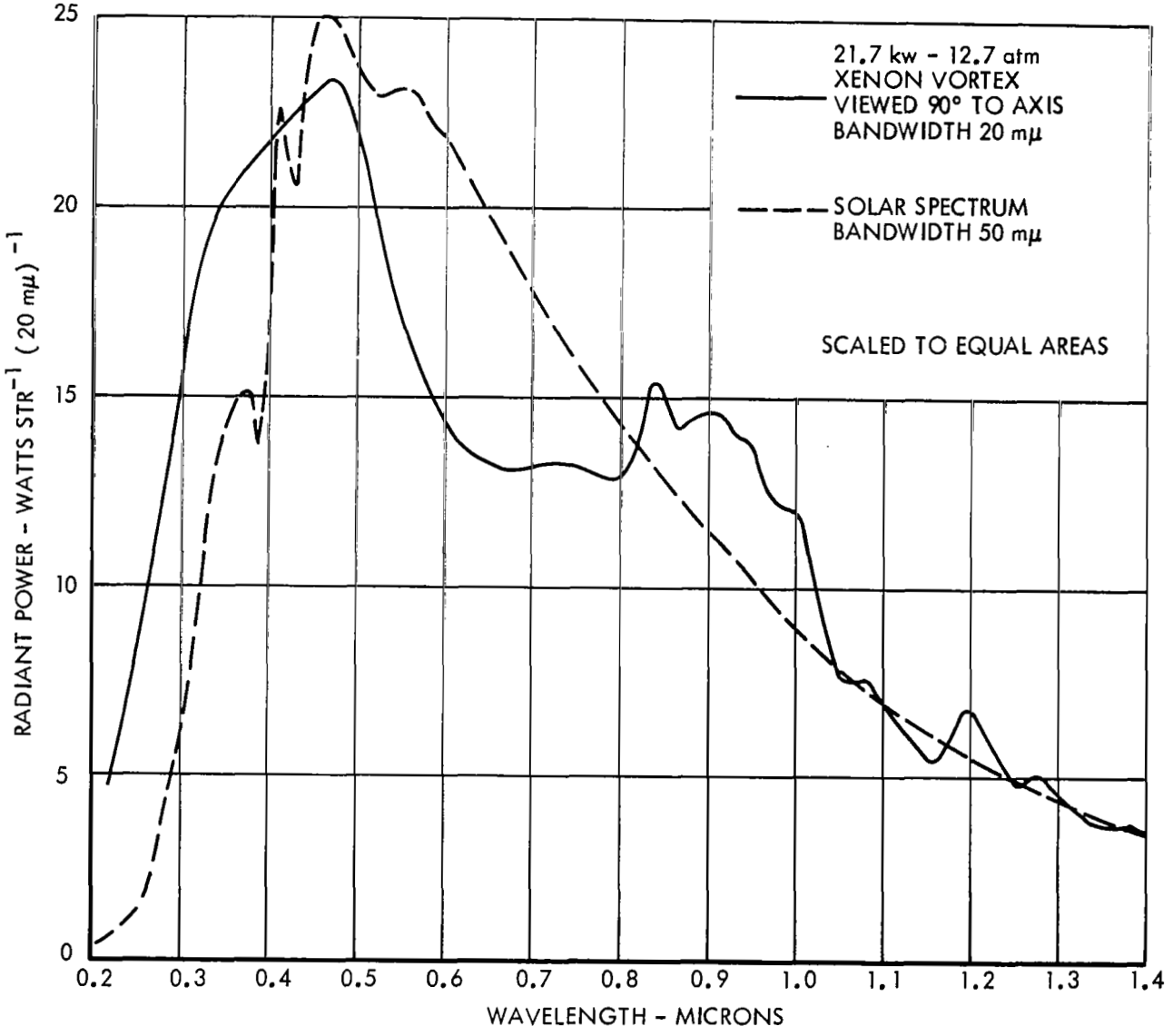

FIGURE 6.3 - SPECTRAL DISTRIBUTION: XENON VORTEX VS SUN

xenon radiation exceeds solar intensity by as much as 33% near 1.0μ. The use of this source with optical elements having transmission losses in the ultraviolet would result in an excellent match to the solar spectrum.

7.0 CONCLUSIONS

The basic investigations showed that the spectral distribution of radiation from the vortex arc can be modified both by injection of additives and by control of electron density. The additives change the spectrum by superimposing line radiations, while the variation in electron density shifts the broad peaks in the continuum radiation.

Line radiations were studied by use of the argon plasma, however, very similar conclusions would be reached with use of krypton. Additive, line emission, studies lead to the conclusion that with the exception of hydrogen all additives result in an increased emission in the ultraviolet. Additives can be selected to add radiation to the visible deficiency zone of the inert gases but when a radiant power comparison is made with the solar beam the increase in the ultraviolet nullifies or minimizes the gain in the visible. Hydrogen gives a real addition in wide bands near 0.49μ and 0.66μ but only with loss of radiative efficiency.

An arc in a constricting vortex flow tends to develop a uniform electron and ion density. This uniform core is surrounded by a thin shell with ion density decreasing rapidly with increasing radius. This means that the ion density can be controlled by input power and by pressure. Continuum emission becomes the dominant radiation process here as in any high pressure plasma. The vortex plasma with its uniformity in electron and ion density should be considered a new radiation standard. With some improvement in theory, its spectral emissivity will be just as predictable from plasma dimensions, pressure and input power as is the radiation of a low reflectivity thermal cavity from its temperature.

The control of pressure and electron and ion density leads to a degree of control over the position of peaks in the continuum. This is possible due to lowering of the ionization potential in high density plasmas. Xenon with the heaviest nucleus of the inert gases is the most susceptible to control. Vortex plasma radiation measurements indicate a lowering of 1.18 v at 12.7 atmospheres and 21.7 kw. Bauer (Ref. 7.1) has measured up to 2.17 v lowering at a pressure of 25 atmospheres. This change in actual ionization potential results in a pronounced shift in the peaks of xenon's continuum.

The 12.7 atmosphere xenon vortex operated at 21.7 kw produces radiation which matches the zero air mass solar spectrum more closely than any other high radiance source of comparable power. It is believed that the xenon spectral match can be improved to an approach to duplication by increasing pressure sufficiently to achieve an estimated 1.63 v lowering of the ionization potential. This is expected with an ion density near 2×10^{18} cm^{-3}.

7.1 Recommendations

a. The investigation indicates that the radiation of the xenon vortex arc when operated at $\approx$ 20 atmospheres pressure may closely approach the spectral distribution of the sun in space. It is recommended that an effort be made to develop a recirculated xenon vortex arc system capable of operation to 25 atmospheres. This would permit test and confirmation of this concept.

b. The investigation indicates that the 12 to 14 atmosphere recirculated xenon vortex arc for operation between 12 kw and 25 kw gives an excellent simulation of solar radiation. Considering the accompanying high radiance of the xenon vortex, it is recommended that this device be considered for the upgrading of existing solar simulator systems as well as installation in those being planned.

REFERENCES

1.1 P. A. Schoeck, 1963: "The Anode Energy Balance of Argon Arcs," in Modern Developments in Heat Transfer, Ibele, Academic Press, Inc., New York, pp 353-400.

1.2 F. S. Johnson, 1954: "The Solar Constant", J. of Meteor, Vol. 11, p 431.

1.3 F. L. Mohler, 1928: "Recombination Spectra of Atomic Ions and Electrons", Phys. Rev., Vol. 31, pp 187-194.

1.4 F. L. Mohler, 1929: "Recombination and Photo-ionization", Phys. Rev. Sup., Vol. 1, pp 216-227.

1.5 F. H. Mies, 1962: "Continuum Radiation from Ionized Rare Gases in Reflected Shock Waves", J. Chem. Phys., Vol. 37, pp 1101-1111.

1.6 M. J. Druyvesteyn and F. M. Penning, 1940: Revised Modern Physics, Vol. 12, p 87.

2.4.1 K. Watanabe and Edward C. Y. Inn, 1953: "Intensity Measurements in the Vacuum Ultraviolet", J. Opt. Soc., Vol. 43, No. 1, pp 32-35.

2.4.2 Donald H. Thurnau, 1956: "Quantum Efficiency Measurements on Several Phosphors under Excitation in the Extreme Ultraviolet", J. Opt. Soc., Vol. 46, No. 1, pp 346-349.

3.0 V. F. Kitayeva and N. N. Sobolev, 1962: "On the Broadening of Hydrogen Lines in the Plasma of Arc and Shock Tubes", Proceedings of the Fifth International Conference on Ionization Phenomena in Gases, Vol. II, North Holland Publishing, Amsterdam, pp 1897-1905.

3.1.1 H. N. Olsen, 1961: "Partition Function Cutoff and Lowering of the Ionization Potential in an Argon Plasma", Phys. Rev., Vol. 124, No. 6, pp 1703-1708.

REFERENCES

3.1.2 D. G. Van Ornum, 1964: "Study of Radiation From Vortex Stabilized Arcs", AEDC-TDR-64-165, Arnold Engineering Development Center.

3.1.3 H. N. Olsen, 1963: "The Electric Arc as a Light Source for Quantitative Spectroscopy", J. Quant. Spectrosc. Radiat. Transfer, Vol. 3, pp 305-333.

3.1.4 Hans R. Griem, 1964: Plasma Spectroscopy, McGraw-Hill Book Company, New York.

3.2.1 Sanborn C. Brown, 1959: Basic Data of Plasma Physics, John Wiley & Sons, New York, p 7 and p 102.

3.2.2 R. B. Brode, 1963: Revs. Modern Phys. 5, 257.

4.0 Lawrence H. Aller, 1953: Astrophysics, The Ronald Press Co., New York, p 78.

4.1 American Institute of Physics Handbook, 1957: McGraw-Hill, New York.

4.2.1 G. H. Reiling, 1964: "Characteristics of Mercury Vapor-Metallic Iodide Arc Lamps", J. Opt. Soc., Vol. 54, No. 4, p 532.

4.2.2 W. F. Meggers, C. H. Corliss and B. F. Scribner, 1961: "Tables of Spectral-Line Intensities", National Bureau of Standards Monograph 32 - Part 1.

4.4 W. E. Thouret and H. S. Strauss, 1963: "Xenon Compact Arcs with Increased Brightness Through Addition of Hydrogen", Illum. Eng., Vol. 58, No. 5, p 37 (May 1963).

7.1 A. Bauer and P. Schulz, 1959: "Constricted Xenon High Pressure Arcs of High Current Density", Zeitschrift fur Physik, Vol. 155, pp 614-627.